ELECTRICAL RESISTIVITY MEASUREMENTS OF MECHANICALLY STABILIZED EARTH RETAINING WALL BACKFILL

by

MICHAEL ANDREW SNAPP

B.S., Colorado School of Mines, 2012

A THESIS

submitted in partial fulfillment of the requirements for the degree

MASTER OF SCIENCE

Department of Civil Engineering
College of Engineering

KANSAS STATE UNIVERSITY
Manhattan, Kansas

2015

Approved by:

Major Professor
Dr. Stacey Kulesza

Copyright

Abstract

In Kansas, mechanically stabilized earth (MSE) retaining walls are typically backfilled with coarse aggregate. Current backfill material testing procedures used by the Kansas Department of Transportation (KDOT) utilize on-site observations for construction quality assurance and the American Association of State Highway and Transportation Officials standard T 288-12 ("Standard Method of Test for Determining Minimum Laboratory Soil Resistivity"). AASHTO T 288-12 is designed to test a soil sample's electrical resistivity (ER) that correlates to its corrosion potential. However, the test, based on material passing through a No. 10 sieve, is inappropriate for coarse aggregates typically used by KDOT as the aggregate will be retained on a No. 10 sieve and potentially leads to over-conservative designs. ER imaging provides a two-dimensional (2D) profile of bulk ER of backfill material, thereby yielding more information regarding backfill uniformity compared to traditional sampling. The objective of this study was to characterize bulk ER of in-place MSE wall backfill aggregates.

In this study, MSE walls selected by KDOT were tested using ER imaging during construction to determine bulk ER of the backfill. Variations within backfill ER may be a result of varying aggregate material, inclusions of fines, thoroughness of compaction, and the presence of water. ER imaging was used on five walls: four MSE walls and one gravity retaining wall that contained no reinforcement. One MSE wall contained metal reinforcement, while the other four walls contained geosynthetic. The ER imaging field method produced a 2D profile that depicted ER uniformity for bulk analysis. A post-processing algorithm was created to remove the subjective nature of the ER imaging results. The program determines the bulk ER based upon the ER imaging results. These results indicate that the laboratory analysis of AASHTO T 288-12 under-estimates the bulk ER of in-situ backfill material. Identification of a material's bulk ER will help characterize the ER of aggregates in a complementary KDOT project. Results of this study will be used to recommend an in-situ test method for aggregate used by KDOT.

Table of Contents

List of Figures

List of Tables

Acknowledgements

I would like to first express my deepest gratitude to my major professor Dr. Stacey Tucker-Kulesza for her allowing me to partake in this project and I thank her for her guidance and patience throughout my time here at Kansas State.

In addition I would like to thank my two other committee members, Dr. Dunja Peric and Dr. Mustaque Hossain for their support. I would also like to extend a thank you to those students who took the time to help in the field testing; including Tri Tran, Abady Al-Ali, John Palma, Weston Koehn, and Zahidul Karim. I would like to thank Sue Wells for her assistance in checking out vehicles through the Kansas State Motor Pool.

I would like to thank the Civil Engineering Department at Kansas State University and the Kansas Department of Transportation (KDOT) for their financial support during my time at Kansas State. I want to specifically thank KDOT for allowing me to be a part of this project and to all the construction-site foreman for allowing us to enter their sites and perform our testing during their construction.

Dedication

I would like to dedicate this research to my parents, David and Debbie Snapp, and my entire family. Without their continued support, I would not be where I am today. Thank you for everything!

Chapter 1 Introduction

1.1 Background

The Kansas Department of Transportation (KDOT) and other state Departments of Transportation (DOTs) typically specify coarse aggregate material for backfill of mechanically stabilized earth (MSE) retaining walls. One major concern for MSE walls is the corrosion of the metallic reinforcement used at times within the walls. Therefore, the American Association of State Highway and Transportation Officials (AASHTO) and other transportation industry leaders have created standard laboratory testing procedures to test the electrical resistivity (ER) of the backfill material, which relates to the corrosion potential. Additionally, researchers such as (Thapalia et al., 2011) have investigated new methods to determine the corrosion potential of a material. These laboratory test methods produce results from a small field sample assumed to be representative of the whole backfill.

KDOT utilizes MSE retaining walls throughout the Kansas State highway system. These walls are commonly used in approach ramps and abutments of overpasses with abrupt elevation changes. MSE walls were first implemented in the United States in the 1970s due to their cost efficiency and strength (Armour et al., 2004). MSE walls are reinforced earth-retaining structures with either solid wall faces or wall faces composed of modular blocks. Fig. 1.1 shows the typical MSE wall attributes. Reinforcement extends from the front face of the wall into the backfilled soil, advantageously utilizing the soil's strength properties and weight to support the wall. KDOT typically uses coarse aggregates as backfill materials because the aggregates allow water behind the wall to freely drain to the base of the wall and then be directed away from the wall by a piping system. Many retaining walls have failed due to increased water pressure within the backfill (Moylan, 2012). Reinforcement and backfill material are analyzed in the laboratory prior to construction to ensure that they are suitable for use in wall construction.

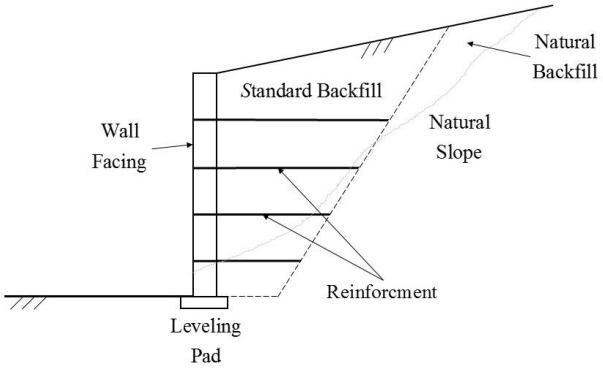

Fig. 1.1. Typical MSE wall attributes

MSE walls use either metal or geosynthetic materials as reinforcement. One primary disadvantage of metal reinforcement, however, is that it is susceptible to corrosion. Corrosion, the process of metal material returning to its stable natural state, is caused by a naturally occurring electric current flowing between two metal objects or two points on the same material when an electrolyte (typically water) is present in the soil (Elias et al., 2009). Inevitable corrosion of metallic reinforcement reduces the strength of the MSE wall due to metal degradation. Therefore, AASHTO has specified rates of reinforcement corrosion and developed a standard test method used to determine a soil's corrosion potential. In addition, AASHTO, the American Society for Testing Materials (ASTM), Federal Highway Administration (FHWA), and state DOTs have created guidelines and standards for construction of MSE walls along with testing procedures and construction quality assurance (CQA) practices, as outlined in Section 2.2.1.

The test directly involved in this study was the AASHTO "Standard Method of Test for Determining Minimum Laboratory Soil Resistivity" (AASHTO method T 288-12), which is used to determine corrosion potential of soils. ASTM has developed a similar test, referred to as the "Standard Test Method for Measurement of Soil Resistivity Using the Two-Electrode Soil Box Method" (G187-12a). Each test method has been described in Section 2.2.1. Both methods require that a sample be collected from the selected backfill material and pass through a No. 10 sieve (2.00 mm). One hundred fifty milliliters of water is added to the material passing through the sieve, allowed to cure for 12 hours, and then placed in a 688 cm^3 box. A resistivity meter is attached to the box and the soil resistance is measured. The sample is then removed from the box, 100 mL of water is added, and the soil resistance is tested again. This process is repeated

until a minimum resistance value is determined. Resistivity is used to determine ER of the soil by multiplying the resistance by a constant for the box. The constant is derived from the relationship of the surface area of one electrode and the distance between the two electrodes at each end of the testing box.

ER imaging is used in fields such as archeology, geology, environmental, geotechnical, and construction. Applications within these fields include determining depth to groundwater (Vaudelet et al., 2011), detecting varying subsurface geology (Chambers et al., 2013), and the presence of subsurface structures (Arjwech et al., 2013). Soil characteristics such as the presence of water, amount of voids, and mineralogy (metallic and non-metallic minerals) affect ER measurements (Zhou et al., 2001). The more water that is present in the subsurface, the lower the ER will be. In addition, more unsaturated void space increases ER values. A larger percentage of clay and metallic minerals in the subsurface will decrease the ER due to conductive behavior of the material. Typical ER values of common geomaterials are outlined in Table 1.1.

Table 1.1. Common ER values of geomaterials (Knight and Endres, 2005; Lucius et al., 2007)

Material	**Resistivity (Ω-m)**
Clay	5-100
Dry Sand and Gravel	>200
Saturated Sand and Gravel	<50
Sandstone	50 -1,000
Shale	5-50
Conglomerates	1,000-10,000
Limestone and Dolomite	>1,000
Igneous Rocks	>1,000
Metamorphic Rocks	>1,000

Traditional ER imaging method utilizes four stakes, commonly referred to as electrodes, to perform the test: two current electrodes and two voltage potential electrodes. Electric current is applied to the two current electrodes, which inject the current directly into the ground, and voltage potential is measured between two voltage potential electrodes. The electrodes are placed

in a straight line along the ground surface. This method has been adapted to an automated system in which multiple electrodes may be used in numerous combinations. Multi-electrode setups always require two current electrodes, but multiple voltage potential electrodes can be used, depending on the data-logger's capacity. ER distribution of the subsurface is determined by forward modeling and data inversion. Additional descriptions of ER derivation and ER imaging are given in Chapter 2.

1.2 Problem Statement

Unfortunately, standard methods for determining the ER of backfill have many flaws. First, samples gathered from the field represent only a small portion of in-place backfill. In addition, MSE walls in Kansas are typically backfilled with coarse aggregates. This material will not pass through a No. 10 sieve (2.00 mm), thereby requiring the material to be crushed. However, crushing can alter material properties, thereby potentially providing misleading ER measurements. AASHTO method T 288-12 develops results from a saturated slurry state, which is not indicative of the MSE wall backfill. Currently, AASHTO method T 288-12 is the only laboratory test used to determine corrosion potential of soil in Kansas. Table 1.2 outlines ranges of ER values and corresponding corrosion potential of a typical aggregate.

The only common field method used to predict and monitor reinforcement corrosion is the addition of metal coupons in the backfill (Elias et al., 2009). Coupons are small samples of metal reinforcement that are inserted near the face of the wall during construction and then removed for degradation testing. However, their removal does not affect the integrity of the MSE wall. Sample degradation is attributed to corrosion. Currently, there is a need for an in-situ testing method that can be used to compare with the AASHTO method T 288-12 corrosion potential laboratory analysis and a laboratory analysis of corrosion potential suitable for coarse aggregates. ER imaging is a field method that will resolve many laboratory analysis disadvantages. The ER imaging in the field can provide results of the entire wall and be performed on the aggregates "as-is" without material being crushed or saturated; more indicative of MSE wall backfill.

Table 1.2 Correlation between resistivity values and corrosion potential (Elias et al., 2009).

Aggressiveness	Resistivity (Ohm-cm)
Very corrosive	< 700
Corrosive	700 to 2,000
Moderately corrosive	2,000 to 5,000
Mildly corrosive	5,000 to 10,000
Noncorrosive	> 10,000

AASHTO method T 288-12 is one of the few laboratory tests used to determine corrosion potential of a soil. Currently, few known field testing methods evaluate corrosion other than the addition of coupons mentioned previously. Laboratory testing require interpretation from a small sample of an entire wall. Therefore, a technical need exists for an in-situ testing method to determine and possibly monitor reinforcement corrosion of an MSE wall. The significance of this research is the application ER imaging to determine bulk ER of aggregate backfill MSE walls. A quantitative analysis of ER imaging results was used to determine bulk ER of the MSE wall rather than relying on qualitative results from the field. Results were compared to the AASHTO method T 288-12 results provided by KDOT.

1.3 Study Objective

This study investigated the application of ER imaging, a near-surface nondestructive geophysical field testing method used to determine the bulk ER of MSE wall backfill. Few known in-situ testing procedures exist for determining ER of aggregate backfill. ER imaging provides a two-dimensional (2D) profile of subsurface ER distribution, thereby providing more information than a small sample tested in a laboratory setting. In this study, ER imaging was applied to four MSE walls specified by KDOT: three walls that contained geosynthetic reinforcement and one wall that had metallic reinforcement. A fifth wall that contained no reinforcement was also tested. As required by the FHWA, KDOT tests all backfill regardless of reinforcement type. A quantitative post-processing algorithm was created to determine bulk ER of in-place backfill rather than relying on qualitative ER imaging results.

1.4 Thesis Outline

This thesis is divided into five chapters. Chapter 1 discusses the background, problem statement, and the study objectives. Chapter 2 presents a literature review deriving ER, the ER imaging field method, applications of ER imaging, background of MSE walls, current testing

procedures and guidelines, and corrosion studies of MSE walls. Chapter 3 discusses equipment used during testing, the ER imaging field testing procedure, and the results of each wall tested. Chapter 4 presents the quantitative post-processing program used to determine the bulk ER of the tested walls. Finally, conclusions, recommendations, and future research are presented in Chapter 5.

Chapter 2 Literature Review

2.1 Electrical Resistivity

ER imaging, developed in the early 1900s, is a near-surface geophysical, non-destructive testing method currently used in various fields due to the availability of equipment, ease of setup, procedure, and interpretation (Lowrie, 2007). ER imaging has applications in fields such as archeology, geology, environmental, geotechnical, and construction with applications in these fields including hydrogeological contamination mapping (Vaudelet et al., 2011), geological subsurface site characterization (Chambers et al., 2013), environmental landfill studies (Bernstone et al., 2000), monitoring of soil moisture content (Zhou et al., 2001), and geotechnical site investigations to determine depth of bridge foundations (Arjwech et al., 2013).

Subsurface characteristics such as water content and saturation, porosity, permeability, mineralogy, clay content, and temperature affect ER measurements (Zonge et al., 2005). ER of a soil tends to decrease with increased water content (ratio of the weight of water in a soil volume to the weight of solids) and saturation (the percent of void spaces in a soil filled with water) (Bai et al., 2013). Materials with large amounts of clay content and high levels of metallic minerals tend to have low ER because the clay and metallic minerals are conductive; allowing the flow of current to easily pass through the material. ER typically decreases with decreased porosity (the percentage of void space in a volume of soil) due to the decrease in void space between particles that prohibit the flow of electric current.

The following sections include discussion of ER derivation and description of the field imaging method used to gather data as well as the general data processing method to obtain ER from the field. Finally, current applications of ER imaging are presented.

2.1.1 Derivation of Electrical Resistivity

ER, an intrinsic material property, defines a material's ability to resist or oppose the flow of electric current. Resistivity (ρ) is represented in units of the Ohm-meter (Ohm-m) and is the inverse of conductivity (σ). ER is fundamentally derived from Ohm's Law (Eq. 1):

$$V = IR, \tag{1}$$

where R is resistance, I is electric current, and V is potential voltage difference. The resistivity of a material is proportional to the length *(L)* of a material and inversely proportional to the cross-sectional area (A) (Fig. 2.1), resulting in Eq. 2:

$$R = \rho \frac{L}{A}. \qquad 2$$

Knowing the resistance from Eq. 2, Eq. 3 is generated by substituting resistance into Ohm's Law. This is done to develop an equation which may be used to determine the ER based on measurable quantities,

$$V = I\rho \frac{L}{A}. \qquad 3$$

The ratio V/L is defined as electric field ($\vec{E}$) when assuming that the potential gradient is constant along the length of the material. Ratio I/A is referred to as current density ($\vec{J}$). Therefore, Eq. 3 can be written as Eq. 4 or rewritten in an alternate three-dimensional (3D) form of Ohm's Law:

$$\vec{E} = \rho \vec{J}. \qquad 4$$

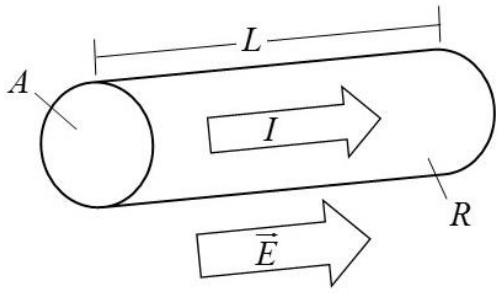

Fig. 2.1. Ohm's Law parameters represented in a conductor (Lowrie, 2007).

Ohm's Law for isotropic homogeneous media is used to derive ER of the subsurface during ER imaging. Section 2.1.2 outlines the process of how the bulk ER image of a soil is determined utilizing four electrodes.

2.1.2 Electrical Resistivity Imaging Method

Traditional ER imaging consists of a four-electrode setup in which direct electric current is injected into the subsurface through two electrodes and the electric voltage potential is measured simultaneously between the other two electrodes. For the two current electrodes, one electrode, referred to as the current source, applies current that expands radially away from the electrode in an assumed isotropic homogenous half space with a surface area of $2\pi r^2$, where r is the radius of the hemi-sphere (Fig. 2.2). The second current electrode receives current from the electrode current source radially inward and is known as the current sink (Fig. 2.3). The generated electric field is parallel to the current flow and is normal to equipotential surfaces. Equipotential surfaces are defined when electric potential is the same across all points on that surface. As defined in Eq. 4, the generated electric field is equal to the product of the resistivity and the current density. As shown in Eq. 5, the current density is the injected current divided by the assumed half space with a surface area $2\pi r^2$:

$$\vec{E} = \rho \frac{I}{2\pi r^2}. \qquad 5$$

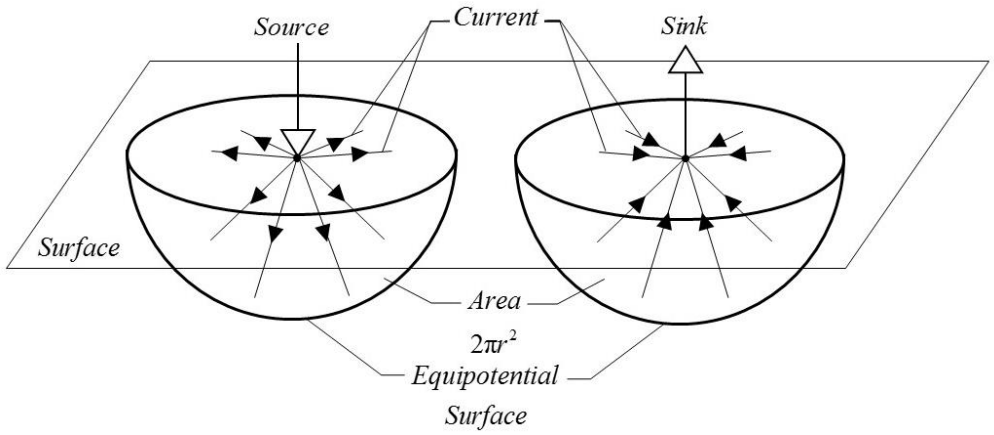

Fig. 2.2. Electric current source and sink expanding radially in a half space.

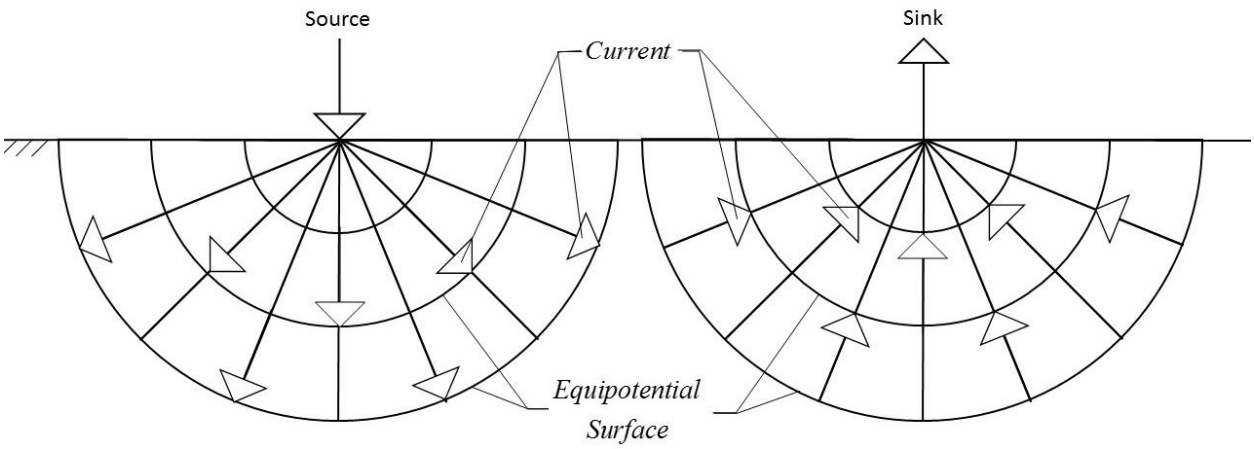

Fig. 2.3. Electric current lines extending radially away from the source and inward toward the sink and equipotential surfaces normal to the current.

The fundamental law of work (Eq. 6) defines the voltage at a point, P, $\left(V_{\mathrm{p}}\right)$ measured in the system as equal to work $\left(W\right)$ done by the electric field to move a charge from the distance r_p (the distance from the current source or sink to the voltage potential measurement) to infinity. The force experienced by a test charge is proportional to the electric field ($\vec{E}$). The derivation of voltage potential $\left(V_p\right)$ of a single electrode using the fundamental law of work is outlined in Eq. 7.

$$W = \int F \bullet \mathrm{d}r \,. \qquad 6$$

$$V_{\mathrm{p}} = \int_{r}^{\infty} \vec{E} \bullet \mathrm{d}r = \int_{r}^{\infty} \frac{\rho I}{2\pi {r_p}^2} dr = \frac{\rho I}{2\pi r_p} \qquad 7$$

Recall that the subsurface is assumed to be a uniform half-space and the electric field lines generated from the input of current expand radially away from the source and are directed radially inward to the current sink (Fig. 2.3). Equipotential lines are assumed to be hemispherical in shape and the potential will increase towards the source remaining positive and will decrease towards the sink and become negative. Therefore, the potential difference between two electrodes, or potential electrodes, at known distances may be measured.

Fig. 2.4 illustrates the general arrangement of two current electrodes, A the sink and B the source, and two voltage potential electrodes, C and D. The voltage potential at electrode C due to the current source A and sink B is represented in Eq. 8.

$$V_{P_C} = \frac{\rho I}{2\pi}\left(\frac{1}{r_{AC}} - \frac{1}{r_{CB}}\right). \quad 8$$

The potential at electrode D is derived in the same manner resulting in Eq. 9:

$$V_{P_D} = \frac{\rho I}{2\pi}\left(\frac{1}{r_{AD}} - \frac{1}{r_{DB}}\right). \quad 9$$

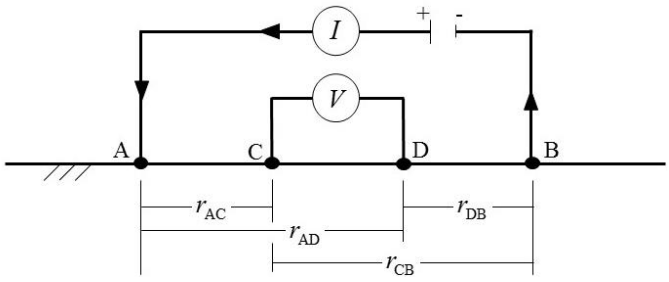

Fig. 2.4. General configuration of current and potential electrodes

The voltage difference measured across the electrodes C and D in Fig. 2.4 is the difference between Eqs. 8 and 9 and is represented in Eq. 10:

$$\Delta V = V_{P_C} - V_{P_D} = \frac{\rho I}{2\pi}\left[\left(\frac{1}{r_{AC}} - \frac{1}{r_{CB}}\right) - \left(\frac{1}{r_{AD}} - \frac{1}{r_{DB}}\right)\right]. \quad 10$$

Eq. 10 is derived under the assumption that the subsurface is a uniform homogenous material with uniform resistivity. In reality, the resistivity of the earth is heterogeneous; therefore, Eq. 11 is rearranged to find apparent resistivity (ρ_a):

$$\rho_a = \frac{2\pi V}{I}\left[\frac{1}{r_{AC}} - \frac{1}{r_{CB}} - \frac{1}{r_{AD}} + \frac{1}{r_{DB}}\right]^{-1}, \quad 11$$

which is interpreted as the resistivity that would be measured if in fact the earth were homogenous. Forward modeling and inversion is used to determine the ER of the subsurface. Apparent ER data from the field are typically plotted into a two-dimensional (2D) profile, or pseudosection, of the subsurface apparent ER. Each subsurface point in a pseudosection

corresponds to a current and potential electrode pair, and the subsurface point is considered average bulk ER of the subsurface. For ease of plotting, the convention is to locate the subsurface point at the intersection of lines that extend from the center of the two pairs of electrodes (current and potential), 45° from the ground surface, as shown in Fig. 2.5 (Hallof, 1957). This method is repeated for each pair of electrodes, thereby generating a pseudosection of apparent ER, as shown in Fig. 2.6. Each array (arrays are defined in section 2.1.3), tested material, and electrode spacing slightly alter the depth of ER imaging investigation (Edwards, 1977; Loke, 1999). However, the pseudosection using 45° plot is a useful method for depicting approximate ER of the subsurface. (Edwards, 1977) defined the effective depth of each data point as described in Eq. 12:

$$z_e = Kc_n a, \qquad 12$$

where z_e represents the effective depth, K a constant for the appropriate absolute scale factor, c_n a coefficient representing the appropriate relative plotting depths for every electrode, and a the spacing between the current and potential electrodes.

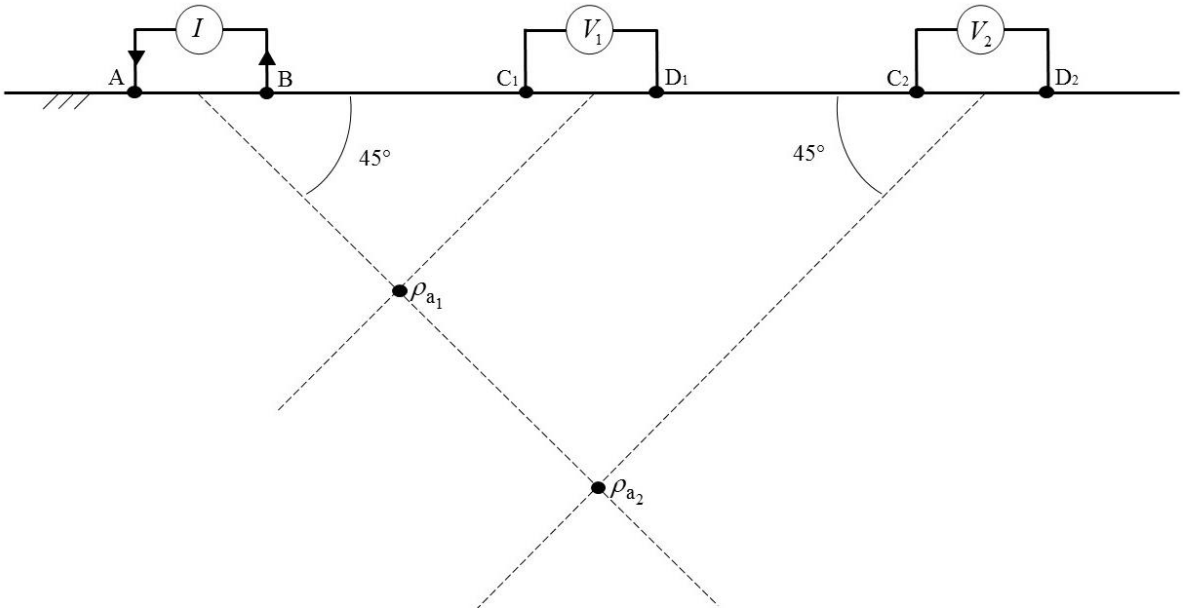

Fig. 2.5. Apparent ER pseudosection of the dipole-dipole array (Hallof, 1957).

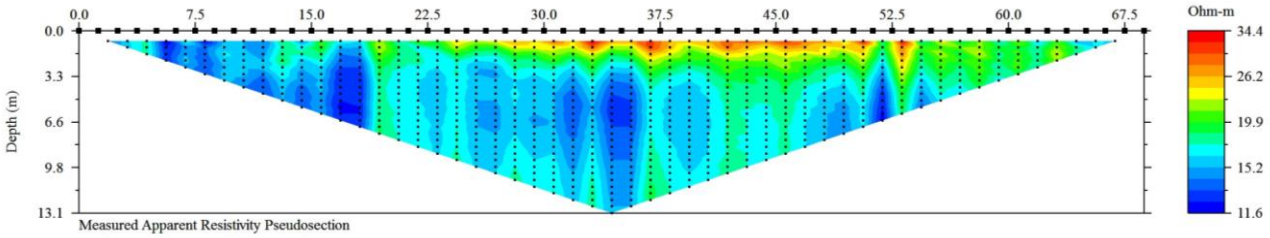

Fig. 2.6. A 2D apparent ER pseudosection from field data.

The traditional method of four electrodes has been modernized into an automated system in which multiple electrodes are connected, thereby increasing the effectiveness and efficiency of ER imaging. Multiple electrodes are attached to a data acquisition system that runs a desired command file. The command file contains information on the spacing of the electrodes and the desired array. From this information, the system relays which electrodes to use as current and potential. Depending on the system, multiple potential readings may be taken per current electrode pair. This allows the process to optimize testing efficiency, decreasing testing time. Where large distances must be continuously imaged, roll-along surveys may be used. A roll-along survey gathers data upon the initial setup and after completion of the first test, the line shifts linearly starting where the location of the last electrode from the previous test. 3D surveys are also possible where the electrodes are arranged in a 3D grid. A 3D test was performed in this study, but because of increased testing time and minimal gain of data, the method was not utilized further. Only 2D surveys are discussed in the following sections. Further information on the equipment and the field setup used in this study is presented in Chapter 3.

2.1.3 Traditional Arrays

An array defines the current and potential electrode configurations used during testing. Three main arrays are used in ER imaging: dipole-dipole, Wenner, and Schlumberger. Each test differs according to electrode configuration or spacing and each has unique advantages and disadvantages. Apparent ER (Eq. 11) can be simplified according to each geometric configuration. When planning a survey, one typically considers the depth necessary to image the medium of interest and the required resolution. In general, as electrode spacing increases, depth of signal penetration increases; and when spacing decreases, depth of signal penetration decreases (Furman et al., 2003); however, there is a trade-off in resolution.

Three areas of concern when comparing and choosing an array include signal-to-noise ratio, electromagnetic coupling (EM), and resolution (vertical and horizontal). Signal-to-noise ratio refers to the ratio of the desired signal to the background noise. EM, also known as cross-wire coupling, is the interference between the transmitter and receiver wires (Zonge et al., 2005). Vertical resolution refers to the ability of the array to provide data with depth, and horizontal resolution refers to the ability to gather data laterally along the survey line. The following sections describe each array and present a pictorial representation of the configuration, the apparent resistivity equation with geometric spacing, and advantages and disadvantages of each array.

Dipole-Dipole Array

The dipole-dipole array consists of the current pair of electrodes and the potential pair of electrodes spaced equal distance a, separated by a factor of na (Fig. 2.7). Eq. 13 simplifies Eq. 11 using the spacing of the dipole-dipole array:

$$\rho_a = \pi an(n+1)(n+2)\frac{V}{I}\ , \qquad 13$$

where a is electrode spacing, n times a spacing represents spacing of the electrode pairs, I is input current, and V is measured voltage.

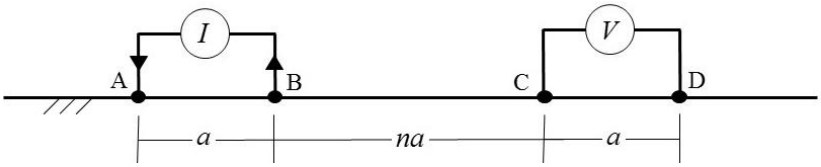

Fig. 2.7. Electrode geometric configuration of the dipole-dipole Array.

The dipole-dipole array provides good lateral and vertical resolutions with minimal EM coupling (Zonge et al., 2005). This array was initially utilized in the study, but due to the increased time to run a survey, it was ultimately not selected as the optimal array. The dipole-dipole array requires approximately 40 minutes utilizing a 56 electrode and 1.2 seconds between measurements.

Wenner Array

Spacing of the Wenner array, as shown in Fig. 2.8, is set to equal distance a between electrodes, allowing the greatest lateral resolution compared to dipole-dipole and Schlumberger arrays (Zonge et al., 2005). Unfortunately, this geometric arrangement limits overall survey depth and increases EM coupling (Stummer et al., 2004). Testing time for a 56 electrode setup is the longest of the three arrays, requiring over an hour. This array was not used in this study due to the amount of time the test takes and lack of resolution with depth. Eq. 14 represents apparent ER with Wenner array geometric spacing:

$$\rho_{\mathrm{a}} = 2\pi a \frac{V}{I}, \tag{14}$$

where a is electrode spacing, I is current, and V is measured voltage.

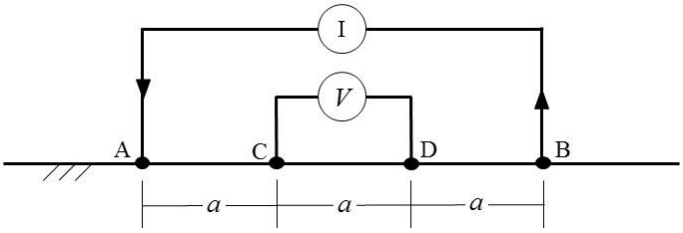

Fig. 2.8. Electrode geometric configuration of the Wenner array.

Schlumberger

The traditional four electrode geometric configuration of the Schlumberger array consists of potential electrodes located inside current electrodes (Fig. 2.9). Electrode arrangement is symmetrical about the center of the test setup. Potential electrodes are spaced at distance a from the center and current electrodes are spaced at distance na. Eq. 15 represents the apparent resistivity from Eq. 11 using the specific electrode spacing of the Schlumberger array.

$$\rho_{\mathrm{a}} = \frac{1}{2}\pi a(n-1)(n+1)\frac{V}{I}, \tag{15}$$

where a is potential electrode spacing from the center of the test, n times a spacing represents spacing of current electrodes from the center of the test, I is injected current, and V measured voltage. The Schlumberger array provides the best vertical resolution of the three arrays with low signal-to-noise ratio (Stummer et al., 2004). However, the Schlumberger array provides poor lateral resolution and high EM coupling (Zonge et al., 2005). This array requires approximately

one hour for a 56 electrode setup. An inverse Schlumberger array, detailed in the following section, was primarily used for this research.

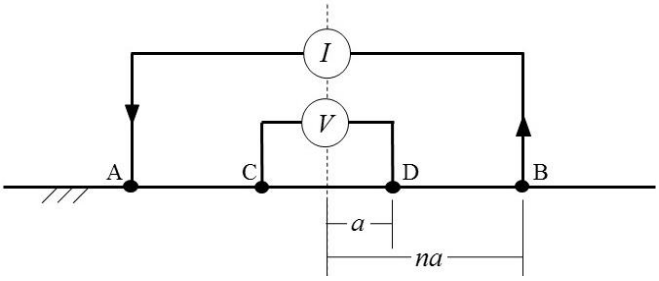

Fig. 2.9. Electrode geometric configuration of the Schlumberger array.

Inverse Schlumberger

The inverse Schlumberger array switches the inner potential electrodes with current electrodes and outer current electrodes with potential electrodes while maintaining spacing configuration of the Schlumberger array (Fig. 2.10). The setup of current and potential electrodes previously mentioned allows multiple potential electrodes to be used per current pairs in the automated system, speeding up testing time from one hour in the Schlumberger array to 32 minutes for a 56 electrode test. The inverse Schlumberger array was primarily utilized in this study because of its relatively fast testing time and optimum data acquisition with good depth resolution.

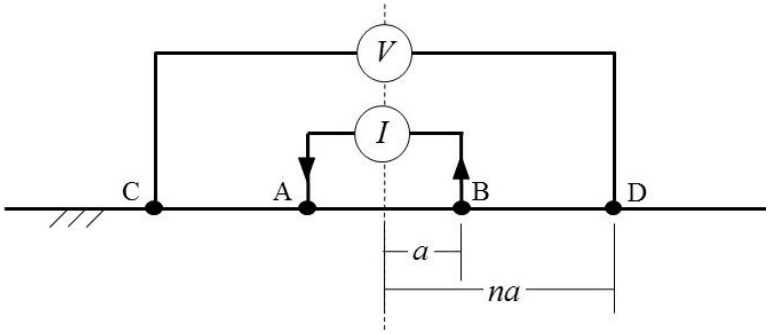

Fig. 2.10. Electrode geometric configuration of the inverse Schlumberger array

2.1.4 Data Processing

Forward modeling and data inversion are used to convert apparent ER determined in the field into inverted ER used for interpretation; however, ER inversion problems are non-unique. Advanced Geosciences Inc. (AGI) commercial software, EarthImager 2D, was used exclusively

for this research. The following paragraphs outline EarthImager modeling and inversion processes.

EarthImager initially graphically displays the measured apparent ER pseudosection (Fig. 2.11A) from field testing, and the modeler sets the desired criteria for data removal. Major spikes in measured data, negative values, maximum and minimum apparent resistivity values, and minimum voltage may be removed at this time. At times, depending on the material being tested and the test setup, insufficient current is injected into the ground. If too low of current is injected, spikes and negative values may occur due to poor potential electrode readings. Once data have been removed, forward modeling and inversion parameters are inputted.

Forward modeling used by AGI is based on the Fourier transformed partial differential equation (Eq. 14) (AGI, 2007). However, Fourier transform partial differential equation is a simplified method, and many other differential equations, such as Poisson's partial differential equation, may be used (Nenna et al., 2011). In order to determine the forward model, the following partial differential equation of the electric potential of the subsurface is used:

$$\frac{\partial}{\partial x}\left(\sigma\frac{\partial V}{\partial x}\right)+\frac{\partial}{\partial z}\left(\sigma\frac{\partial V}{\partial z}\right)-k^2\sigma V=-I\cdot\delta(x)\cdot\delta(z), \qquad 16$$

where V is scalar electrical potential, I is electric current source, k is wavenumber, and σ is electrical conductivity as a function of (x,z)(AGI, 2007). Finite element modeling was used with four nodes between each electrode. Neumann boundary conditions are applied at the surface while Dirichlet boundary conditions are used at the sides and base of the model (AGI, 2007). The partial differential equation is used to estimate the potential at each of the node locations. The forward model is solved using the Cholesky decomposition.

Inversion is an iterative process used to determine the subsurface ER distribution based upon gathered data and model parameters. It is used to reduce the data misfit between the field data and the calculated data in the model. In other words, inversion determines the resistivity model (predicted data) which best fits the measured field data. The root mean squared (RMS) error is used to describe the goodness of fit of the model (Eq. 17).

$$RMS = \sqrt{\frac{\sum_{i=1}^{n}\left(\frac{d_i^{Pred} - d_i^{Meas}}{d_i^{Meas}}\right)}{N}} \times 100\%, \quad 17$$

where N is the total measurements, d^{Pred} is predicted data, and d^{Meas} is the measured data. In general, an RMS of less the 5% is acceptable, between 5 and 10% is acceptable but questionable, and greater than 10% is unacceptable.

Four types of inversion methods are available in EarthImager: forward modeling only, damped least squares, smooth model inversion, and robust inversion. Damped least squares inversion attempts to minimize weighted misfit data. Smooth model inversion, commonly referred to as Occam's inversion, determines the smoothest model in which the model and data fit to an a-priori Chi-squared statistic (AGI, 2007). Robust inversion combines damped least squares and smooth inversion. Occam's inversion, the most common method, was used in this study. Once the inversion method is chosen, the stop criteria are chosen based on a number of iterations, RMS, or error reduction percent. The modeling and inversion are completed once one of the stop criteria is reached.

Once inversion and model settings are established, the model and inversion process can begin. The forward model and inversion process are performed by comparing the measured apparent resistivity pseudosection (Fig. 2.11A) to the calculated apparent resistivity pseudosection (Fig. 2.11B). The calculated apparent resistivity pseudosection is solved using Eq. 12. The inverted resistivity section is determined from the evaluation and transformation of the electric potential at each electrode location. The inverted resistivity section and the calculated apparent resistivity pseudosection is adjusted until it reaches an acceptable RMS value when compared to the measured apparent resistivity pseudosection or another stop criteria is reached.

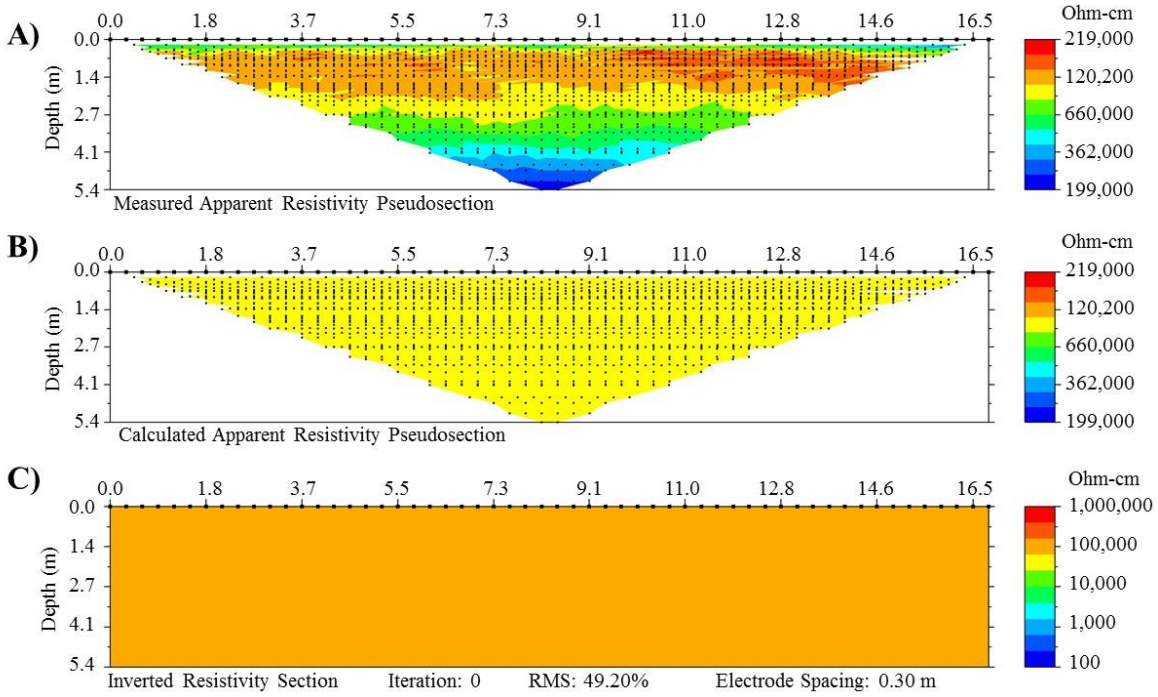

Fig. 2.11. Beginning of the computer modeling and inversion

2.1.5 Electrical Resistivity Imaging Applications

A variety of studies related to ER imaging have been conducted to characterize subsurface geology and in infrastructure investigation. ER is commonly used with other nondestructive testing methods such as ground penetrating radar (GPR), seismic reflection and refraction, and induced polarization (IP). However, two limiting features of these nondestructive testing methods include their inability to produce laboratory test specimens and the subjective nature in data interpretation. Therefore, drilling is typically used to gather a sample in order to verify the interpretation and to provide laboratory testing specimens. The following sections describe selected studies involving ER.

Subsurface Geology Characterization

One application of ER is to determine subsurface geology. Numerous studies of ER use have been conducted to determine subsurface geology for general site characterization, groundwater detection, and groundwater contamination. The following paragraphs introduce and discuss case studies involving ER imaging.

ER imaging, vertical electrical sounding (VES), and direct-push soil sampling were used in a shallow groundwater investigation in Benin, West Africa (McInnis et al., 2013). Prior research and numerical analysis indicated possible salinity movement into the coastal city's water supply; therefore, the source, extent, and movement of salt water had to be defined. ER imaging and VES surveys were used to verify variability of subsurface geology and delineate fresh and salt water interface for testing. Soil sampling was used to determine the possible source of salt water intrusion.

McInnis et al. (2013) utilized ER imaging in 18 test locations and a total of 24 tests. Each survey was approximately 120 m in length, electrodes were spaced at 5 m, and the use of the Wenner array achieved a depth of approximately 18 m. A few data points were taken using a potential electrode immediately after the electrode was used as a current electrode, thereby allowing data results to be bias due to polarization effects. VES is an ER imaging method in which a one-dimensional "borehole" of data is gathered instead of a two-dimensional profile view along the survey line. This testing consists of maintaining a constant center point of the survey and moving electrodes away from the center location. The Schlumberger array was used for 38 VES surveys, achieving a maximum depth of 60 m. Groundwater samples (121 samples) were collected using a manual direct-push drill and analyzed for chemical composition.

ER imaging and VES surveys identified the salt water intrusion front and provided locations from which water samples for testing should be gathered (Fig. 2.12). Laboratory analysis of the water samples concluded that the salt was ocean-based rather than due to human contamination. The study validated the use of ER with other nondestructive methods in order to locate and provide data for sampling of a shallow aquifer system.

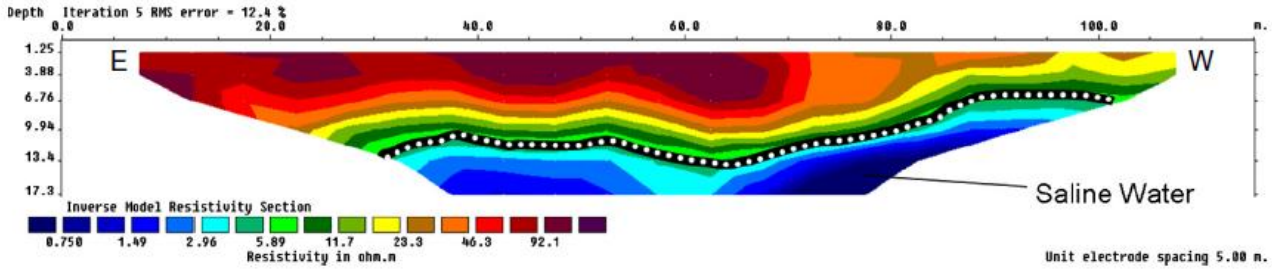

Fig. 2.12. ER image showing the boundary between fresh and saline water (McInnis et al., 2013)

The United States Geological Survey (USGS) performed a study in the Amargosa Desert in Nevada that utilized three ER methods (ER imaging, VES surveys, and capacitive coupled resistivity) to determine gravel layers thought to control contamination migration (Lucius et al., 2008). The site was an active chemical waste disposal with an inactive low-level radioactive waste area. Wells located around the landfill contained high levels of contamination in the form of water vapor. The local geology was dominantly sandy gravel material with a clay layer as a base. It was determined that the sandy gravel layer was the region in which contaminated water vapor was moving. The goals of the study were to determine continuity of the clay layer across the region, especially to the southwest due to groundwater flow from the northeast to the southwest, and to map the sandy gravel layer.

Lucius et al. (2008) used ER imaging VES, and capacitive coupled resistivity to map the interface across the site. ER imaging was used to develop five profiles ranging from 600 m to 1,150 m in length, with electrode spacing of 4 m or 5 m, using the inverse Schlumberger array (Lucius et al., 2008). VES surveys were performed at 54 locations using the Schlumberger array. Capacitive couple resistivity provides ER data by using alternating current and electrodes resting on metal plates instead of the traditional method in which electrodes are placed in the ground. Electrodes are towed behind an all-terrain vehicle and arranged in a dipole-dipole configuration. The process of the electric field passing from electrodes into the earth without direct contact is referred to as capacitive coupling and is advantageous due to its ability to inject current through the plate and into the ground rather than through a stake which must be hammered into the surface. Capacitive coupling was used around the perimeter of the site (four locations).

All three testing methods detected the two major layers (sandy gravel and clay) throughout the entire site and to the southwest. Results showed that the sandy gravel layer regressed to the southeast, thereby allowing successful mapping of the possible water vapor contaminant pathway (Fig. 2.13). In addition to the geophysical testing, drilling should be conducted to verify and quantify contamination transport in the previous study findings.

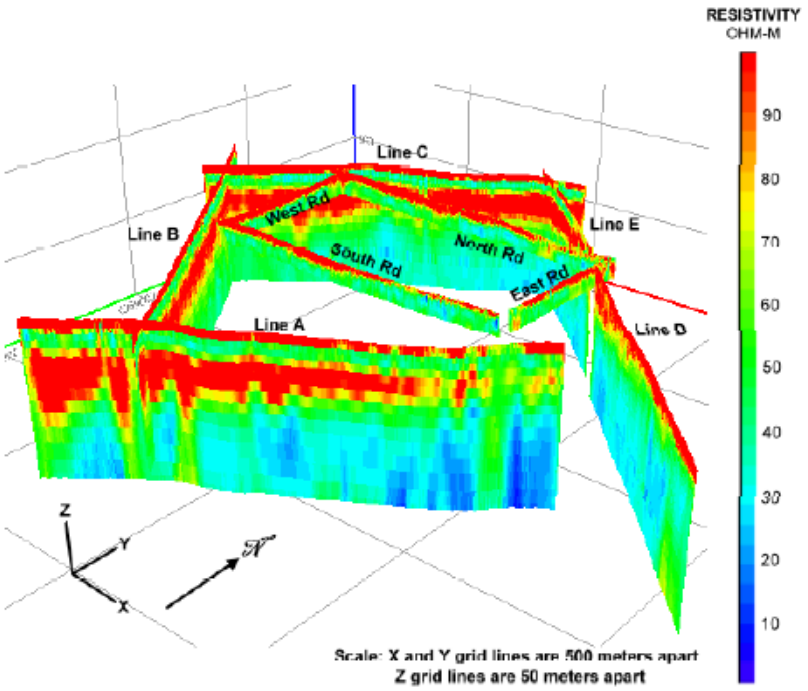

Fig. 2.13. 3D view of ER imaging and capacitive coupling testing (Lucius et al., 2008).

Infrastructure Investigation

ER imaging has recently been used in infrastructure investigation such as determining the depth of unknown bridge foundations, landfill investigations, and concrete assessments. Results of infrastructure investigations are typically known and any irregularities may indicate potential problems. The following sections introduce two infrastructure studies that describe the problem, method, and conclusions drawn from the study results.

A new landfill was being constructed near a preexisting landfill in southern Italy in the Apulia region. During initial construction, leachate was found. Drilling was an undesirable investigation technique because it could potentially cause a new leachate pathway through the borehole. Two ER methods were used to verify liner integrity and determine whether or not leachate had passed through the high-density polyethylene (HDPE) liner approximately 20m below the ground surface (De Carlo et al., 2013). They utilized three ER imaging lines that were approximately 235 m long with 5 m electrode spacing utilizing the Wenner-Schlumberger array, thereby providing sufficient depth of investigation. A second ER method, known as the mise-à-la-masse (MALM), was utilized to determine liners degradation. This survey uses two current

electrodes, one placed inside the landfill area and the other outside, to produce a voltage map that shows current pathways.

ER imaging results detected an irregular shape of a conductive zone (thought to be leachate) located 40 m below the ground surface, 20 m below the HDPE liner. As shown in Fig. 2.14, a funnel shape of lower resistivity formed beneath the HDPE liner thought to be leachate. MALM results, however, indicated that the liner was continuous. Irregularities in the results were attributed to leachate passing through the HDPE liner.

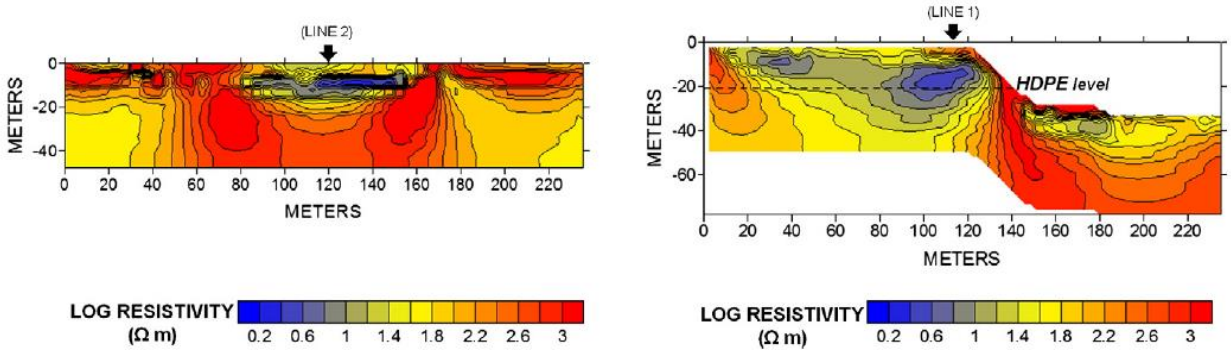

Fig. 2.14. ER imaging over the covered landfill (left) and over the covered landfill and into the excavation of the new landfill (right) (De Carlo et al., 2013).

In another infrastructure study, ER was successfully utilized to determine the depth of unknown foundation in which the original construction plans were inaccessible, leading to unreliable scour assessment. A study in Texas used ER imaging to identify the depths of unknown bridge foundations (Arjwech et al., 2013). This study utilized ER imaging and the dipole-dipole array with spacing variation dependent on the diameter of supporting piers and foundations. In general, spacing's ranged from 1 m to 1.5 m. Larger diameter piers required larger spacing due to the structure's tendency to be embedded deeper than smaller diameter piers. Arjwech et al. (2013) determined that ER applicability depends on the material in which the foundation is embedded; hard rock produced ER values similar to concrete, rendering the technique invalid as the foundation and geology were not distinguished.

The diameter of the drilled shaft imaged in the controlled setting increased with depth, which is not indicative of the actual shaft that has a constant diameter. Even though the test was unable to image the diameter of the pile accurately it was able determined that the foundation reached a depth greater than 5 m; a conservative depth for safe scour potential. Due to the success in

imaging pile depth in the controlled studies, ER imaging was applied to two bridges: a roadway bridge and a railway bridge. Each study consisted of two ER imaging lines: one line that followed the bridge span direction and the other line that was perpendicular to the bridge span. The roadway bridge used slender piles similar to that in the test in the controlled environment. As shown in Fig. 2.15, the slender nature of the piles was not imaged, but their depth was greater than the 5 m desired for safe scour potential. The railway bridge used a larger hexagonal foundation compared to the roadway bridge, and results showed that the foundation did not extend more than 4 m in depth (Fig. 2.16).

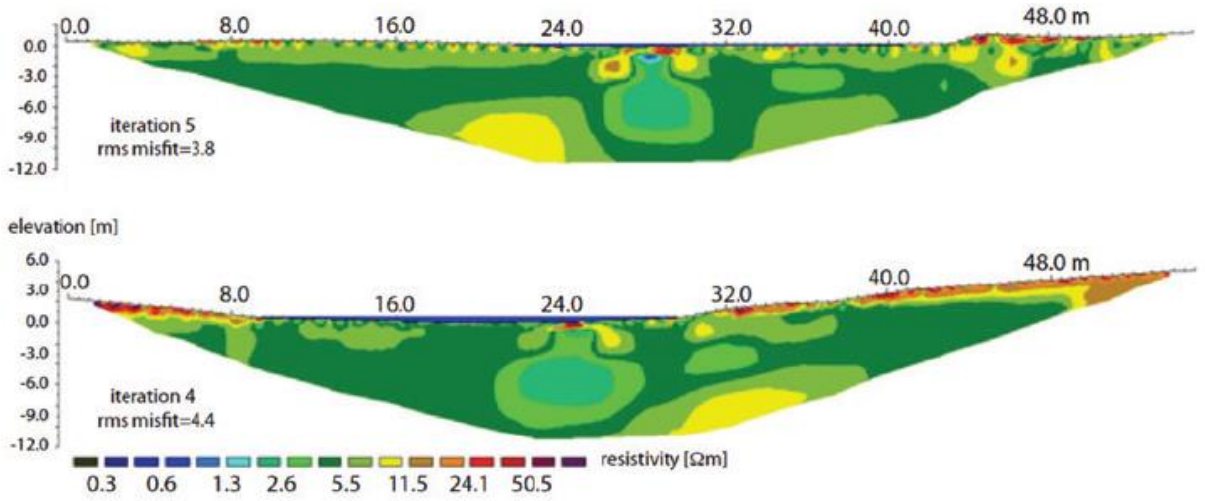

Fig. 2.15. Roadway bridge ER imaging results (Arjwech et al., 2013).

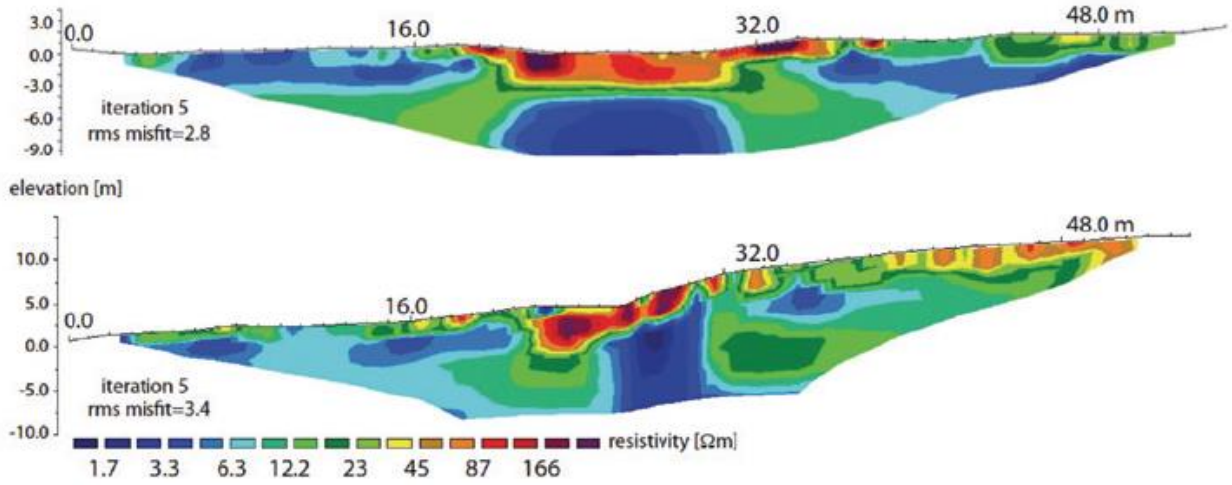

Fig. 2.16. Railway bridge ER imaging results (Arjwech et al., 2013)

2.1.6 Summary

As demonstrated in the previous studies, ER imaging is a valid nondestructive technique used in a variety of applications within the engineering field and is becoming increasingly popular. The technique may be used as a stand-alone method but is more valuable when used in conjunction with other nondestructive and drilling methods to verify ER imaging. ER imaging is an easy nondestructive testing method with respect to its setup procedure, automated system, and data processing with provided software.

2.2 Mechanically Stabilized Earthen Retaining Walls

Retaining walls are common structures with applications for transportation infrastructure, water retention, and residential and commercial building industries. Retaining walls are used in areas in which elevation changes sharply in a confined area. Various retaining wall designs include cantilever (Fig. 2.17A), piles (Fig. 2.17B), gravity structures (Fig. 2.17C), and mechanically stabilized earthen (MSE) retaining walls (Fig. 2.17D).

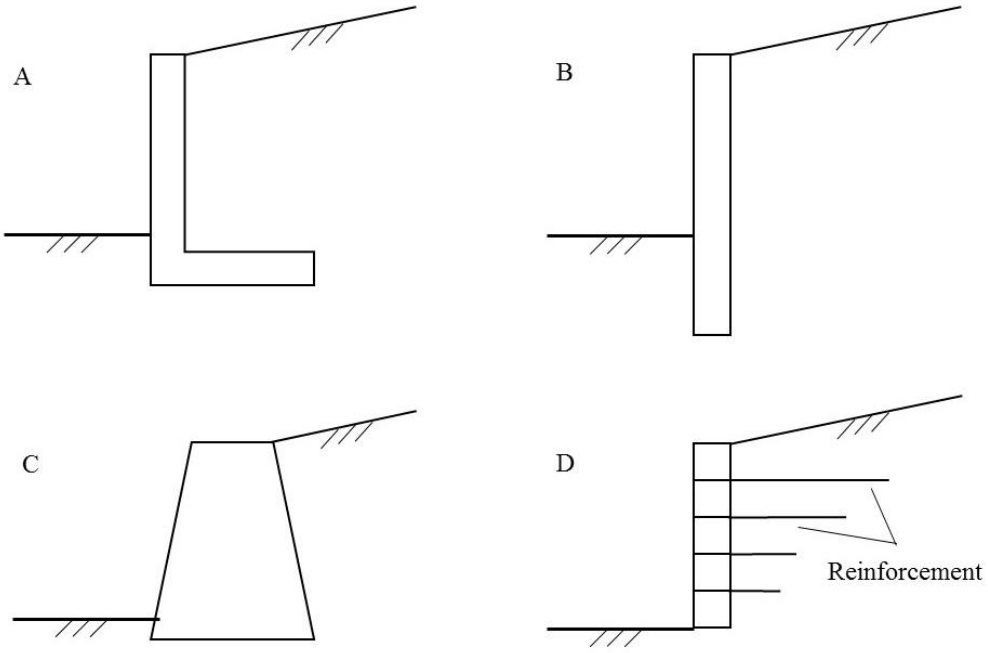

Fig. 2.17. Common retaining walls

MSE walls, introduced into the United States in the 1970s, are becoming increasingly popular because they are less expensive, have high structural capacity, and can be much larger than the traditional walls (Armour et al., 2004). The disadvantage of MSE walls, though, is that they are complex to construct, thereby increasing labor required to add reinforcement and compaction between each layer. However, the advantages of MSE walls outweigh the few disadvantages.

MSE retaining walls can be constructed many ways and will contain three main elements; the face, reinforcement, and backfill (Fig. 2.18). Although MSE walls may appear to have a solid-face, a majority of MSE walls are comprised of modular blocks or panels. MSE walls contain reinforcement that attaches to the wall and extends into the compacted backfill material. This

reinforcement joins the wall to the soil, increasing system strength by providing an anchor and advantageously utilizing the weight of the soil and other properties to support the wall. Typical reinforcements are galvanized steel strips or geosynthetics mesh structure. Geosynthetics are man-made polymer based material used to assist in stabilizing structures and slopes. Reinforcement degradation over time is a concern for the walls stability since the reinforcement supports the wall. Corrosion of metal reinforcement reduces the strength of the reinforcement causing many failures, as discussed later. Advancements in geosynthetics technology have helped reduce failures due to corrosion as geosynthetics are not vulnerable to corrosion.

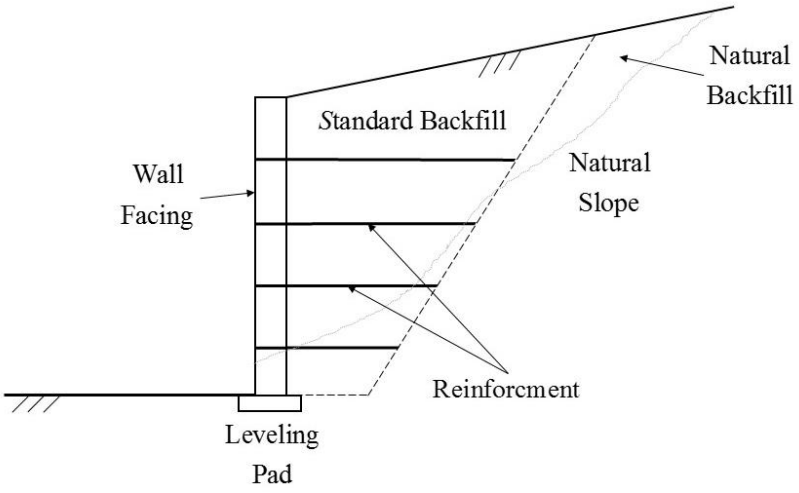

Fig. 2.18. Typical MSE wall attributes.

Another essential feature of any retaining wall is the backfill material. Free-draining material is ideal as backfill material in order to decrease the potential of hydro-static pressure buildup, a leading cause of retaining wall failures. The backfills material should be analyzed to determine its properties, specifically the corrosion potential. The following section outlines current laboratory tests and construction specifications for the backfill materials.

2.2.1 Current Testing and Construction Quality Assurance Practices

AASHTO, ASTM, FHWA, and state DOTs, have developed guidelines, standards, testing procedures, and CQA practices for retaining wall backfill materials. Current MSE wall construction testing and practices are primarily laboratory analyses with limited in-situ investigation. Field observations and inspections by an engineer are the only current in-situ

testing procedures. The following paragraphs outline current laboratory tests and field techniques for retaining walls.

2.2.2 American Association of State Highway and Transportation Officials

AASHTO has developed and published specifications and testing (field and laboratory) procedures primarily to be used in transportation infrastructure construction. AASHTO has developed a test that may be used for MSE wall backfill referred to as the "AASHTO Standard Method of Test for Determining Minimum Laboratory Soil Resistivity" (T 288-12). In addition to AASHTO method T 288-12 and other applicable test procedures, AASHTO has also published specifications and guidelines for MSE retaining wall construction.

AASHTO method T 288-12 determines ER of a soil sample which is an indicator of its corrosion potential. The test can also identity the soil conditions that may accelerate metal corrosion in an MSE wall or underground metallic elements. It involves gathering a sample from the borrow material and determining minimum soil resistivity through laboratory testing. The sample is pulverized to pass a 2 mm sieve (No. 10) and mixed with distilled water. After the soil has been cured for 12 hours, it is remixed thoroughly and compacted into layers in a soil box (two box sizes outlined in the standard). The soil box contains two electrodes at opposite ends that are connected to a resistivity meter. Resistance is measured between two electrodes and soil resistivity is calculated. After the test is completed, the soil is removed, water is added to the soil, remixed, placed back into the box, and another measurement is taken. Measurements are repeated until a minimum soil resistivity value is obtained. The relationship of resistivity and corrosion is discussed in Section 2.2.3: Soil Corrosion. AASHTO is a major implementer of CQA practices and testing procedures, but there is still a need of in-situ testing methods. Fig. 2.19 depicts the AASHTO method T 288-12.

Fig. 2.19. AASHTO method T 288-12 (Reinforced Earth,).

American Society of Testing and Materials

ASTM has also produced standards and specifications, such as the "Standard Test Method for Measurement of Soil Resistivity Using the Two-Electrode Soil Box Method (G157-12a)." This test determines soil resistivity to predict corrosion potential and is a laboratory analysis method that is commonly paired with the in-situ test method, "Standard Test Method for Field Measurement of Soil Resistivity Using the Wenner Four-Electrode Method" (G 57-06). Both tests are outlined in the following paragraphs.

ASTM standard test G 157-12a is similar to the AASHTO method T 288-12 test in that it requires a soil sample to be wetted and placed in box with specific dimensions outlined in the standard with the ability to connect a resistivity meter. Water is added, the soil is remixed, and resistance is again measured until a minimum measurement is recorded. The ASTM standard does not require material sieving nor directly comment on soil types appropriate for testing. The

only recommendation mentioned for the test sample is the removal of "foreign material such as gravel, small stones, roots, twigs, and so forth" (ASTM, 2012), possibly implying that the testing method is not suitable for coarse aggregate backfill material.

ASTM has also published the "Standard Test Method for Field Measurement of Soil Resistivity Using the Wenner Four-Electrode Method (G 57-06)." This test method measures soil resistivity to determine the expected corrosion rate and design protection of buried structures (ASTM, 2006). This test method is one of the few in-situ testing methods for soil corrosion, but provides no information in regards to its use on MSE wall backfill or its use in coarse aggregate material. Similar to AASHTO, no in-situ testing methods currently exist specifically for coarse backfill material of an MSE wall.

Federal Highway Administration

FHWA has developed many detailed standards and guidelines that outline construction of MSE walls, including documents such as "Design and Construction of Mechanically Stabilized Earth Walls and Reinforced Soil Slopes Volume I and II" and "Corrosion/Degradation of Soil Reinforcements for Mechanically Stabilized Earth Walls and Reinforced Soil Slopes" (FHWA, 2015). These documents provide information regarding the design process and construction practices of MSE walls. The following paragraphs outline backfill standards and testing procedures for corrosion and in-situ testing methods.

The "Corrosion/Degradation of Soil Reinforcements for Mechanically Stabilized Earth Walls and Reinforced Soil Slopes" document describes methods that may be used to prevent corrosion and outlines testing methods and specifications that should be considered for MSE wall construction. The report recommends specific backfill material properties when using metal reinforcement, as shown in Table 2.1.

Table 2.1 Recommended testing methods and standards of MSE wall back fill material (Elias et al., 2009)

Attribute	Recommended Value	Test Method
Electrical Resistivity	> 3,000 Ohm-cm*	AASHTO T-288
pH	5 to 10	AASHTO T-289
Organic Content	Max 1%	AASHTO T-267
Chlorides	< 100 PPM	ASTM D4327
Sulfates	< 200 PPM	ASTM D4327

*Minimum resistivity value for metal reinforcement

FHWA also provides monitoring methods of metal reinforced MSE walls. One method is the retrieval of coupons. These coupons, which are reinforcement materials placed during construction with access during post-construction, are removed and analyzed for degradation (Elias et al., 2009). Their degradation relates to the corrosion within the wall. However, removal of coupons does not affect the stability of the wall. This methods requires installation during construction to monitor the wall. FHWA has significantly contributed to the policy and testing methods of MSE walls. But, no in-situ non-destructive testing method has yet been developed.

Kansas Department of Transportation

Each state DOT has their own standards that closely adhere to those outlined by AASHTO, ASTM, and FHWA. Because this study was performed in the state of Kansas and the project was sponsored by KDOT (only KDOT guidelines and CQA procedures for backfill material are included). Specifications may be found on KDOT's website (http://www.ksdot.org/hwycont.asp) in the "Specifications and Manuals" section.

KDOT's "Bridge Construction Manual", "Geotechnical Manual", and the "Construction Manual" provide information regarding materials to be used in MSE retaining wall construction, required laboratory testing, the factor of safety required for design, and more. These manuals are similar to the FHWA manuals with slight variations.

The "Geotechnical Manual" recommends the use of either well or poorly-graded gravel or sands that contain less than 15% fines or the material passing the No. 40 sieve (KDOT, 2007). FHWA makes no specific recommendation in regards to the material that may be used as backfill

material. KDOT “Geotechnical Manual”, the “Construction Manual” requires the use of sand or coarse aggregate material but also provides aggregate testing procedures and standards similar to those provided by FHWA, as outlined in Table 2.1. However, KDOT provides guidelines for little field testing procedures in their manuals.

As discussed, limited in-situ testing procedures and laboratory methods currently exist for backfill material of an MSE wall. AASHTO method T 288-12 requires using the minimum soil ER value obtained once the sample becomes a slurry mix from the addition of water. This is not indicative of materials used in MSE walls constructed by KDOT as most are constructed with free-draining coarse aggregates; water is typically not present. AASHTO method T 288-12 also requires the material to pass through a No 10 (2 mm) sieve essentially excludes coarse aggregates. Thus though this study and a complimentary study of AASHTO method T 288-12, new laboratory and field testing procedures may be developed.

2.2.3 Soil Corrosion

Reinforcement of MSE walls can either be metal or geosynthetic material. Metal is used at times because it is less expensive than geosynthetics. However, metal is a corrosive material and this has caused many failures of MSE walls. Recent advancements of geosynthetics have decreased the use of metals as MSE wall reinforcement. Despite the lack of corrosion potential in a geosynthetics, many agencies still prefer metal reinforcement.

Corrosion is the degradation of metals through environmental electrochemical reactions and is the process of the metals returning to their natural state. Moisture that penetrates the soil typically contains dissolved compounds, resulting in an acidic environment and providing an electrolyte in the soil. The presence of these electrolytes cause voltage differences between the metal and the soil allow natural current to flow between the two materials (Elias et al., 2009). The current flows from the anode (metal) to the cathode (soil and electrolyte) and back again to the anode completing the circuit. Due to the loss of metal ions to the electrolyte, the metal becomes corroded (Elias et al., 2009).

Tests discussed in the previous sections require soil material to be tested for resistivity. As stated in the ASTM Standard G 187-12, high resistivity values of soil typically result in a low corrosive environment, while low resistivity values are typically indicative of a highly corrosive environment. Lower resistivity values, indicative of finer-grained material, correlate to higher

corrosive values due to typically the increase of particle contact allowing for the flow of current and also the retention of water, the electrolyte. Table 1.2 showed the range of resistivity values for potential corrosion.

2.2.4 Corrosion Studies of Mechanically Stabilized Earth Retaining Wall Reinforcement

Many studies have investigated corrosion of metal reinforcement of MSE walls prior to complete catastrophic wall failure. The following paragraphs describe selected investigations performed on failing MSE walls.

Corrosion Effect on MSE Retaining Walls

A case study in Nevada examined preexisting MSE wall reinforcements thought to have been affected by corrosion. The reinforcement corrosion was accidentally discovered in two MSE walls, leading to uncertainty with the remaining MSE walls within the State of Nevada. Corrosion of reinforcement of one wall was found during construction of an additional sound-wall above the preexisting wall. The corrosion of the reinforcement of the second wall was found during demolition of a small portion of the wall for an expansion project (Thornley and Siddharthan, 2010).

Reinforcement and backfill samples were taken directly from the walls and tested. Both walls were well documented during construction, and each wall had test results for the Nevada test method. This test measures conductivity of water from a saturated soil solution with reinforced fill, which is different from the AASHTO T 288-12 test (Thornley and Siddharthan, 2010). Statistical analysis of metal loss was performed on the corroded reinforcement based on the original diameters (Thornley and Siddharthan, 2010).

Test results showed that the Nevada T 235B (which classified the material as only moderately corrosive) underestimated the corrosion potential of the backfill material compared to the AASHTO T 288-12 (which classified the material as highly corrosive). A statistical analysis of the corrosion and also a model used to determine the behavior of the MSE wall under static and seismic loading conditions showed results that the walls were unable to retain stability for the designed life of 75 years (Thornley and Siddharthan, 2010). Fortunately, the state of

Nevada identified the corrosion and design issues and took corrective action prior to catastrophic wall failures.

MSE Wall Repair due to Reinforcement Corrosion

In 2002, six panels failed at the base of a MSE wall designed and constructed in 1978 (Armour et al., 2004). The wall was part of an overpass structure over a railroad in Soda Springs, Idaho. Upon visual inspection, the metal reinforcement was determined to have experienced severe corrosion, thereby causing the failure. Reinforcement strength decreased from the degradation, causing panels to detach from the face of the wall. Due to unstable conditions caused by the initial failure, additional panels began to fail, ending when the surrounding reinforcement formed an arch-shaped support and the failure was stabilized. Approximately 15 m^3 of material fell from the wall. Laboratory testing was performed on the backfill materials to determine the reason for the accelerated corrosion rate of the reinforcement. According to AASHTO standards and the Idaho DOT standards, the backfill material was classified as very corrosive. Remediation of the MSE wall consisted of the installation of soldier piles, rock anchors, and reinforced shotcrete pilasters at each soldier pile in order to support the wall.

2.2.5 Summary

As seen in the previous case studies, reinforcement corrosion is a concern when constructing an MSE wall. Many testing procedures may be utilized to prevent these failures, but the majority of testing procedures are laboratory-based. Visual inspections and engineering judgment are the only known field methods currently used for MSE wall construction quality assurance practices.

Chapter 3 Experimentation

3.1 Introduction

This chapter describes ER imaging equipment used in the study and the ER imaging field procedure. Software used to analyze the data is introduced, including a brief explanation of the modeling process. Finally, the five testing locations, with ER imaging results presented by date at each MSE wall are described.

3.2 Equipment and Software

ER data were collected using the SuperSting Earth Resistivity, IP & SP System (SuperSting) produced by Advance Geosciences Inc. (AGI) (Fig. 3.1a). The SuperSting can take up to eight potential readings simultaneously per each current injection. The system is powered by two 12-volt direct current batteries (used in this study) or electric generators. AGI provided the electrodes used for ER imaging in this research. Fourteen cables of four electrodes per cable (total of 56 electrodes) were used. The electrodes were spaced at maximum distances of approximately 2.7 m (Fig. 3.1b), and they were attached to stainless steel electrodes that were 46 cm long and 2.2 cm in diameter. The electrode stakes are hammered into the ground and the electrodes are connected by a spring attachment (Fig. 3.1c).

Prior to performing an ER imaging survey, a command file must be uploaded to the SuperSting. This command file informs the SuperSting regarding the sequence in which the electrodes will be used to inject current and which electrodes will be used to measure the voltage potential difference. Administrator software provides general information about the anticipated depth of the survey, data density and coverage, and the time estimation for the duration of the test. Once the command file is created, it is transferred to the SuperSting and ready to be used in the field.

Arrays used in this test were chosen based on time of the test and vertical resolution of data. All tests were performed on active construction sites, and limiting total time required for testing was critical since construction typically was stopped during testing. Vertical resolution was essential to determine the interface between the native material and the base of the MSE wall. Two traditional arrays discussed in Chapter 2 were considered for this study: the dipole-dipole and inverse Schlumberger arrays. The Wenner array was originally investigated but not used

further because the array provides limited vertical resolution and extended testing time (over 1 hour and 15 minutes). The dipole-dipole array was used during early stages of testing because the array provides lateral and vertical resolution in less time than other arrays (approximately 1 hour). Ultimately, the inverted Schlumberger array was used exclusively because the array provided optimum vertical resolution in 30 minutes.

Stainless steel electrode stakes were hammered in the ground at desired equal distance spacing, measured with a tape measure along a straight line on the surface. The stakes were driven into the ground as deep as possible, thereby increasing contact between the stake and ground in order to minimize contact resistance, as discussed in the following paragraphs. The cables were attached to stainless steel electrodes stakes by a spring attachment. The SuperSting was attached at the middle of the testing line. Fig. 3.1d shows a typical field setup.

One 3D test was performed, but due to increased testing time (3 hours) and no additional gain of useful data; 3D testing was not used further. As stated in Chapter 2, survey depth depends on the array used and electrode spacing; in general, the larger the spacing, the greater the depth of investigation. An approximation for investigation depth is seven times the electrode spacing for the inverted Schlumberger array: one meter electrode spacing would generate a survey with a depth of approximately seven meters. The most efficient method for testing MSE walls is to test the entire height of the wall and reach a depth in which the native material below the foundation of the wall is imaged.

a)

b)

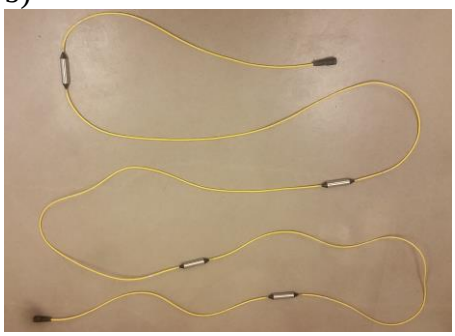

c)

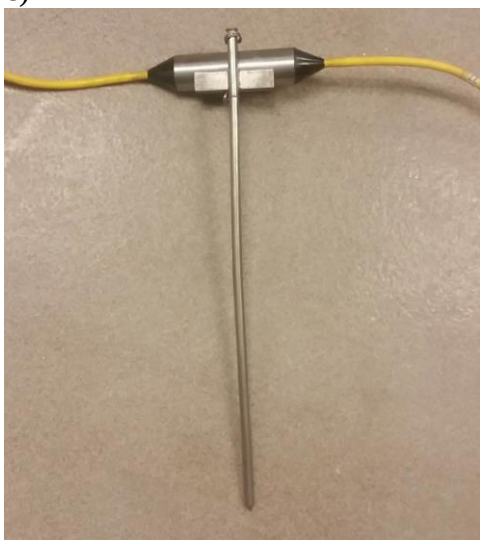

d)

Fig. 3.1. (a) SuperSting, (b) cable (yellow) connecting four electrodes (silver) with adapters at the end to connect to another cable (black), (c) stainless steel electrode setup, and (d) equipment setup in the field

After completing the setup, the contact resistance test was performed to verify that the cables were connected and the electrodes connected to the electrode stakes. An error such as *HVOVL* typically indicates poor contact between the electrode and the ground. An *INOVL* error indicates a loose or improper connection. An issue with testing coarse aggregates is the difficulty obtaining proper contact between the electrode stake and the aggregates. The coarse angular aggregates do not contact the electrode stake as well as the fine-grained soil. Fig. 3.2 shows the correlation of injected current and contact resistance. A lower contact resistance leads to an increased amount of current injected into the ground. The stronger the current signal, the more

accurate the measurement. Trends of lower RMS values with decreased contact resistance are discussed later.

The contact resistance test performed prior to ER imaging was vital in this study. A contact resistance between 0 and 20,000 Ohm provides adequate results with little noise (RMS values below 10%), data becomes uncertain and noisy between 20,000 to 40,000 Ohm (RMS around 10% typically), and more than 40,000 Ohm results in unusable data of poor quality (RMS greater than 10% typically). The larger the contact resistance, the lower the amount of injected current and the more inaccurate and noisy the measurement and vice versa.

Several techniques can improve the contact between the electrodes and the contact materials. Water, preferably salt water, may be added around electrodes to increase contact. However, this method was not investigated in this study because the aggregates were free-draining materials, (a material that prevents water from being retained around the electrodes) and cause water to seep into the wall, creating preferential current pathways and erroneous ER measurements. A second method to improve the contact between electrodes and the ground is the installation of a second stainless steel electrode in contact with the electrode that demonstrates high contact resistance. The second stainless steel electrode increases the surface area in contact with the ground, thus allowing increased injection of current. Adding a second electrode was used in this study, but it had very little impact on reducing the contact resistance test results. The final method includes compacting the material around the electrode with a hammer, thereby increasing the contact between the electrode and the ground. However, this method provided little improvement in lowering the contact resistance test when used in this study. Therefore it was determined if results of the contact resistance test are high (greater than 40,000 Ohm) the entire ER imaging survey should be moved to an area that has recently been compacted as these regions of recent compaction provided better contact between the aggregate and the electrode stakes. Fig. 3.2 shows the correlation of the injected current and the contact resistance at multiple testing locations.

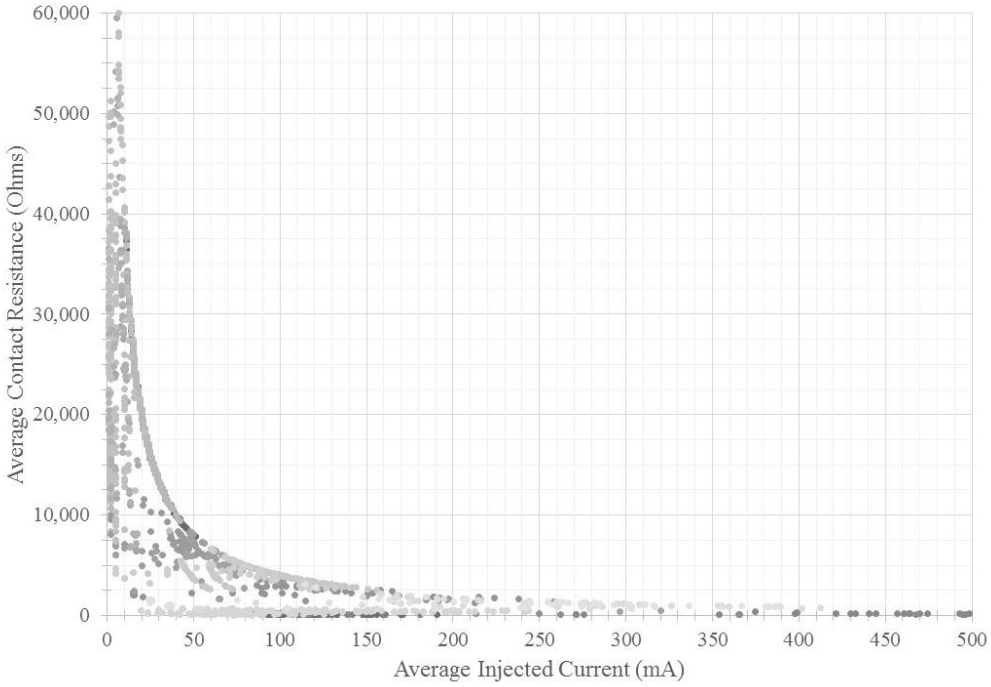

Fig. 3.2. Correlation of average injected current and average contact resistance.

Once appropriate contact resistance was achieved in this study, data were collected for the survey. After completion of the ER imaging survey, data were processed using AGI EarthImager 2D Version 2.4.0 software. Data removal criterion was set to remove negative values, measurements in which the injected current or measured voltage was too small to obtain an accurate reading or extreme irregular spikes were present in the data. The percentage of noise was estimated due to the limited contact between the electrode stakes and the ground increasing the noise in the testing. Estimation of large amounts of noise leads to over-smoothening of the data in the inversion, while under-estimation may produce artifacts due to the inversion trying to fit the noisy data (LaBrecque et al., 1996). The smooth model, commonly referred to as Occam's inversion, was used with the finite element model response in this study. The finite element model mesh consisted of four blocks between two electrodes, with Neumann boundary conditions at the surface and Dirichlet boundary conditions applied at the sides and base of the model. Once the desired settings were applied, the inversion and forward modeling begin. Quality of the data is based upon the RMS from the inversion. The RMS is the measure of the misfit between the calculated and the measured apparent resistivity's. The lower the RMS and lower contact resistance test, the better quality the data (RMS of 0% to 5% and contact resistance of 0-20,000Ohm). Lesser quality data (RMS of 6% to 10% and contact resistance of 20,000-

40,000 Ohm) implies that the data misfit has increased due to possible mathematical artifacts and/or the prediction of ER that is not representative of aggregate. Detailed information of data processing has been outlined in Section 2.1.4.

3.3 Electrical Resistivity Imaging Data

Five walls were designated by KDOT for testing: four MSE walls and one gravity retaining wall. The gravity retaining wall, located in Lawrence, Kansas, near the intersection of Haskell Ave. and East 31st Street, is part of the South Lawrence Trafficway Project (Fig. 3.3 "Gravity Wall"). Three of the four tested MSE walls contained geosynthetic reinforcement and one wall contained metal reinforcement. The metal-reinforced MSE wall is located at the interchange of Kansas Highway 10 and Ridgeview in Lenexa, Kansas (Fig. 3.3 "Metal Wall"). One geosynthetic wall is located northwest of Bonner Springs, Kansas, at the overpass of 118th Street and Interstate 70 (Fig. 3.3 "Geosynthetic Wall 1"). Another geosynthetic wall is located north of Bonner Springs, Kansas, at the interchange of US Route 73 and Interstate 70 (Fig. 3.3 "Geosynthetic Wall 2"). The final geosynthetic wall is located in Pittsburg, Kansas, near the intersection of South Broadway Street and Centennial Drive (Fig. 3.3 "Geosynthetic Wall 3"). The following sections describe each site and present ER imaging data.

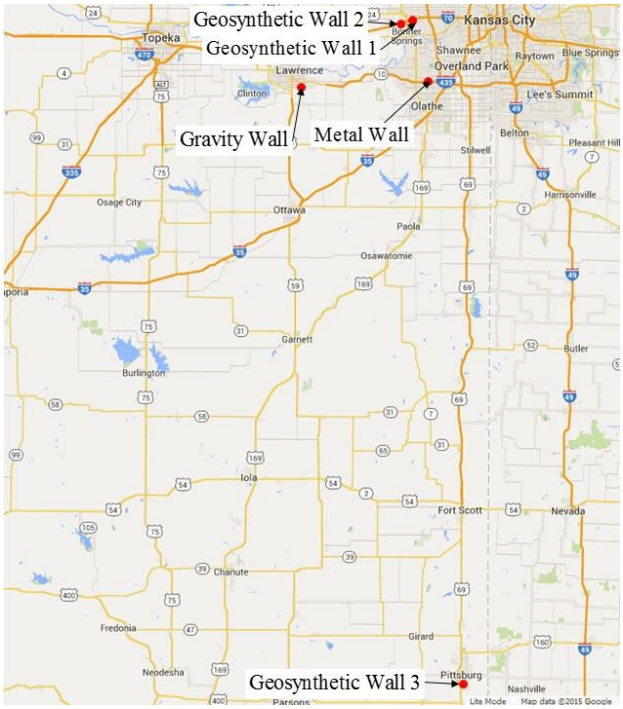

Fig. 3.3. Wall locations (Google Maps, 2013).

3.3.1 Geosynthetic Wall 1: Interchange of US Route 73 and Interstate 70

An MSE wall was built at the interchange of US Route 73 (US73), also referred to as Kansas Highway 7 (K7), and Interstate 70 (I70). The interchange was reconstructed for traffic flow, and the MSE wall was constructed to support the ramp structure. The site is located approximately 23 km west of Kansas City, Kansas. Compaction equipment was used from the face of the wall to 1.5-3.0 m from the face. Heavier compaction equipment and truck traffic were allowed 3.0 m and further from the face of the wall. Attributes of the wall are outlined in Table 3.1. This wall was tested on the following dates in 2014: June 18, June 20, July 9, and August 12.

Table 3.1. Characteristics of MSE wall located at US73 and I70.

Attribute	Value
Length	353.6 m
Height	1.5-11.0 m
Reinforcement	Geogrid
Backfill Resistivity*	3,808 Ohm-cm

*Source KDOT

Two tests were performed on June 18, 2014. Each test used the dipole-dipole array because of the array's ability to provide lateral resolution of data with depth and minimal noise. Both tests were in a region of the wall with no surface elevation change. Heavy-compaction equipment and truck traffic for placing backfill material were allowed in this region of the wall. Table 3.2 outlines characteristics of Test 1 followed by a resistivity profile in Fig. 3.4.

Table 3.2. Characteristics of Test 1.

Attribute	Value
Wall Height	9.1 m
Distance from Walls Face	9.1 m
Electrode Spacing	0.3 m
Array	Dipole-dipole
Average Contact Resistance	Data not found
Data Removed	0.8%
RMS	4.7%
Number of Iterations	6
Noise Estimation	5.0%

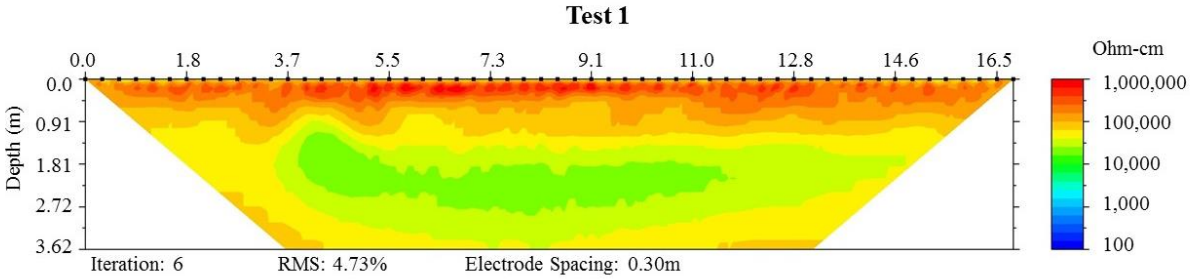

Fig. 3.4. Test 1 inverted resistivity profile.

The test imaged a depth of 3.6 m, but was unable to image the full height of the wall due to limited spacing of electrodes. The profile in Fig. 5 depicts an ER within the range of a noncorrosive gravel material. High surface resistivity values were attributed to insufficient contact between the electrode stakes and gravel backfill. Decreased resistivity at depths of 1.4-2.7 m was possibly due to increased compaction within this region or a region in which finer material was present. Increasing compaction or utilizing finer-grained material decreases resistivity due to a decrease in the void space. However, the relationship between compaction and ER is outside the scope of this project.

The starting electrode of the second test coincided with the starting electrode of Test 1, but electrode spacing of Test 2 was greater than Test 1. Characteristics of Test 2 are outlined in Table 3.3. Test 2 experienced two inversions due to the high RMS value in the first inversion. Prior to the start of the second inversion, additional data were removed based on the data misfit. The inverted resistivity section of Test 2 is depicted in Fig. 3.5.

Table 3.3. Characteristics of Test 2.

Attribute	Value
Wall Height	9.1 m
Distance from Wall's Face	9.1 m
Electrode Spacing	0.9 m
Array	Dipole-dipole
Average Contact Resistance	Test was not found
Number of Inversions	2
Data Removed (1st Inversion)	5.5%
RMS (1st Inversion)	9.2%
Number of Iterations (1st Inversion)	8
Data Removed (2nd Inversion)	3.1%
RMS (2nd Inversion)	7.1%
Number of Iterations (2nd Inversion)	5
Noise Estimation	8.0%

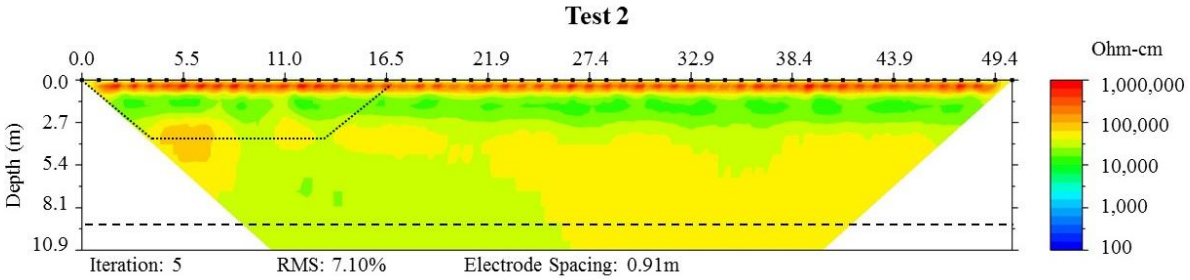

Fig. 3.5. Test 2 inverted resistivity profile with Test 1 represented in dashed lines and the base of the wall located at approximately 9.1 m.

ER values were representative of a mildly to noncorrosive gravel material. The high ER values near the ground surface and the lower resistivity region between 1.0 and 2.7 m were also observed in Test 1. The band of decreased ER between 1.0 and 2.7 m was continuous throughout the profile, possibly due to increased compaction or integration of finer material during construction. The region from 2 m to the base of the profile depicted a uniform ER inverted section with regions of low and high ER values. Low ER regions (dark to light green/yellow) were attributed to finer-grained material or increased compaction, while high ER regions (dark yellow to red) may be due to coarser material or decreased compaction. The test was unable to image native material below the wall at approximately 9.1 m of depth.

Test 3, completed on June 20, was conducted closer to the wall's face compared to testing performed on June 18. The test was located where compaction equipment changed from light-compaction units to heavy-compaction equipment. Unloading truck traffic for fill placement (which would increase compaction) was not allowed in this region, and no surface elevation change was present within the testing area. The dipole-dipole extension array was used to provide more data points than the dipole-dipole array because it utilizes more combinations of current and potential electrodes (repeating measurements). However, the testing time increased to over one hour. Test characteristics are outlined in Table 3.4, and a resistivity inverted section is represented in Fig. 3.6.

Table 3.4. Characteristics of Test 3.

Attribute	Value
Wall Height	9.1 m
Distance from Wall's Face	2.1 m
Electrode Spacing	1.2 m
Array	Dipole-dipole extension
Average Contact Resistance	20,000 Ohm
Number of Inversions	2
Data Removed (1st Inversion)	3.4%
RMS (1st Inversion)	7.5%
Number of Iterations (1st Inversion)	5
Data Removed (2nd Inversion)	5.6%
RMS (2nd Inversion)	6.0%
Number of Iterations (2nd Inversion)	4
Noise Estimation	8.0%

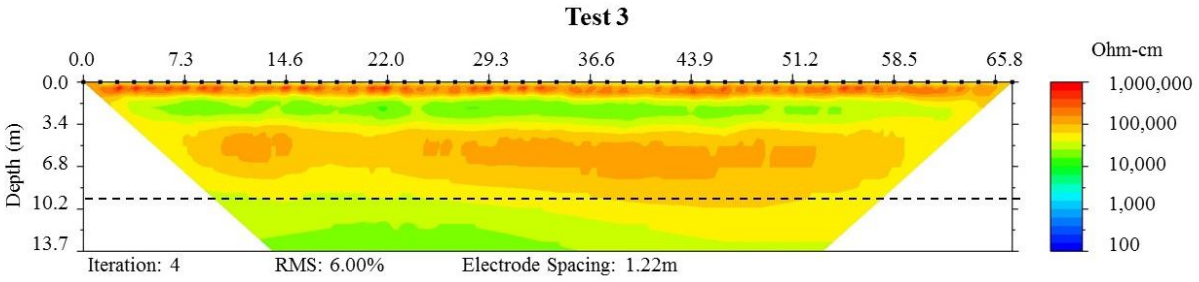

Fig. 3.6. Test 3 inverted resistivity profile with approximate base of wall at 9.1 m.

A contact resistance average of 20,000 Ohm showed that contact between electrodes and the ground was moderate, resulting in an acceptable RMS value of 6.0%. As in Tests 2 and 3, high

resistivity was observed near the ground surface due to contact between the electrodes and ground. Decreased resistivity values were also observed at depths of 1-2.5 m. Overall resistivity of the wall was higher than Test 1 and Test 3, with an approximate average of 70,000 Ohm-cm; classified as a noncorrosive aggregate. The increased values may be due to prevention of heavy-compaction equipment and unloading truck traffic within this region. Test 3 imaged the complete height of the wall (bottom shown as dashed lines) and part of the native material, as shown in the lower left portion of the profile in which ER decreased below 10,000 Ohm-cm.

The third site visit was on July 9. The testing location was moved to a different section of the wall due to active construction at the previous testing locations. The height of the wall varied from approximately 4.0-6.0 m, but no surface elevation change was present. This test was conducted near the interface where light-compaction and heavy-compaction equipment were used. The inverse Schlumberger array was used instead of the dipole-dipole array in order to increase vertical resolution. Attributes of Test 4 are depicted in Table 3.5, followed by a resistivity inverted section in Fig. 3.7.

Table 3.5. Characteristics of Test 4.

Attribute	Value
Wall Height	4.5-6.0 m
Distance from Wall's Face	3.1 m
Electrode Spacing	0.6 m
Array	Inverse Schlumberger
Average Contact Resistance	8,000 Ohm
Number of Inversions	2
Data Removed (1st Inversion)	0.3%
RMS (1st Inversion)	6.6%
Number of Iterations (1st Inversion)	8
Data Removed (2nd Inversion)	3.0%
RMS (2nd Inversion)	3.5%
Number of Iterations (2nd Inversion)	4
Noise Estimation	5.0%

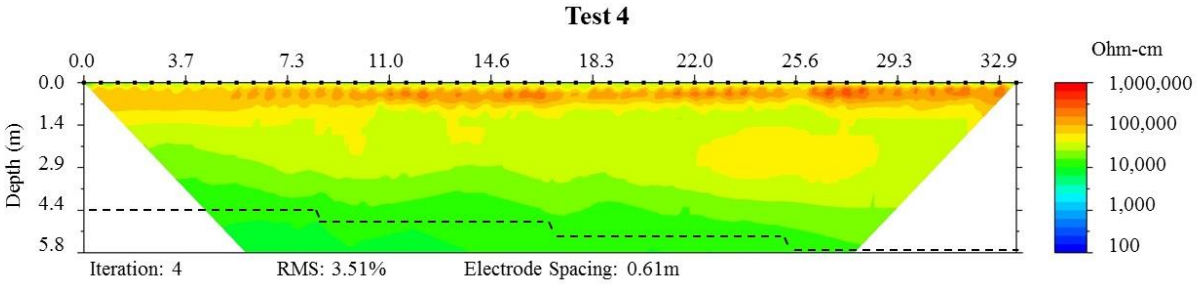

Fig. 3.7. Test 4 inverted resistivity profile with approximate base of the wall.

The contact resistance test depicted low contact resistance between gravel material and electrode stakes, resulting in a decreased RMS value; however, ER values at the surface were high. The profile in Fig. 8 depicts a uniform ER profile of the wall representing a mildly to noncorrosive aggregate, similar to previous tests. Test 4 imaged the full height of the wall and detected native material below the wall where values decreased to below 10,000 Ohm-cm.

The final test was performed on August 12 (Test 5). The testing location returned to the original testing area, and the wall was at its final height of 11.0 m. The test was again at the interface of light and heavy-compaction equipment and truck traffic was prohibited. Table 3.6 outlines attributes of Test 5, followed by the inverted resistivity section in Fig. 3.8.

Table 3.6. Characteristics of Test 5.

Attribute	Value
Wall Height	11.0 m
Distance from Wall's Face	3.1 m
Electrode Spacing	0.9 m
Array	Inverse Schlumberger
Average Contact Resistance	4,500 Ohm
Data Removed	0.1%
RMS	3.6%
Number of Iterations	2
Noise Estimation	5.0%

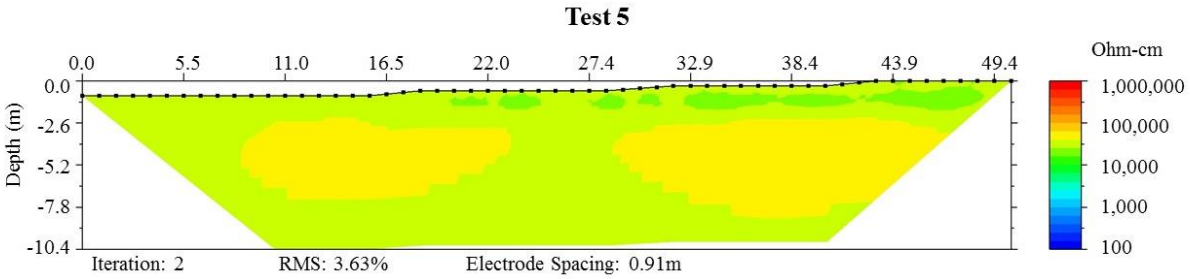

Fig. 3.8. Test 5 inverted resistivity profile.

The inverted section showed a uniform profile with an ER of approximately 40,000 Ohm-cm; a mildly to none-corrosive aggregate. Electrode spacing was insufficient to image the full height of the wall. Previous tests showed a high zone of ER values near the ground surface, but that zone was not present in Test 5 due to a decreased average contact resistance value. The lower contact resistance indicates adequate contact between electrodes and the gravel resulting in a low RMS value in the inversion. Low ER values at the ground surface were assumed to be a finer-grained material or attributed to increased compaction.

At this location test T 288-12 was 3,808 Ohm-cm; a moderately corrosive aggregate. General observations of ER imaging results showed values ranging from 10,000-1,000,000 Ohm-cm, which were significantly larger than the laboratory value but within the ER range of a mildly to noncorrosive gravel. The laboratory test value is based on a slurry mixture of finer-grained material (dust from the aggregate) or crushed aggregate material passing the No. 10 sieve. These finer grains and slurry mixture (water dominated mixture) result in decreased ER values, and are not representative of the aggregates. Test results also showed that geosynthetic reinforcement does not affect ER imaging, and compaction and presence of finer-grained materials impacted ER results.

3.3.2 Geosynthetic Wall 2: Overpass of 118th Street and Interstate 70

Because of limited space due to residential structures and a golf course, an MSE wall was constructed as an overpass structure at 118th Street over I70. The site is located 19.0 km west of Kansas City, Kansas. Light-compaction equipment was used to compact the fill materials. Testing occurred on three dates: June 18, 2014; July 9, 2014; May 21, 2015. Attributes of the

MSE wall are outlined in Table 3.7. The aggregate backfill was from the same source as the Geosynthetic Wall 1.

Table 3.7. Characteristics of MSE wall located at 118th St. and I70.

Attribute	Value
Length	76.2 m
Height	2.0 m to 7.0 m
Reinforcement	Geogrid
Backfill Resistivity*	3,808 Ohm-cm

*Source KDOT

The first test was performed on June 18, 2014. Only one test was completed due to the small stature of the wall and because ER imaging causes construction to cease during testing. Test 6 details are outlined in Table 3.2, followed by the inverted ER section in Fig. 3.9.

Table 3.8. Characteristics of Test 6.

Attribute	Value
Wall Height	3.5 to 4.8 m
Distance from Wall's Face	0.6 m
Electrode Spacing	0.3 m
Array	Dipole-dipole
Average Contact Resistance	Data not found
Data Removed	0.0%
RMS	4.2%
Number of Iterations	3
Noise Estimation	5.0%

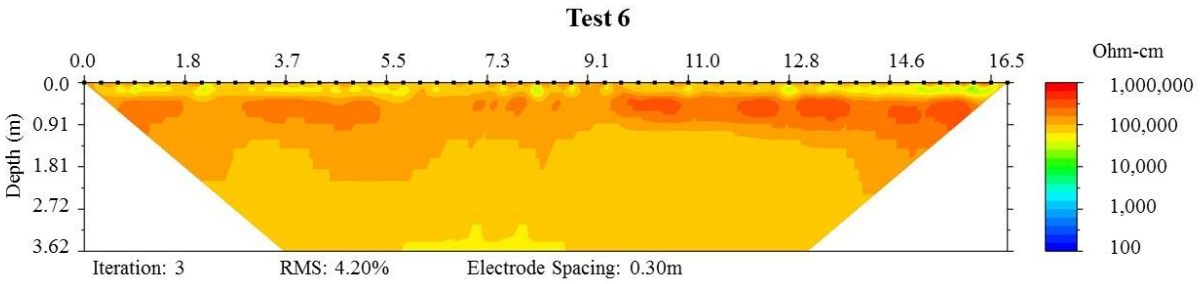

Fig. 3.9. Test 6 inverted resistivity profile.

Test 6 was performed close to the face of the wall where compaction effort is typically less. Since only light-compaction was used at the site, it might lead to increased ER values compared to Geosynthetic Wall 1. Values of this wall were comparable to that of the high-end of gravel

material and classified as noncorrosive. The survey was unable to image the entire height of the wall.

A second test was performed on July 9, 2014 (Test 7). Only one test was completed on this date due to limited space which requires construction to stop during testing. Test 7 was performed near the final stages of the construction and close to the face of the wall, similar to Test 6. Details of the test are outlined in Table 3.9, followed by the inverted resistivity section in Fig. 3.10.

Table 3.9. Characteristics of Test 7.

Attribute	Value
Wall Height	3.0 to 6.7 m
Distance from Wall's Face	0.6 m
Electrode Spacing	0.6 m
Array	Inverted Schlumberger
Average Contact Resistance	2,800 Ohm
Data Removed	0.0%
RMS	3.6%
Number of Iterations	2
Noise Estimation	5.0%

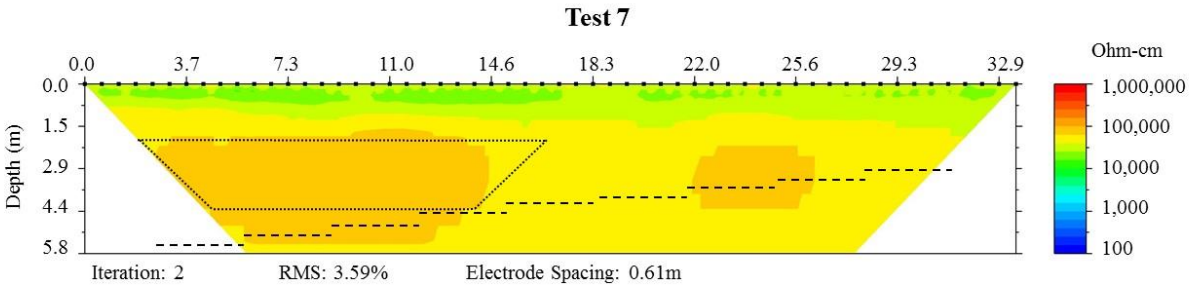

Fig. 3.10. Test 7 inverted resistivity profile with Test 6 outlined in small dashed lines (lower left) and approximate base of the wall in large stair-stepped dashed lines.

Test 7 was performed close to the face of the wall, similar to Test 6, but near the end of construction when the wall was almost complete. Overall ER of the wall decreased compared to Test 6, possibly due to the added weight of material and active construction activity that further compacted the gravel. High surface values from previous testing were not observed, and average contact resistance was low at the site, resulting in a low RMS value in the inversion. The

approximate location of Test 6 is represented in Fig. 3.10 as dotted lines in the shape of the inverted section. Test 7 shows that the region of Test 6 had higher ER values, as represented in Fig. 3.9. Again, ER values were within the ER range of a mildly to noncorrosive gravel, and the test was unable to detect native material below the base of the wall.

Test 8 was completed on May 22, 2015. The wall had been completed for almost a year, and the roadway did not cover the entire wall and allowed space to perform ER imaging. Test 8 was set back further from the face of the wall then previous tests at the site. The top of the wall contained a transition zone of native grass and soil overlaying the aggregate portion of the wall. This native grass and soil zone was approximately 0.3 m thick, thereby providing adequate contact to the electrode stakes and a low RMS value in the inversion. Attributes of Test 8 are outlined in Table 3.10, followed by the ER pseudosection in Fig. 3.11.

Table 3.10. Characteristics of Test 8.

Attribute	Value
Wall Height	3.0 to 7.0 m
Distance from Wall's Face	1.2 m
Electrode Spacing	0.91 m
Array	Inverted Schlumberger
Average Contact Resistance	250 Ohm
Number of Inversions	1
Data Removed	0.0%
RMS	2.9%
Number of Iterations	8
Noise Estimation	3.0%

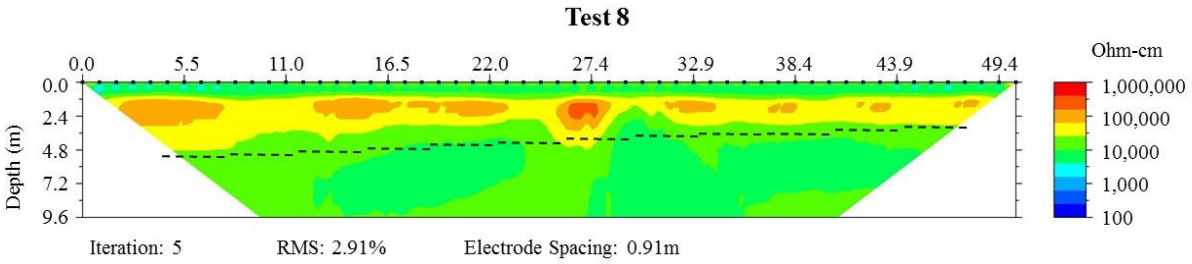

Fig. 3.11. Test 8 inverted resistivity profile with approximate base of wall.

Test 8 provided quality data (low RMS) due to the contact from the ground to the electrode stake. The test imaged the transition between surface fine-grained soils (vegetative supporting

material) to coarse aggregates used to construct the wall. ER imaging was able to image the base of the wall. The lower resistant native material below the foundation may be affecting the aggregate results near the base of the wall; lowering the values in this region. A drainage structure near the center of the profile possibly resulted in high ER values at the horizontal mark of 27.4 m. Overall, MSE wall ER results showed a uniform material similar to previous testing, with results in the ER range of non- to mildly-corrosive gravel material.

Results at Geosynthetic Wall 2 were similar to the results observed at Geosynthetic Wall 1. ER values of the field test indicted that aggregate has ER similar to non- to mildly-corrosive gravel material (greater than 10,000 Ohm-cm). ER values are significantly higher than the laboratory results provided by KDOT in which the aggregate had a resistivity of 3,808 Ohm-cm; moderately corrosive. Post-construction results were similar to the test results performed during construction.

3.3.3 Geosynthetic Wall 3: South Broadway Street and Centennial Drive

A sidewalk was added at the intersection of South Broadway Street and Centennial near a mall in Pittsburg, Kansas. Sharp topographic relief was present into the mall parking lot, and a small MSE wall was added with a handrail to support a sidewalk and road above without disturbing the mall's parking lot. Only light-compaction equipment was used at the site due to the small stature of the wall. Testing was conducted only on July 25, 2014. The wall's attributes are outlined in Table 3.11.

Table 3.11. Characteristics of the MSE wall at Broadway and Centennial.

Attribute	Value
Length	118.0 m
Height	0.8 m to1.8 m
Reinforcement	Geogrid
Backfill Resistivity	Not Known

Test 9 was performed during the final stages of wall construction, and only a small portion of the wall was tested due to active construction. Electrode stakes were placed into the ground surface with minimal effort compared to the previous testing sites, indicating that compaction at this site was minimal, thereby leading to inadequate results in ER imaging. KDOT was unable to

apply additional compaction in the testing region. Attributes of Test 9 are outlined in Table 3.12, followed by the inverted resistivity section in Fig. 3.12.

Table 3.12. Characteristics of Test 9.

Attribute	Value
Wall Height	2.0 m
Distance from Wall's Face	0.9 m
Electrode Spacing	0.3 m
Array	Inverted Schlumberger
Average Contact Resistance	30,000 Ohm
Data Removed	0.0%
RMS	6.88%
Number of Iterations	8
Noise Estimation	5.0%

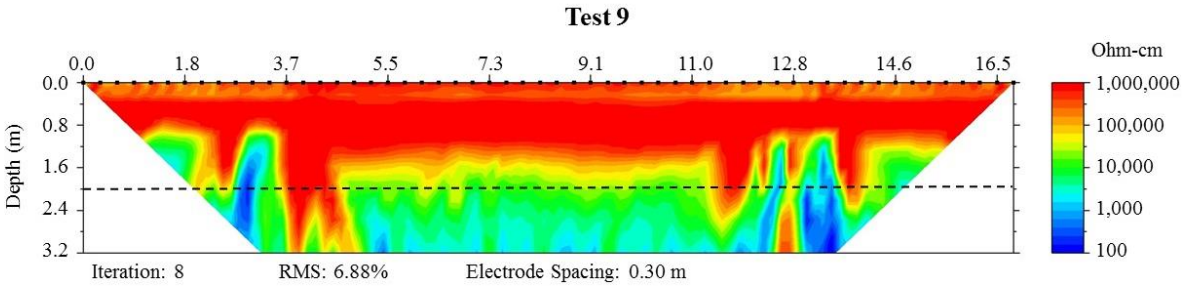

Fig. 3.12. Test 9 inverted resistivity profile with approximate base of wall at 2 m.

The contact resistance test showed extremely inadequate contact between the ground and electrode stakes, leading to high ER values. The poor contact is due to lack of compaction at the site. Double-staking of electrode stakes in order to increase the surface area for contact and sledge hammer compaction around the electrodes was applied with minimal decrease in the contact resistance test. Results depicted an inverted section with extremely high ER values of 1,000,000 Ohm-cm; noncorrosive. The survey was able to image the native material below the foundation, but due to the poor quality data, the accuracy is questionable.

The third and final geosynthetic reinforced MSE wall produced extremely high ER results, as compared to previous MSE walls. The extreme high value is thought to be caused by poor compaction at the site. However, further analysis is need to define the relationship of compaction and ER. AASTHO method T 288-12 laboratory results were not provided, but are assumed to be consistent with previous MSE geosynthetic reinforced walls. If AASHTO method T 288-12

results would be similar, the results from Test 9 are substantially higher than that obtained from the laboratory test.

3.3.4 Metal Wall: Interchange of Ridgeview and Kansas Highway 10

The overpass of Ridgeview above route K-10 was expanded to accommodate increased traffic flow. Abutments on the north and south of K-10 utilized MSE walls for support. These walls contained metal strip reinforcement approximately 0.6 cm thick and 5 cm wide that were anchored into the face of the wall. Reinforcement was placed at maximum horizontal spacing of 0.75 m and maximum vertical spacing of 0.5 m. Due to active construction during testing, only the northwestern MSE wall abutment was tested. Light-compaction equipment was used from the face to 1.5 m from the face, and heavy-compaction equipment was used beyond 1.5 m. When the wall was at its final height, the site was visited four times: September 2, 2014; September 19, 2014; October 3, 2015; January 22, 2015. Characteristics of the wall are defined in Table 3.13.

Table 3.13. Characteristics of MSE wall at Ridgeview and K-10.

Attribute	Value
Length	20 m
Height	1.4 to 7.0 m
Reinforcement	Metal Strips
Backfill Resistivity*	6,036 Ohm-cm

*Source KDOT

On September 2, 2014, Test 10 was performed in a region in which heavy-compaction equipment was used. Due to surface elevation changes, a relative survey of the electrodes was performed. Test attributes are outlined in Table 3.14, followed by the ER inverted section in Fig. 3.13.

Table 3.14. Characteristics of Test 10.

Attribute	Value
Wall Height	1.4 to 7.0 m
Distance from Wall's Face	3.1 m
Electrode Spacing	0.3 m
Array	Inverted Schlumberger
Average Contact Resistance	900 Ohm
Data Removed	0.0%
RMS	3.7%
Number of Iterations	8
Noise Estimation	3.0%

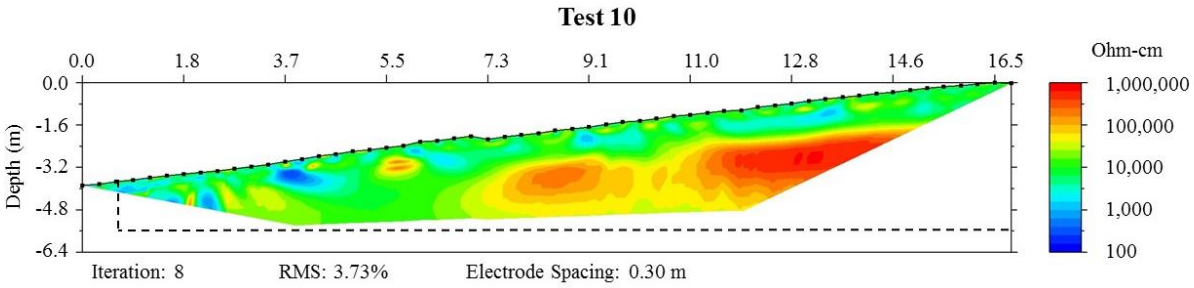

Fig. 3.13. Test 10 inverted resistivity profile with approximate base and edge of wall.

Test 10 had a low average contact resistance test results, implying adequate contact between the electrode stakes and aggregate, resulting in a low RMS value. Imaging produced a non-uniform profile compared to previous testing. Low values near the ground surface were caused by metal reinforcement and/or the presence of fine-grained materials. Reinforcement seemed to have minimal effect after depths of approximately 1.2 m from the ground surface. Near the first electrode (as shown on the left side of Fig. 3.13), the low values were attributed to mixing of the native fine-grained soil and aggregates during construction and the recent rain events. Inadequate compaction may have been the cause of the increased ER values at depths of 2.4-5.2 m and horizontal locations between 7.3 and 14.6 m. However, the test was unable to image the entire height of the wall due to limited electrode spacing induced by the small testing area. Based upon the inverted section, the aggregates range from very corrosive to noncorrosive.

On October 19, 2014, Test 11 was completed in the same region as Test 10. The test was performed in a location allowing heavy-compaction equipment. A second inversion was

performed due to the high RMS value in the first inversion. Table 3.15 outlines test details, and Fig. 3.14 depicts the ER inverted section.

Table 3.15. Characteristics of Test 11.

Attribute	Value
Wall Height	1.4 to 7.0 m
Distance from Wall's Face	3.1 m
Electrode Spacing	0.3 m
Array	Inverse Schlumberger
Average Contact Resistance	1,300 Ohm
Number of Inversions	2
Data Removed (1st Inversion)	1.6%
RMS (1st Inversion)	6.2%
Number of Iterations (1st Inversion)	8
Data Removed (2nd Inversion)	4.0%
RMS (2nd Inversion)	3.9%
Number of Iterations (2nd Inversion)	6
Noise Estimation	4.0%

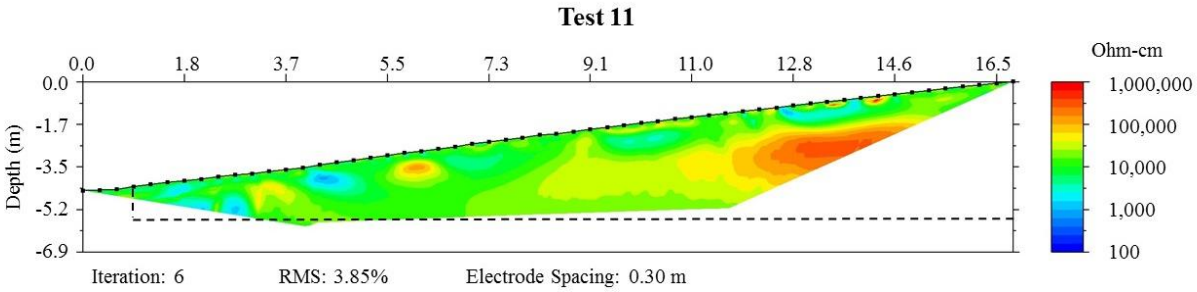

Fig. 3.14. Test 11 inverted resistivity profile with approximate base and edge of wall.

Overall ER of Test 11 was similar to Test 10 but the inverted section depicts a more uniform ER. Low values near the ground surface increased slightly, possibly due to recent rains washing the finer-grained materials out of the system or water was draining to the bottom of the wall. Metal reinforcement near the surface lowered ER values compared to typical values for gravel material. The region of high values from decreased substantially, potentially due to construction activities and weight of material (which increased compaction), the presence of water in the system from recent rains, and/or the addition of finer material being washed through the wall from the surface. The profile depicts a corrosive to noncorrosive environment.

Significant rain events had occurred prior to October 3, 2014, when Test 12 was completed, and a slight mist of rain was present during testing. The test was performed in the same area as Tests 10 and 11 with the wall remaining at the same height. Test 12 details are described in Table 3.16, and the ER inverted section is depicted in Fig. 3.15.

Table 3.16. Characteristics of Test 12.

Attribute	Value
Wall Height	1.4 to 7.0 m
Distance from Wall's Face	3.1 m
Electrode Spacing	0.3 m
Array	Inverted Schlumberger
Average Contact Resistance	1,300 Ohm
Data Removed	0.0%
RMS	4.5%
Number of Iterations	8
Noise Estimation	4.0%

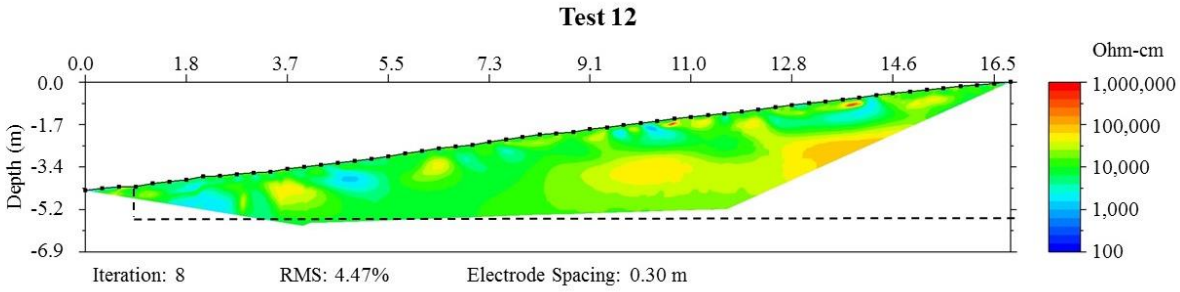

Fig. 3.15. Test 12 inverted resistivity profile with approximate base and edge of wall.

Overall ER of the inverted section decreased due to the presence of water from previous rain events and rain during testing. The region (9.1m to 14.6 m) in which high ER values were observed continued to decrease, but low surface values stayed relatively constant. The low ground surface values are attributed to the presences of metal reinforcement. The overall ER has decreased due to the presence of water in the wall. The inverted section represents corrosive to noncorrosive aggregates.

Two tests were completed on January 22, 2015: Test 13 and Test14. Test 13 was completed in the same area as previous tests, in locations of heavy-compaction equipment utilization. Test 14 was completed near the face of the wall where only light-compaction equipment was used.

Both tests were completed on the previously tested wall, but the survey was oriented in the reverse direction, resulting in flipped inverted sections. Test 13 details are outlined in Table 3.17, followed by the ER profile in Fig. 3.16. Test 14 is outlined in Table 3.18, and the inverted section is depicted in Fig. 3.17. Each test went through two iterations due to the high RMS value in the first iteration.

Table 3.17. Characteristics of Test 13.

Attribute	Value
Wall Height	1.4 to 7.0 m
Distance from Wall's Face	3.1 m
Electrode Spacing	0.3 m
Array	Inverse Schlumberger
Average Contact Resistance	6,000 Ohm
Number of Inversions	2
Data Removed (1st Inversion)	0.7%
RMS (1st Inversion)	5.0%
Number of Iterations (1st Inversion)	8
Data Removed (2nd Inversion)	3.0%
RMS (2nd Inversion)	4.0%
Number of Iterations (2nd Inversion)	7
Noise Estimation	4.0%

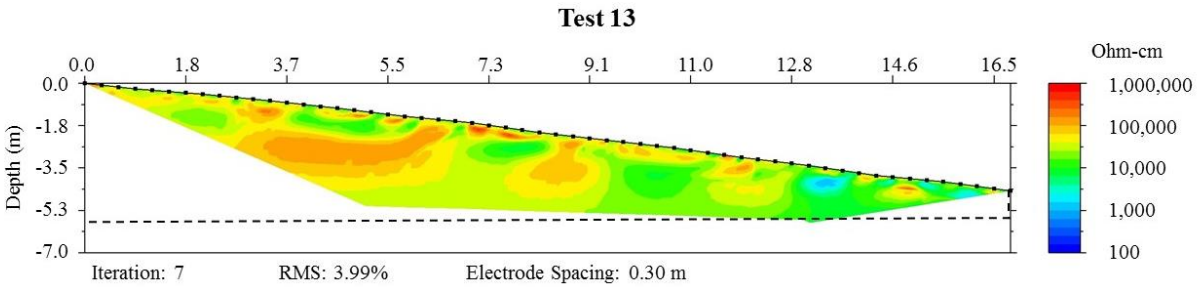

Fig. 3.16. Test 13 inverted resistivity profile with approximate base of wall.

Test 13 had an average contact resistance of 6,000 Ohm, resulting in a decreased RMS value. Results followed the trend of a more uniform profile, and regions near the surface depicted low ER values attributed to metal reinforcement. The right side of the inverted section contained lower values not typically representative of aggregate materials, possibly due to the mixing of native material with aggregates during construction or the presence of water. The more uniform

profile may be attributed to water loss and fine-grained material being washed out from within the wall. The aggregates are classified as corrosive to noncorrosive.

Table 3.18. Characteristics of Test 14.

Attribute	Value
Wall Height	1.4 to 7.0 m
Distance from Wall's Face	0.6 m
Electrode Spacing	0.3 m
Array	Inverse Schlumberger
Average Contact Resistance	8,000 Ohm
Number of Inversions	2
Data Removed (1st Inversion)	0.7%
RMS (1st Inversion)	7.4%
Number of Iterations (1st Inversion)	8
Data Removed (2nd Inversion)	3.7%
RMS (2nd Inversion)	5.0%
Number of Iterations (2nd Inversion)	8
Noise Estimation	5.0%

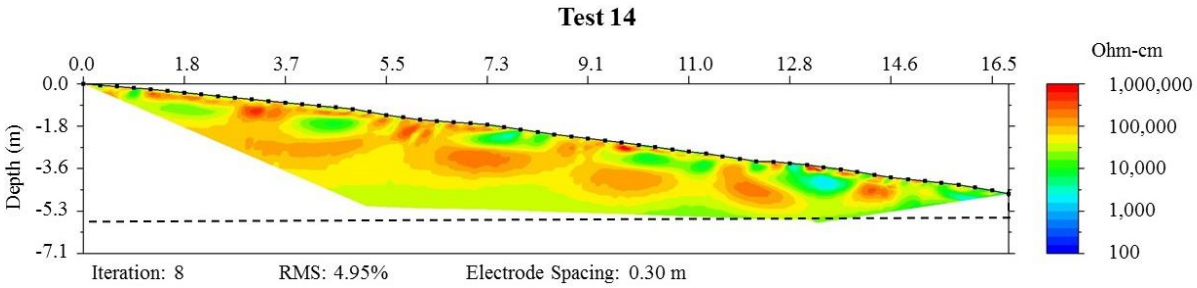

Fig. 3.17. Test 14 inverted resistivity profile with approximate base of wall.

Test 14 was performed close to the face of the wall in locations of lesser compaction, resulting in increased average contact resistance and RMS value. The inverted section depicts a more uniform profile with higher ER values compared to previous testing. Again, the profile close to the face of the wall produced higher results than tests farther from the wall's face, possibly due to compaction variability. However, further research is needed to define the correlation of compaction and ER. ER near the ground surface are lower due to the less resistant metal reinforcement. The environment describes a moderate to noncorrosive aggregate.

The MSE wall with metallic reinforcement at the intersection of Ridgeview and K-10 produced results similar to previous testing. KDOT laboratory tests showed the aggregates had

an ER of 6,036 Ohm-cm; mildly corrosive. After omitting the lower values thought to be caused by the metal reinforcement, presence of water, and native fine-grained material, the ER imaging results showed values similar to previous testing; mild- to non-corrosive. In addition, ER imaging produced results significantly higher than AASHTO method T 288-12 laboratory testing. Metal reinforcement may have minimally affected ER imaging results near the surface, but the effect dissipated with depth. Additional testing of MSE walls containing metal reinforcement is desired in order to further define the effect of metal reinforcement on ER imaging.

3.3.5 Gravity Wall: Intersection of Haskell Avenue and East 31st Street

The final wall tested was a gravity wall located near the intersection of Haskell Ave. and East 31st St. in Lawrence, Kansas. The South Lawrence Trafficway was expanded, and a gravity retaining wall was added to retain a steep soil slope near one of the new roads. The wall was compacted using heavy equipment, except in a region where the wall was not wide enough to allow passage for a roller. In this particular region, vibratory compaction of a steel plate was used. Hard sandstone bedrock was present across the site. The site was visited four times: February 24, 2015; March 31, 2015; April 10, 2015; May 21, 2015. The gravity wall contained no reinforcement. Characteristics of the wall are outlined in Table 3.19.

Table 3.19. Characteristics of the MSE wall located at Haskell Ave. and East 31st St.

Attribute	Value
Length	92.1 m
Height	0 m to 6.8 m
Reinforcement	None
Backfill Resistivity*	3,895 Ohm-cm

*Source KDOT

Test 15 was completed on February 24, 2015, after a recent snow event. No snow was present, but the ground was frozen. Testing was completed midway through construction. Test attributes are presented in Table 3.20, followed by the ER inverted section in Fig. 3.18. Roller compaction was used through most of the wall except between 16.5 to 35.5 m, where vibratory plate compaction was applied.

Table 3.20. Characteristics of Test 15.

Attribute	Value
Wall Height	2.0 to 4.6 m
Distance from Wall's Face	1.8 m
Electrode Spacing	0.9 m
Array	Inverse Schlumberger
Average Contact Resistance	40,000 Ohm
Number of Inversions	2
Data Removed (1st Inversion)	25.5%
RMS (1st Inversion)	17.8%
Number of Iterations (1st Inversion)	8
Data Removed (2nd Inversion)	7.9%
RMS (2nd Inversion)	9.3%
Number of Iterations (2nd Inversion)	8
Noise Estimation	8.0%

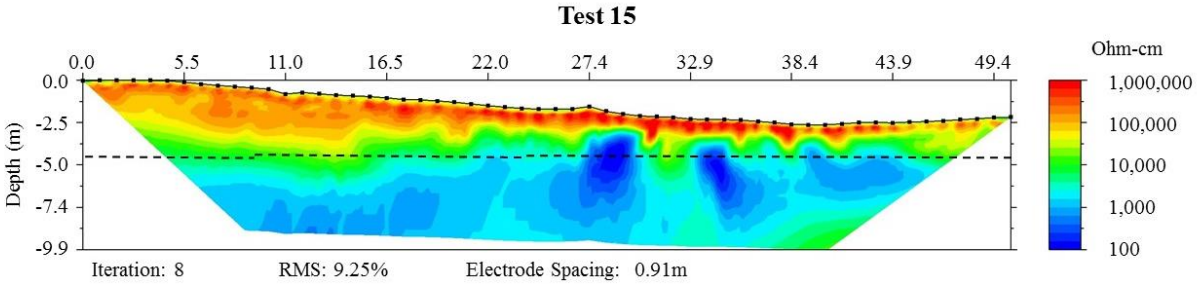

Fig. 3.18. Test 15 inverted resistivity profile with approximate base of wall.

The frozen ground provided inadequate contact resistance, leading to a high RMS value; however, the test produced valuable results. The inverted section imaged the wall height and native material below the foundation. The profile also showed results on the high end of the range of gravel material due to poor contact resistance. Due to the large spacing of the test, most of the imaging is of the native foundation material. The smoothening of the inversion process is lowering the ER results near the base of the wall due to the low ER of the native foundation material. Results of Test 15 were similar to previously tested geosynthetic reinforced walls. The region that had vibratory plate compaction (16.5-35.5 m) may have provided lesser compaction than a roller, thereby resulting in increased ER values. The inverted section represents a corrosive to noncorrosive gravel.

Test 16 was completed on March 31, 2015, and the first electrode of Test 16 correlated to the 38 electrode of Test 15. The ground had thawed, and heavy-compaction method was used throughout this portion of the wall. Table 3.21 outlines test attributes, and Fig. 3.19 shows the ER inverted section.

Table 3.21. Characteristics of Test 16.

Attribute	Value
Wall Height	2.0 to 5.0 m
Distance from Wall's Face	1.8 m
Electrode Spacing	0.9 m
Array	Inverse Schlumberger
Average Contact Resistance	4,300 Ohm
Number of Inversions	2
Data Removed (1st Inversion)	17.4%
RMS (1st Inversion)	9.3%
Number of Iterations (1st Inversion)	8
Data Removed (2nd Inversion)	7.6%
RMS (2nd Inversion)	5.1%
Number of Iterations (2nd Inversion)	6
Noise Estimation	6.0%

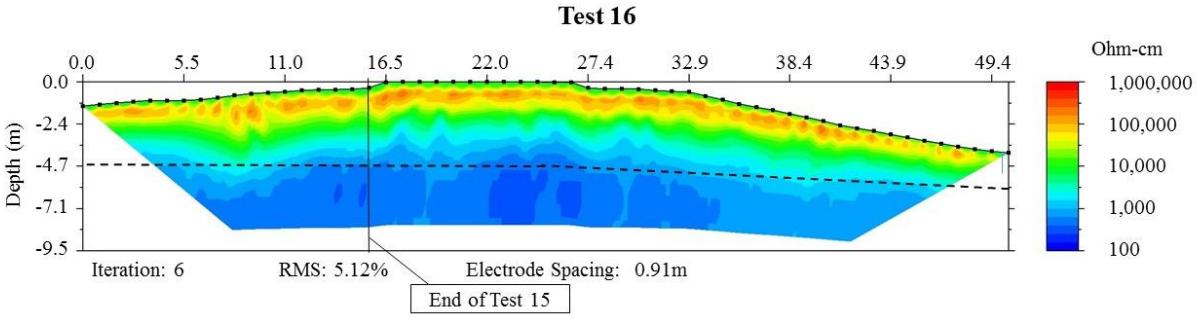

Fig. 3.19. Test 16 inverted resistivity profile with approximate base of wall and end of Test 15.

Test 16 imaged the entire MSE wall and foundation where the material changed from aggregate to native material. Surface values were low due to contact between the electrodes and the ground, thereby providing a low RMS value. Like Test 15, the low resistance foundation material is altering the ER values near the base of the wall. ER imaging depicts a corrosive to noncorrosive environment.

On April 10, 2015, Test 17 was completed in the same region as Test 15. Test 17 had smaller electrode spacing and was completed in the reverse direction of Test 15, resulting in a flipped ER inverted section. Characteristics of Test 17 are described in Table 3.22, followed by the ER inverted section in Fig. 3.20. Two inversions were performed due to the high RMS value in the first inversion.

Table 3.22. Characteristics of Test 17.

Attribute	Value
Wall Height	2.0 to 4.0 m
Distance from Wall's Face	1.8 m
Electrode Spacing	0.9 m
Array	Inverse Schlumberger
Average Contact Resistance	5,000 Ohm
Number of Inversions	2
Data Removed (1st Inversion)	7.8%
RMS (1st Inversion)	5.7%
Number of Iterations (1st Inversion)	8
Data Removed (2nd Inversion)	2.5%
RMS (2nd Inversion)	4.4%
Number of Iterations (2nd Inversion)	7
Noise Estimation	5.0%

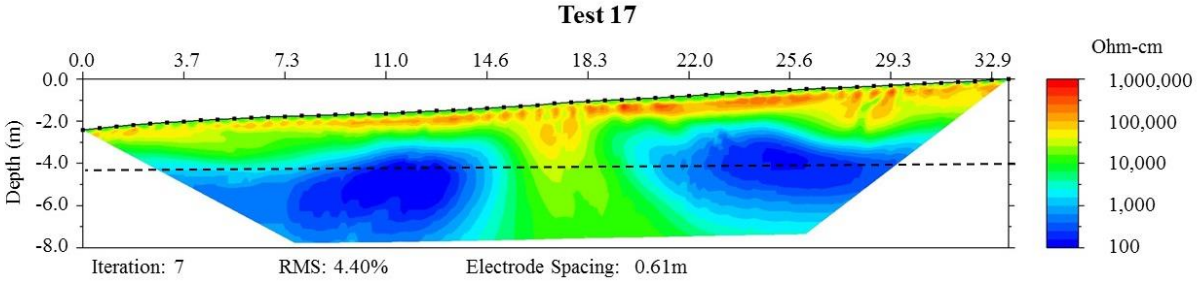

Fig. 3.20. Test 17 inverted resistivity profile with approximate base of wall.

Test 17 had a lower average contact resistance and RMS value than Test 15. Test 17 imaged the foundation of the wall where it changed from backfilled aggregate (greater than 10,000 Ohm) to native soils (less than 10,000 Ohm). The high ER values between 14.6 and 18.3 m has become more prominent than represented in Test 15 due to better contact and non-frozen ground yielding better quality results. The low resistive foundation material continues to alter the results near the foundation of the wall; lowering the ER. Test 17 depicts a corrosive to noncorrosive backfill.

Test 18 and Test 19 were completed on May 21, 2015. The wall was near completion during this time, with native material placed over the top of the aggregates in order to support vegetation. The native material provided adequate contact between the electrode stakes and the ground, resulting in lower RMS values. However, the native material was almost saturated due to heavy rains during previous weeks. Test 18 was performed in the same region as Tests 15 and 17. Test 19 was completed in the same section of the wall as Test 16. The first electrode of Test 19 was located where the last electrode of Test 18 was placed. Table 3.23 and Fig. 3.21 show results from Test 18, and Table 3.24 and Fig. 3.22 represent Test 19.

Table 3.23. Characteristics of Test 18.

Attribute	Value
Wall Height	2.0 to 4.0 m
Distance from Wall's Face	1.8 m
Electrode Spacing	0.6 m
Array	Inverse Schlumberger
Average Contact Resistance	75 Ohm
Number of Inversions	2
Data Removed (1st Inversion)	1.0%
RMS (1st Inversion)	9.1%
Number of Iterations (1st Inversion)	8
Data Removed (2nd Inversion)	3.9%
RMS (2nd Inversion)	4.8%
Number of Iterations (2nd Inversion)	6
Noise Estimation	5.0%

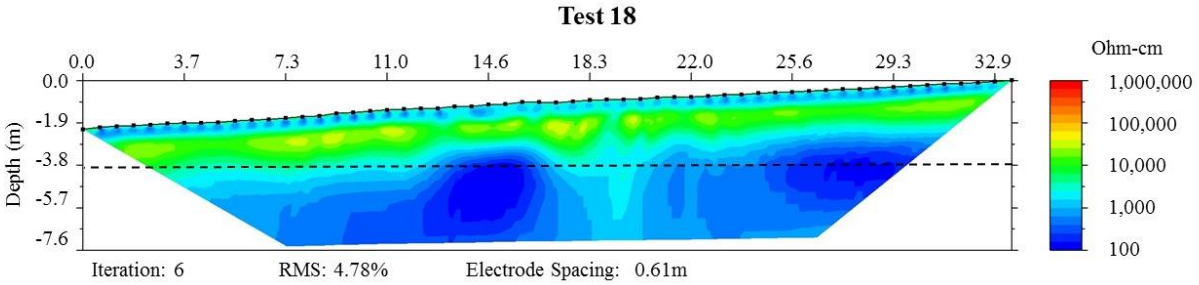

Fig. 3.21. Test 18 inverted resistivity profile with approximate base of wall.

Test 18 imaged the native material at the ground surface (approximately 1,000 Ohm-cm), the aggregate backfill (approximately 10,000 Ohm-cm), and the native soil below the foundation (less than 1,000 Ohm-cm). Resistivity of the aggregate backfill portrays uniform ER, but results

showed a material with a lower ER than previous testing but within the range of mildly to noncorrosive aggregate. Lower values are attributed to the presence of water within the wall due to recent rain events. Low ER of the foundation material continues to alter the ER of the aggregates near the base of the wall.

Table 3.24. Characteristics of Test 19.

Attribute	Value
Wall Height	2.3 to 7.0 m
Distance from Wall's Face	1.8 m
Electrode Spacing	0.9 m
Array	Inverted Schlumberger
Average Contact Resistance	150 Ohm
Data Removed	0.5%
RMS	2.8%
Number of Iterations	0.9
Noise Estimation	3.0%

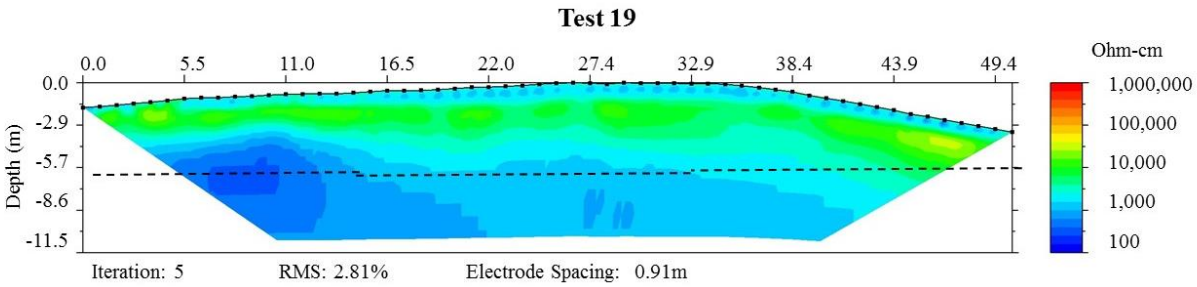

Fig. 3.22. Test 19 inverted resistivity profile with approximate base of wall.

Test 19 results were similar to results of Test 18. The test imaged the ground surface and foundation native material (approximately 1,000 Ohm-cm) and aggregate backfill (approximately 10,000 Ohm-cm). Results of the backfill were lower than that from previous testing due to recent rain events that resulted in the presence of water in the wall. Native low resistance foundation material alters the aggregate ER results near the base of the wall. The aggregate is represented as a mildly to noncorrosive material.

Results from the gravity wall were similar to the results from the geosynthetic and metal reinforced MSE walls. KDOT test method T 288-12 results showed that the aggregate had an ER of 3,895 Ohm-cm (moderately corrosive), while ER imaging produced higher ER results between 5,000 and 100,000 Ohm-cm (mildly to noncorrosive). The compaction effort and

methods and the presence of water within the wall also altered ER imaging results. Due to the wall being a small part of the ER imaging, the low resistant foundation material below the wall is altering the inversion results; lowering the resistivity of the aggregates near the wall base.

3.4 Summary

ER imaging results from the five walls demonstrated that the field method can be applied to measure the ER of retaining wall aggregate backfill. These results, however, were constantly higher than ER results gathered in the laboratory using AASHTO method T 288-12. Geosynthetic reinforcement had no effect on the ER results. Metal reinforcement altered ER values near the surface, but the effect dissipated with depth. Compaction of the backfill may affect ER results, with the trend of increased compaction yielding decreased ER values. Further testing and analysis are needed to understand the relationship of compaction and water to ER imaging. Water within the backfill materials was shown to lower ER results. ER imaging of the full height of the retaining is valuable, but too deep of imaging of the native foundation material may alter aggregate results near the base of the wall. Due to the subjective nature of the geophysics results, a post-processing data algorithm was generated to determine the bulk ER at each wall. The methodology has been discussed in the next chapter.

Chapter 4 Quantitative Post-Processing Algorithm

4.1 Introduction

A quantitative post-processing algorithm was applied to 18 of the 19 tests; Test 9 was excluded due to poor experimental data from the field. Quality of data was discussed in Chapter 3, Section 3.1. In general, a lower RMS provides better quality with decreased data noise, and more accurate ER data. The larger the contact surface area between the electrodes and the aggregates, the larger the injected current and the more reliable the ER measurement is from the field.

4.2 Methodology

The post-processing program, which was generated in MatLab, used the inverted ER section values generated in EarthImager to determine bulk resistivity of each wall. This post-processing procedure removed the objective interpretation presented by the inverted ER section in EarthImager. Only ER values representative of the walls were taken into account to determine the bulk ER. Values below the foundation of the wall were removed from the algorithm and not taken into account for bulk resistivity calculations. After removal of data were completed, the data was graphed into a histogram that provided a general understanding of the distribution of ER values within the wall (Fig. 4.1). Histograms for all tests are shown in the Appendix.

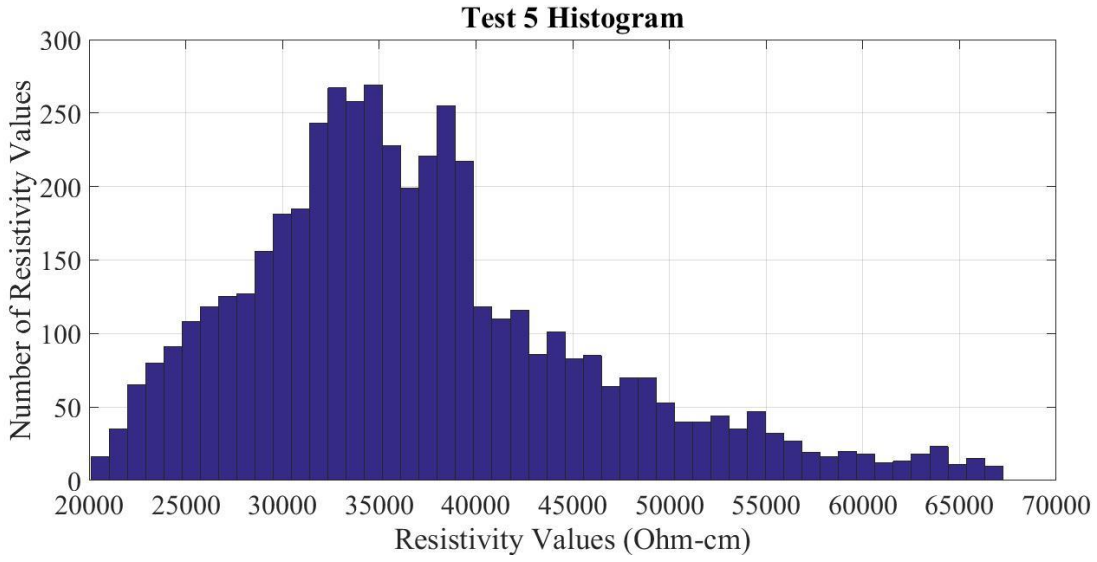

Fig. 4.1. Histogram of Test 12.

The data and log of the data were plotted in a normal distribution and compared in a Cumulative Density Function (CDF) plot in order to verify which distribution provided the best fit to data described by (Baecher and Christian, 2005). A linear fit indicated a good fit of the data to the distribution. The norm of the residuals was used to estimate the goodness of fit of the data to a linear approximation. The mean μ and standard deviation σ were needed to determine the CDF:

$$\mu = \frac{\sum x_i}{n} \ , \tag{18}$$

where the numerator is the sum of all observations, and the denominator is the total number of observations (n). The standard deviation is as follows:

$$\sigma = \sqrt{\frac{1}{n}\sum_{i=1}^{i=n}\left(x_i - \mu\right)^2} \ , \tag{19}$$

where x_i is an observation and the other terms previously have been defined.

The normal CDF is determined by:

$$F(x|\mu,\sigma) = \frac{1}{\sigma\sqrt{2\pi}}\int_{-\infty}^{x} e^{\frac{-(t-\mu)^2}{2\sigma^2}}\,dt \tag{20}$$

in which μ and σ have been defined, t is each data value, and x is the interval of data. The result is that the probability of an observation will lie in the given interval from a normal distribution. In order to determine the lognormal CDF, the mean μ and standard deviation σ of the log data were calculated. Lognormal distribution with mean m and variance v is represented as follows:

$$\mu = log\left(m^2 \Big/ \sqrt{v+m^2}\right) , \tag{21}$$

$$\sigma = \sqrt{log\left(v/m^2+1\right)} \ , \tag{22}$$

where μ and σ are the mean and standard deviation of the log, respectively. The lognormal CDF is defined as:

$$F(x|\mu,\sigma) = \frac{1}{\sigma\sqrt{2\pi}} \int_0^x \frac{e^{\frac{-(ln(t)-\mu)^2}{2\sigma^2}}}{t} dt \quad (23)$$

in which all variables have been previously defined. As mentioned, the norm of the residuals was used to estimate the goodness of fit of the linear fit of the data. Norm of residuals is defined as

$$norm = \sqrt{\sum_{i=1}^{n} d_i^2} \quad (24)$$

where d_i represents the difference between the *ith* predicted data and the measured data. A perfect linear fit of the data would produce a norm of residual of 0. Table 4.1 contains the norm of residuals from the normal distribution of the data and the log of the data plotted in CDFs. The lognormal norm of residuals is less than the normal norm of residuals for each test, implying that the lognormal distribution was a better fit of the data. The lognormal distribution was also used because each test was independent and the results were only positive.

Table 4.1. Norm of residuals from the normal distribution of normal and lognormal CDFs.

Test		**1**	**2**	**3**	**4**	**5**	**6**	**7**	**8**	**10**
Norm of Residuals	**Normal**	4.8	3.5	2.3	5.3	4.6	5.9	3.6	4.6	5.3
	Lognormal	2.6	2.7	2.1	3.3	3.9	4.7	2.9	2.2	3.8
Test		**11**	**12**	**13**	**14**	**15**	**16**	**17**	**18**	**19**
Norm of Residuals	**Normal**	6.0	9.4	7.6	9.0	5.4	5.1	5.9	3.0	4.5
	Lognormal	4.0	3.6	4.7	4.5	3.4	2.2	3.7	2.4	3.1

After determining that the lognormal distribution was the best fit of the data, the lognormal CDF and the lognormal Probability Density Function (PDF) of the data were used to determine bulk resistivity of each test at the first and second geosynthetic walls, the metal reinforced wall, and the gravity wall. Geosynthetic Wall 3 was excluded from the processing due to the poor quality of the data (Test 9). The lognormal PDF equation is:

$$f\left(x|\mu,\sigma\right) = \frac{1}{x\sigma\sqrt{2\pi}} e^{\frac{-(\ln x-\mu)^2}{2\sigma^2}}, \quad (25)$$

in which the variables have been previously defined. The PDF (Fig. 4.2) was used to understand the distribution of the data. The peak of the PDF may be greater than 1, as shown in Fig. 4.2,

because the PDF represents probability density, or the probability per unit value of ER, which can exceed 1. The integral of the density function may not exceed 1, however, and it is represented as the CDF, which must remain between zero and 1 (Fig. 4.3). The peak of the PDF is 50% of the data (50% of the data lies to the left or right of the peak) and correlated with the 0.5 probability in the CDF. The smaller the confidence interval, the tighter the PDF tails became and the slope of the CDF became steeper. These attributes suggest uniform ER imaging results. The larger the confidence interval range, the wider the tails of the PDF and the line of the CDF was less steep, implying non-uniformity. Variation of the mean and confidence interval was due to the type of array used, the spacing of electrodes, location of the test on the wall, the type and extent of compaction, and the presence of water in the backfill.

The PDF and CDF of each test were used to set bounds on the data and remove outliers to determine bulk resistivity. The decision of which outliers to remove was based upon the RMS value determined from EarthImager. An RMS value between 0 and 5% represented good quality data, and 95% of the data were used in the bulk analysis. RMS between 6 and 10% represented lower data quality then previously (but still acceptable), and only 90% of the data were used in the bulk calculation. No tests were analyzed with an RMS greater than 10%. Data were removed from both “tails” of the PDF (95% removed 2.5% on each side, while 90% removed 5% from each side) (Fig. 4.2). Bounds of 95% and 90% were chosen due to their ability to remove lower and upper outliers of the data. PDFs and CDFs of each test are organized by site in the Appendix.

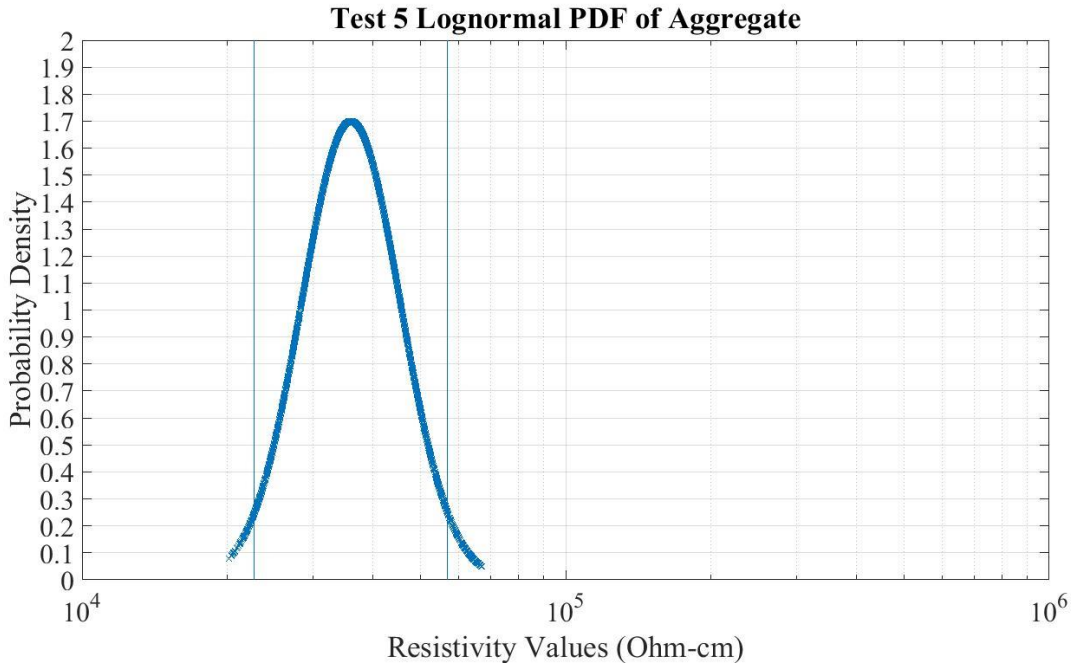

Fig. 4.2. PDF of Test 5 with an RMS of 3.6% removing 5% of outliers (vertical blue lines represent bounds of data removal).

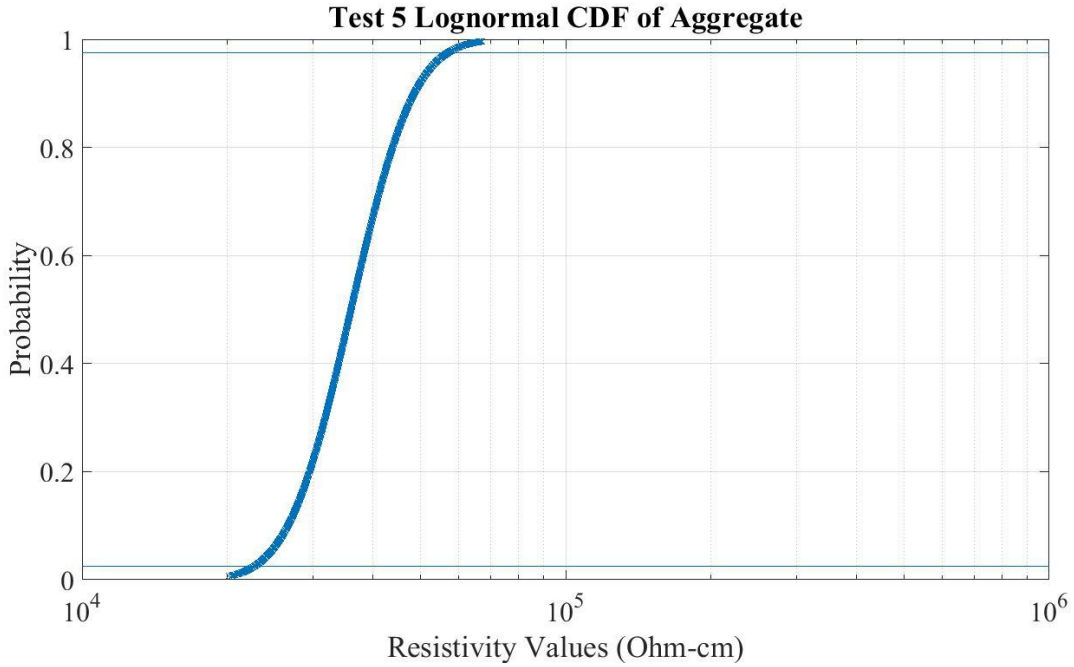

Fig. 4.3. CDF of Test 5 (horizontal blue lines represent the bounds of data removal).

The confidence interval was also determined for each test. A confidence interval of 95% implies that 95% of sampling would provide an interval that includes the mean (μ), and only

5% of sampling would provide an inaccurate interval (Devore, 2004). In other words, a confidence interval of 95% means that 95% of any sample taken from that particular ER imaging test will produce a mean within the calculated confidence interval.

A random sample (bound data that removed outliers) was taken from a non-normal distribution of a population (entire data set in this case) with a mean (μ) and standard deviation (σ). Assuming that the population n is large, the Central Limit Theorem implies that the sample is approximately normal even though the population distribution is not, an implication that is applicable to this case of a lognormal distribution with a large population of ER values. The large-sample confidence interval for the population mean for any population distribution is represented in the following equation:

$$\bar{x} \pm z_{\alpha/2} \frac{s}{\sqrt{n}} \qquad 26$$

in which $\bar{x}$ represents the samples mean, $z_{\alpha/2}$ represents the critical value, s represents the sample standard deviation, and n represents the number of observations. The critical value is a set constant based on the desired confidence. In this particular case, a 95% confidence was represented with a 1.96 critical value and 90% confidence was represented with a 1.645 critical value. A confidence interval with a small range suggests that more is known about the mean; a wide range suggests a larger range of variability of the mean. In other words, a small range implies more uniform ER imaging results, while a wide range implies a less uniform distribution of ER results.

4.3 Analysis of Results

The following sections present findings of the post-processing algorithm used on four of the five walls tested. Results from Geosynthetic Walls 1 and 2, the metal-reinforced wall, and the gravity wall are presented in the following sections. Each site results are presented in a table that describes the confidence value used (either 90 or 95%), the upper and lower bounds for data removal, and the mean and confidence interval within the bounds. A discussion of results follows the tables. At the end of the chapter, PDFs and CDFs of each test under similar conditions are compared.

4.3.1 Geosynthetic Wall 1: Interchange of US Route 73 and Interstate 70

Geosynthetic Wall 1 results from the post-processing algorithm are presented in Table 4.2. Test T 288-12 yielded an ER of 3,808 Ohm-cm. Fig. 4.4 and Fig. 4.5 depict the PDF and CDF, respectively, of data at Geosynthetic Wall 1.

Table 4.2. Geosynthetic Wall 1 results.

Test	Confidence Interval (%)	Bounds Placed to Remove Outliers in PDF (Ohm-cm)		Sample Mean (Ohm-cm)	Confidence Interval (Ohm-cm)	
		Upper Bound	Lower Bound		Lower Value	Upper Value
1	95	228,990	18,068	74,246	72,317	76,834
2	90	66,159	17,334	38,282	37,939	38,840
3	90	127,280	22,141	62,662	61,720	64,307
4	95	143,180	14,558	48,696	47,164	49,506
5	95	57,044	22,726	36,411	36,164	36,656

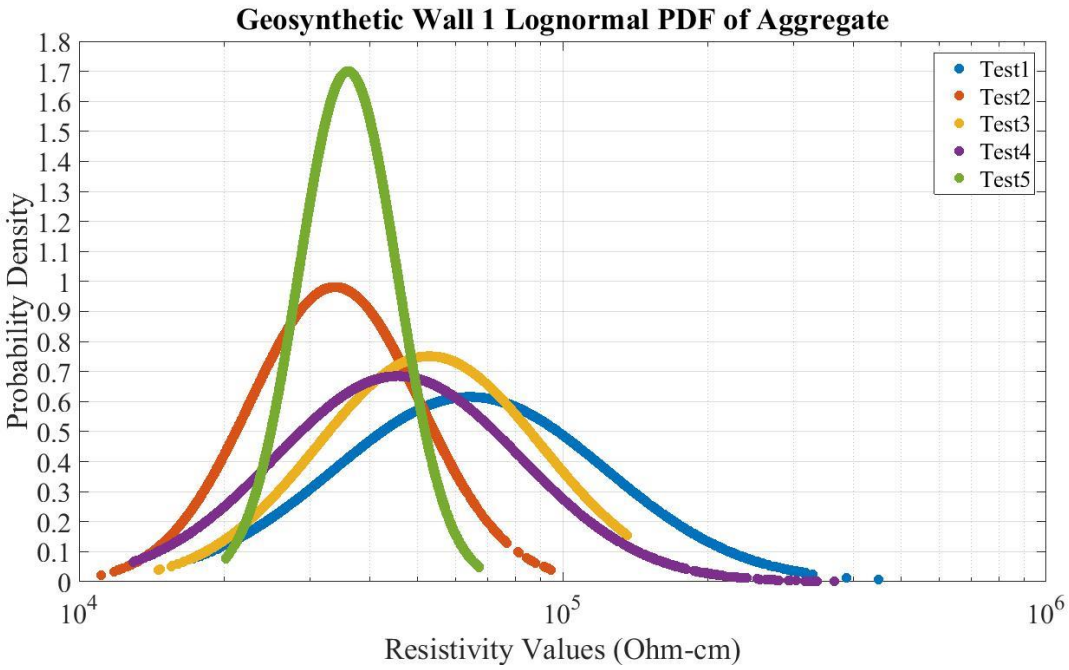

Fig. 4.4. PDF of geosynthetic Wall 1 Tests 2, 4, and 5.

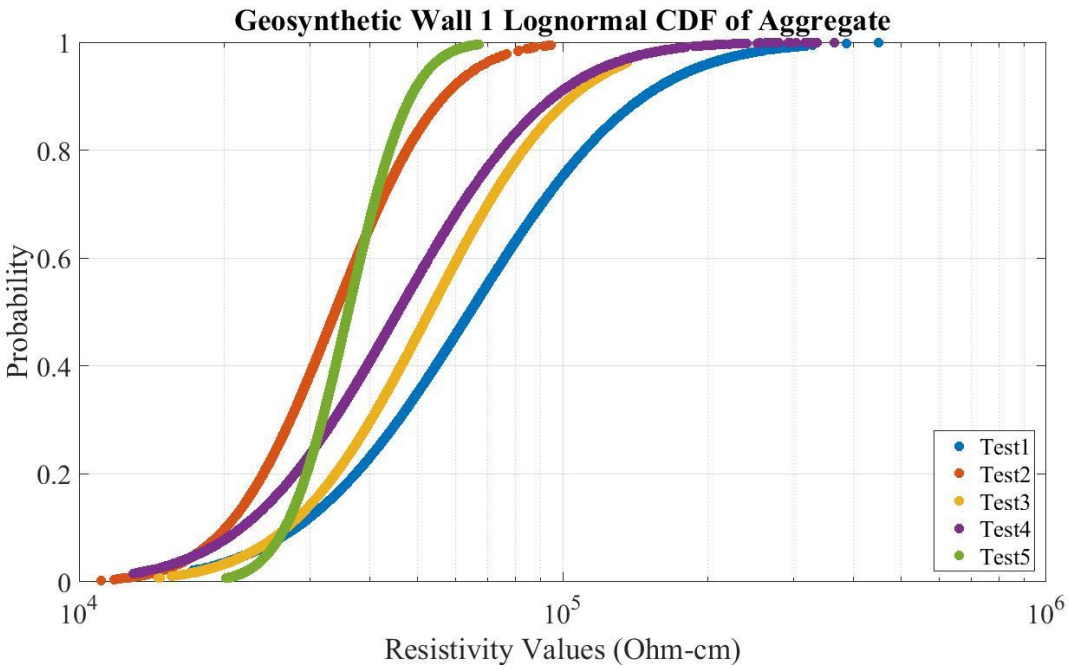

Fig. 4.5. CDF of Geosynthetic Wall 1.

Test 1 and Test 2 were performed in the same region of the wall, with the same array (dipole-dipole), during the same day. The only difference in the two tests was spacing of the electrodes from 0.3 to 0.9 m. Results from Table 4.2 indicate large variability between the two tests: Test 1 had 74,246 Ohm-cm and Test 2 had 38,282 Ohm-cm as a mean.

Test 1 results were near the ground surface where little compaction and construction activity had influenced the region. Due to limited construction activity and compaction, the mean was high and the range of the confidence interval was wide, leading to a shallow slope of the CDF and wide-tailed PDF.

Test 2 provided results with depth in which a majority of the testing profile had overburden weight with added construction activity and compaction to further compact the aggregate, resulting in a lower ER values than Test 1. The PDF had tighter tails then Test 1 and a steeper slope in the CDF, portraying a more uniform profile. A more uniform profile was also observed in the decreased range of confidence interval and lower mean.

Test 3 was performed in the same region as Test 1 and 2. Although the spacing was larger than the previous tests, Test 3 utilized the same array but was closer to the face of the wall (2.13 m compared to 9.1 m). Test 3 results were similar to results of Test 1. The high ER values were

attributed to compaction since this test was performed near the transition between light- and heavy-compaction equipment. Due to limited compaction, uniformity of the wall decreased, as demonstrated by the wide-tailed PDF, shallow-sloped CDF, and wide confidence interval.

Test 4 was performed at a different region of the wall than the previous tests. The Schlumberger inverted array was used at a spacing of 0.6 m, and the test was closer to the face of the wall at 3.1 m than Tests 1 and 2, similar to Test 3. At this distance, a transition occurred from the use of heavy to light-compaction equipment. This region of the wall had larger amounts of construction activity than the previous tests that contributed to increased compaction. Therefore, Test 4 confidence interval, mean, PDF, and CDF ranged in between those for Test 2 and Test 3.

Test 5 had the lowest ER at the site. This test was completed near the area of the first three tests but closer to the face of the wall at 3.1 m. Although light-compaction equipment was used, intense construction activity was ongoing, thereby increasing compaction throughout the wall and producing low ER values. Test 5 had the smallest confidence interval, tightest PDF tails, and steepest slope in the CDF, implying uniformity as demonstrated in the pseudosection (Fig. 3.8).

Geosynthetic Wall 1 results showed that ER imaging generates results more than 10 times greater than AASHTO method T 288-12 results (3,808 Ohm-cm). However, the degree of compaction altered the results, with a continuing trend throughout the other walls. Tests 4 and 5 were used as bulk ER results for Geoysnthetic Wall 1 because they had similar testing procedures, each portrayed a uniform wall, and had 95% confidence (Table 4.3). These tests depicted an ER of 35,000 to 50,000 Ohm-cm (noncorrosive).

Table 4.3. Geosynthetic Wall 1 bulk ER.

Test	Confidence Interval (%)	Sample Mean (Ohm-cm)	Confidence Interval (Ohm-cm)	
			Lower Value	Upper Value
4	95	48,696	47,164	49,506
5	95	36,411	36,164	36,656

4.3.2 Geosynthetic Wall 2: Overpass of 188th Street and Interstate 70

Geosynthetic Wall 2 post-processing results are outlined in Table 4.4. Aggregates from the Geosynthetic Walls 1 and 2 came from the same source. AASHTO test T 288-12 yielded an ER of 3,808 Ohm-cm. Fig. 4.6 represents the PDF, and Fig. 4.7 depicts the CDF of Geosynthetic Wall 2 data.

Table 4.4. Geosynthetic Wall 2 results.

Test	Confidence Interval (%)	Bounds Placed to Remove Outliers in PDF (Ohm-cm)		Sample Mean (Ohm-cm)	Confidence Interval (Ohm-cm)	
		Upper Bound	Lower Bound		Lower Value	Upper Value
6	95	260,290	49,513	117,880	116,070	119,160
7	95	101,350	20,677	49,702	49,033	50,609
8	95	119,410	4,806	29,663	28,147	31,360

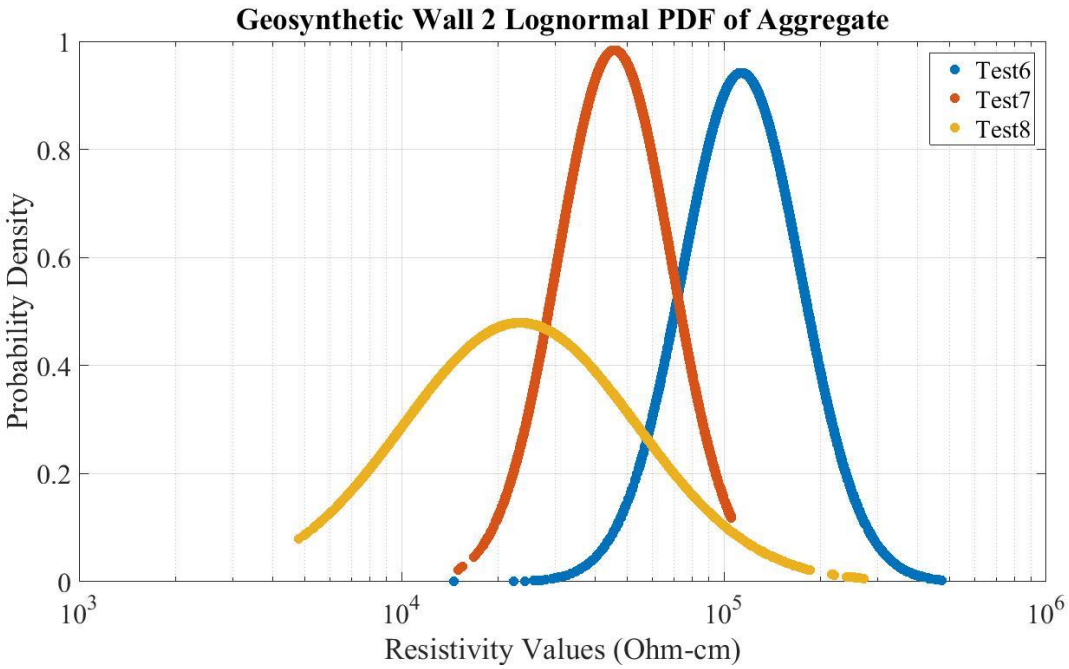

Fig. 4.6. PDF of Geosynthetic Wall 2.

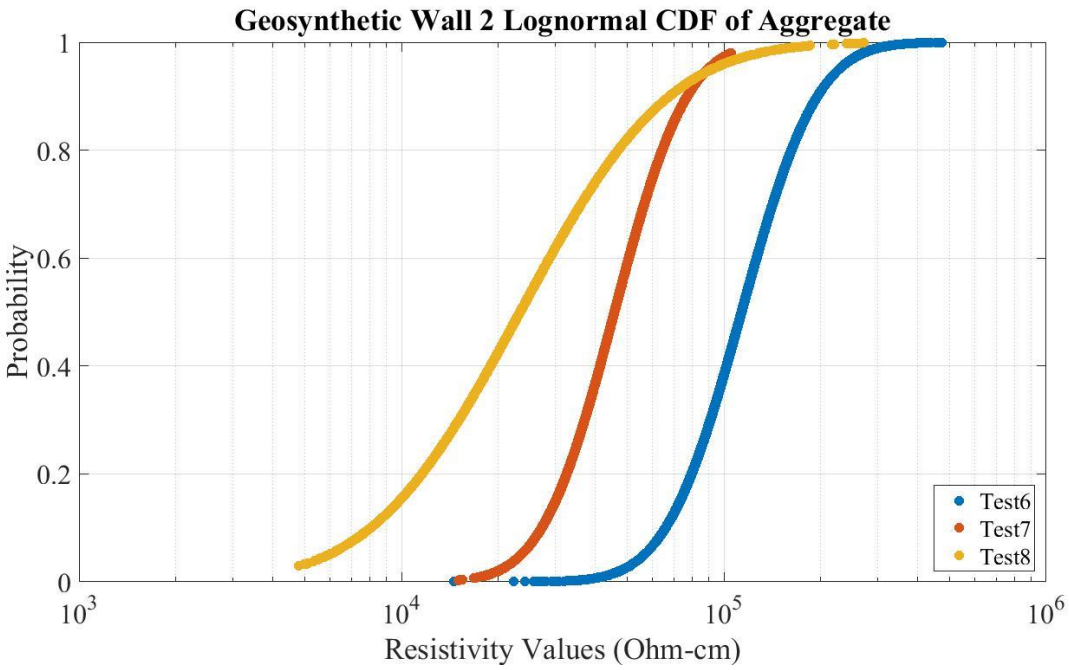

Fig. 4.7. CDF of Geosynthetic Wall 2.

Test 6 had a relatively high ER mean compared to the previous site because only light-compaction equipment was used at the site, testing was close to the walls face, and the test was completed during the early stages of construction when construction activity was light. Test 7 ER was substantially lower than Test 6 because of continued construction and compaction activities on the backfill of the wall. The PDF and CDF were depicted with a small confidence interval, indicating a uniform profile. Test 8 was performed after-construction following a recent rain event in which the aggregate was wet, thereby lowering ER values to below 30,000 Ohm-cm. Due to presence of water, the PDF and CDF were shifted to a lower resistivity.

Geosynthetic Wall 2 post-processing results showed that ER imaging was 10 to 100 times greater than AASHTO test T 288-12 results (3,808 Ohm-cm). Test 7 was taken as the bulk ER result for Geosynthetic Wall 2, and test results, which were similar to Geosynthetic Wall 1 results, were representative of the backfill material, leading to classification of the aggregate as noncorrosive. The wide confidence interval ranges, wide tails of the PDF, and steep slopes of Geosynthetic Wall 2 suggest a less uniform backfill than Geosynthetic Wall 1. This is attributed to the light-compaction equipment, decreased stature of wall, and less construction activity that consequently provided lower compaction. Test 8 showed effect of water decreasing ER imaging results.

Table 4.5. Geosynthetic Wall 2 bulk ER.

Test	Confidence Interval (%)	Sample Mean (Ohm-cm)	Confidence Interval (Ohm-cm)	
			Lower Value	Upper Value
7	95	49,702	49,033	50,609

4.3.3 Metal Wall: Interchange of Ridgeview and Kansas Highway 10

Post-processing results from the MSE wall reinforced with metallic strips are outlined in Table 4.6. AASHTO test T 88-12 showed the ER of the backfill to be 6,036 Ohm-cm. Test data are depicted in the PDF in Fig. 4.8 and the CDF in Fig. 4.9.

Table 4.6. Metal reinforcement wall results.

Test	Confidence Interval (%)	Bounds Placed to Remove Outliers in PDF (Ohm-cm)		Sample Mean (Ohm-cm)	Confidence Interval (Ohm-cm)	
		Upper Bound	Lower Bound		Lower Value	Upper Value
10	95	225,590	693	22,556	19,235	22,048
11	95	131,260	1,754	20,556	19,348	21,213
12	95	71,320	1,839	16,094	15,627	16,957
13	95	162,610	4,632	39,425	38,890	41,569
14	95	260,760	6,693	59,296	58,828	63,075

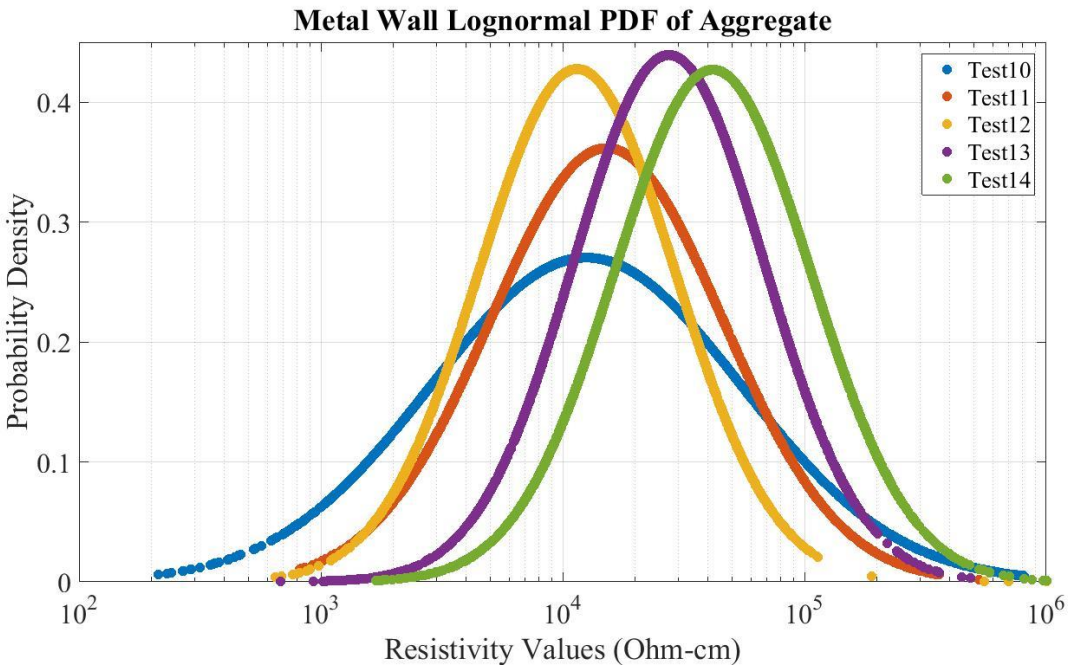

Fig. 4.8. PDF of the metal-reinforced MSE wall.

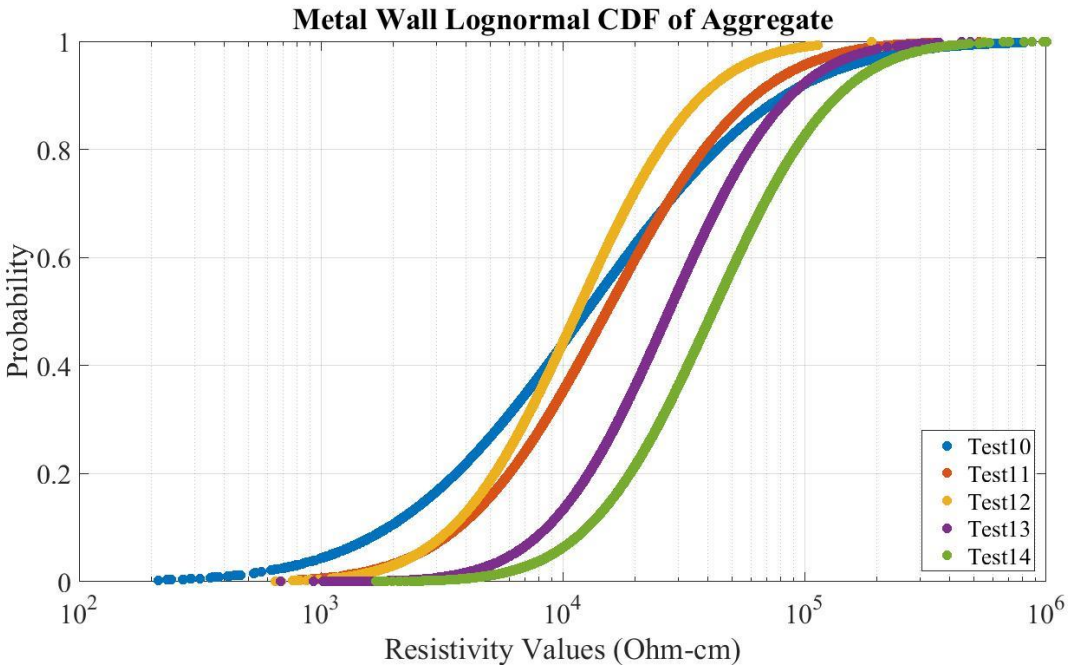

Fig. 4.9. CDF of the metal-reinforced MSE wall.

Wide tails in the PDF and shallow slopes of the CDF support wider confidence intervals as compared to those in previous testing. Tests 10 through 13 were performed 3.1 m from the face of the wall, while Test 14 was performed only 0.6 m. Tests 10 and 11 showed lower ER results

than Geosynthetic Walls 1 and 2 due in part to the metallic reinforcement and water present in the wall from recent rains. Test 12 was performed in a misty rain condition, and results were even lower than results of Tests 10 and 12, implying that water influences ER results. Test 13 was performed when little or no water was present, and results were similar to results from previous tests. The final test at the site, Test 14, was completed near the face of the wall where light-compaction equipment was used, consequently resulting in increased ER values. Because of compaction efforts, ER results near the face of the wall continually trended towards larger values than ER values away from the face.

ER results from the MSE wall with metal reinforcement were more than 10 times greater than results of AASHTO method T 288-12 (6,036 Ohm-cm). The small range of confidence intervals shows that ER imaging provides uniform results of the backfill material. These results, however, vary from test to test due to compaction and the presence of water. Results from Tests 10, 11, and 12 were similar to the results of Test 8 at Geosynthetic Wall 2 where water was present within the wall. Test 14 was performed close to the face of the wall where compaction was limited, thereby providing results comparable to the results of previous testing near faces of MSE walls. Test 13 was used to define the bulk ER of the metal wall; results are outlined in Table 4.7, and the aggregate was classified as noncorrosive. Testing conditions were similar to other tests used to determine the bulk ER from previous walls.

Table 4.7. Metal wall bulk ER.

Test	Confidence Interval (%)	Sample Mean (Ohm-cm)	Confidence Interval (Ohm-cm)	
			Lower Value	Upper Value
13	95	39,425	38,890	41,569

4.3.4 Gravity Wall: Intersection of Haskell Avenue and East 31st Street

Results from the gravity retaining wall are outlined in Table 4.8. AASHTO method T 288-12 results indicated an ER of 3,895 Ohm-cm. The PDF and CDF of the gravity wall are depicted in Fig. 4.10 and Fig. 4.11, respectively.

Table 4.8. Gravity wall results.

Test	Confidence Interval (%)	Bounds Placed to Remove Outliers in PDF (Ohm-cm)		Sample Mean (Ohm-cm)	Confidence Interval (Ohm-cm)	
		Upper Bound	Lower Bound		Lower Value	Upper Value
15	90	743,940	1,391	94,721	110,840	133,290
16	90	146,190	1,100	29,833	32,665	38,142
17	95	257,260	2,046	42,132	41,815	47,708
18	95	39,044	864	9,678	9,538	10,943
19	95	19,882	1,222	6,018	5,932	6,271

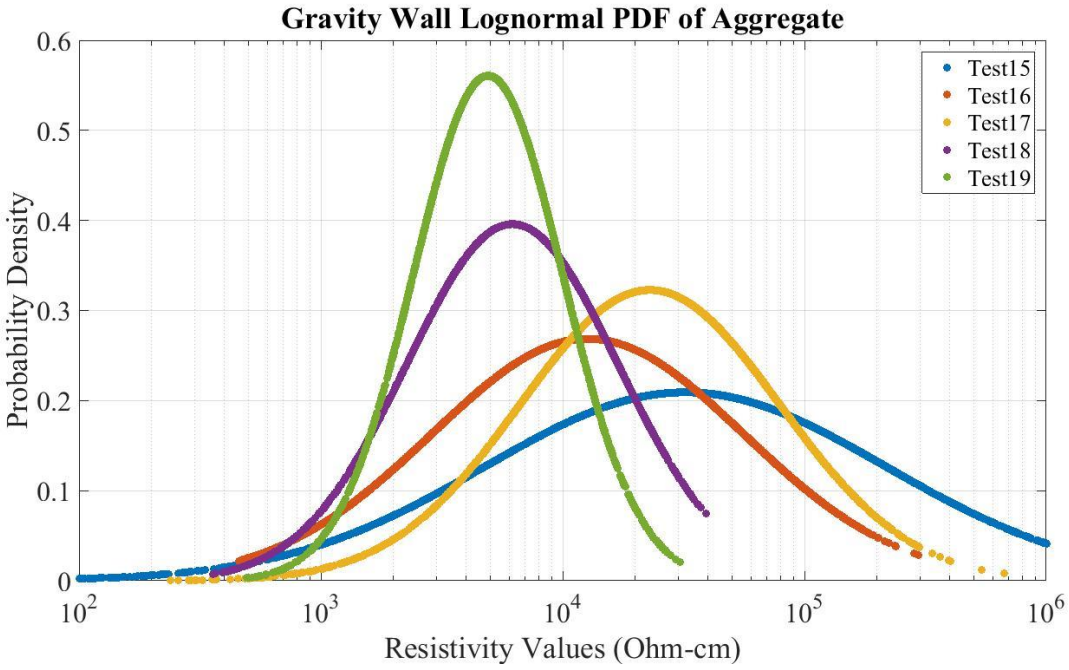

Fig. 4.10. PDF of the gravity wall.

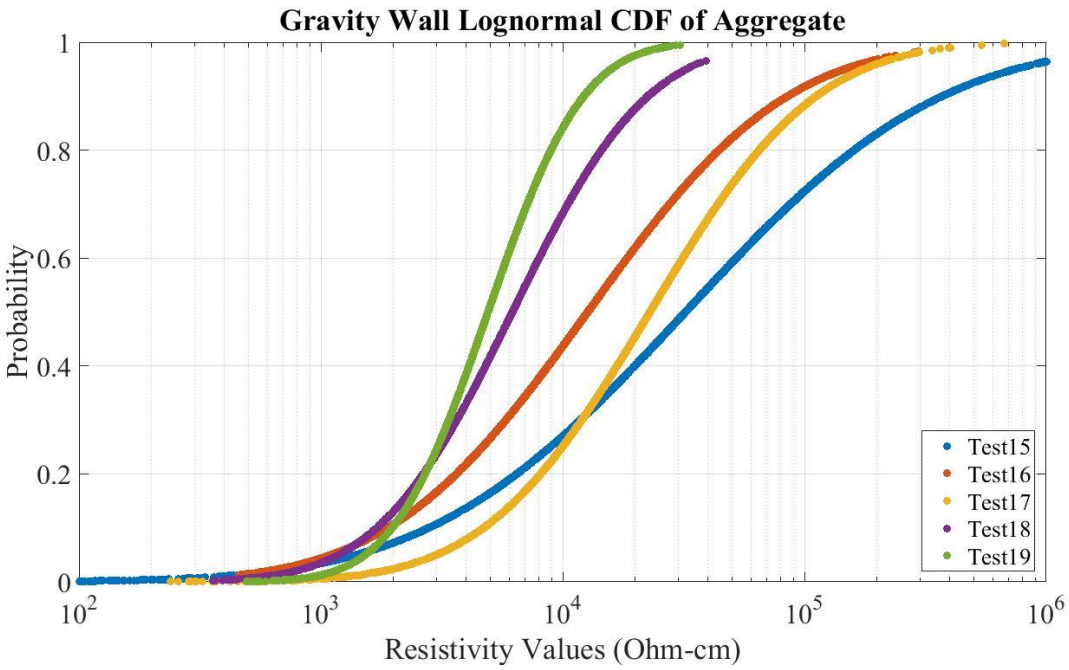

Fig. 4.11. CDF of the gravity wall.

The mean of the result from Test 15 was high and the confidence interval was large due to the frozen ground during testing. Tests 16 and 17 were performed at different sections of the wall: Test 16 was performed in a region in which heavy-compaction equipment was used, and vibratory plate and roller compaction were used in the region of Test 17. Vibratory plate compaction provided lower compaction than the roller, resulting in a higher mean and confidence interval. The extremely low resistant layer below the foundation of the wall influenced values near the foundation and attributed to the lower values and wide confidence intervals observed at the gravity wall in Tests 15 and 16. The final two tests at the site were completed after construction and after a recent heavy rain event. Water present in the backfill lowered the ER values.

Results from the gravity wall produced ER values more than 10 times greater than AASHTO T 288-12 laboratory test. Results from Tests 16 and 17 were similar to those tests from previous walls in which water was not in the backfill and compaction was consistent. Tests 18 and 19 had lower results similar to previous tests in which water was known be present in the backfill. The highly conductive (low resistant) foundation material skewed the results near the base of the wall, causing ER values to be lower than they actually may have been. Test 17 was used to classify the bulk ER of the gravity wall due to the similar testing conditions and the 95%

confidence. Test 17 results are outlined in Table 4.9. The aggregate was classified as noncorrosive.

Table 4.9. Gravity wall bulk ER.

Test	Confidence Interval (%)	Sample Mean (Ohm-cm)	Confidence Interval (Ohm-cm)	
			Lower Value	Upper Value
17	95	42,132	41,815	47,708

4.3.5 Comparison of Test Sites

Post-processing results indicated that ER imaging can provide representative ER data if testing conditions are similar such as electrode spacing, aggregate dryness, and compaction efforts. Compaction effects are better represented by examining results site-by-site, as discussed. In general, the closer the test is to the face of the wall, the lesser the compaction and the higher the ER. Testing further from the wall where heavier compaction equipment is used and intense construction activity is common increases compaction and lowering ER results. The following section examines results of tests performed in similar conditions across sites, including the effects of water.

Fig. 4.12 (PDF) and Fig. 4.13 (CDF) compare the results from Tests 4, 5, 7, 13, and 17, all of which had similar testing conditions with 95% confidence. Most, if not all of the wall had been constructed, the tests were mostly set back from the face of the walls where heavy-compaction equipment was used, and no water was present during testing. Table 4.10 outlines the bulk ER of Tests 4, 5, 7, 13, and 17.

Table 4.10. Tests 4, 5, 7, 13, and 17 bulk ER results.

Test	Confidence Interval (%)	Sample Mean (Ohm-cm)	Confidence Interval (Ohm-cm)	
			Lower Value	Upper Value
4	95	48,696	47,164	49,506
5	95	36,411	36,164	36,656
7	95	49,702	49,033	50,609
13	95	39,425	38,890	41,569
17	95	42,132	41,815	47,708

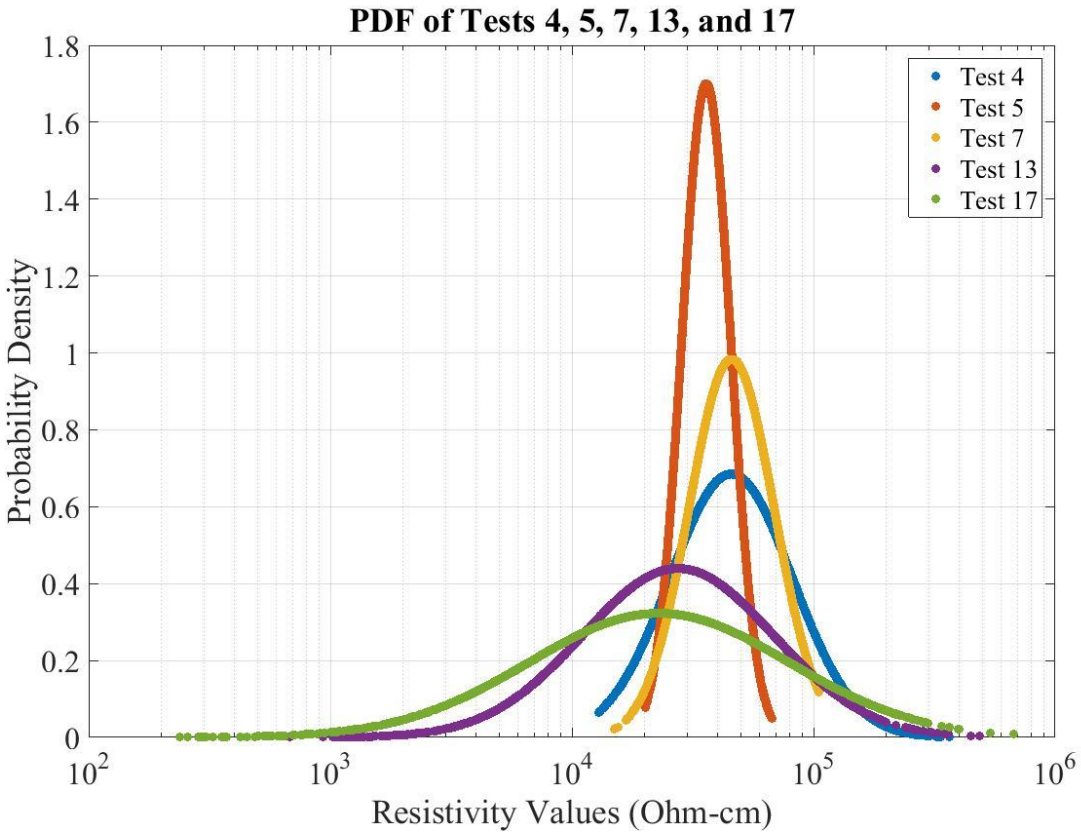

Fig. 4.12. PDF of Tests 4, 5, 7, 13, and 17.

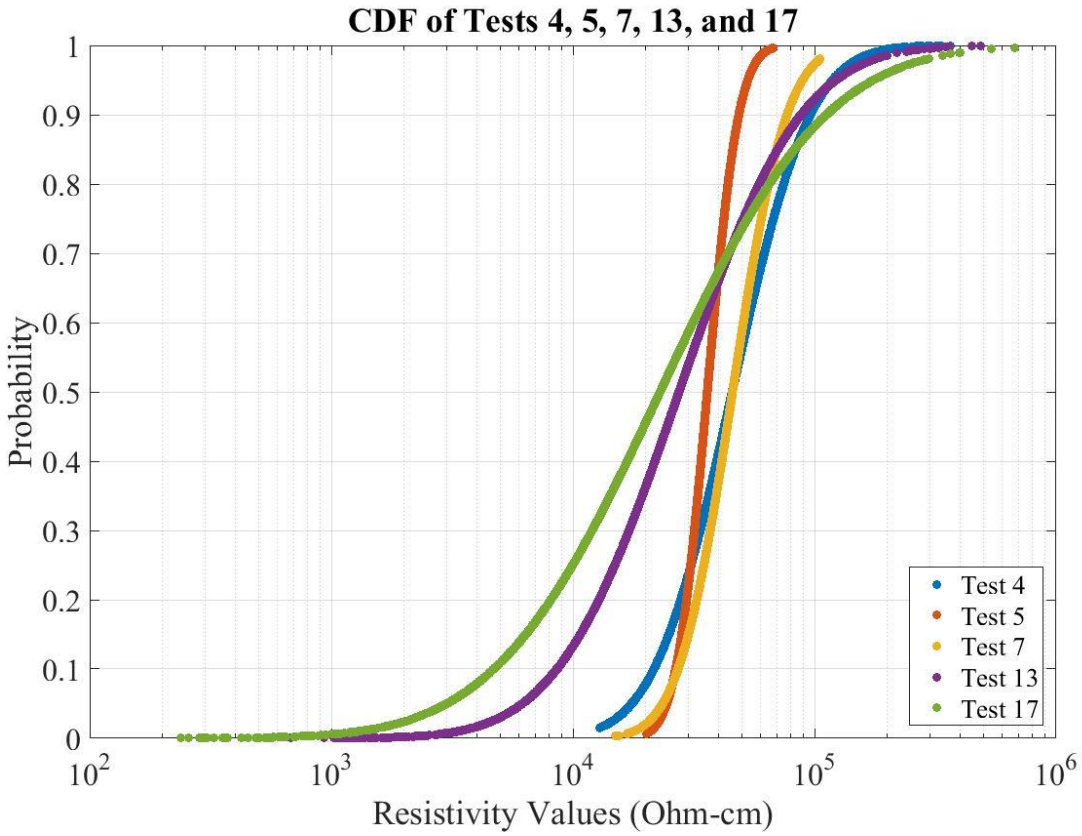

Fig. 4.13. CDF of Tests 4, 5, 7, 13, and 17

Fig. 4.12 and Fig. 4.13 depicts tests performed under similar conditions produce similar results. The means of these eight tests lie within the range of 36,400 to 50,000 Ohm-cm. This range of data is not significant when compared to the ER classification of dry gravel material, which is greater than 20,000 Ohm-cm. Tests 4, 5, and 7 represented a small range in the PDF, and steep slopes in the CDF demonstrated uniformity of the backfill. Test 13 was similar to Tests 4, 5, and 7, but because of the metal reinforcement and presence of fine-grained material, the ER values were lower. Test 17 imaged a highly conductive (low resistance) material below the foundation, which skewed results of the backfill near the foundation, resulting in large variability, as demonstrated by the large-tailed PDF and less steep slope of the line in the CDF.

Fig. 4.14 (PDF) and Fig. 4.15 (CDF) show the effects of water in the backfill. Tests 8, 10, 11, 12, 18, and 19 were known to have water within the wall backfill. Table 4.11 outlines ER post-processing results.

Table 4.11. Tests 8, 10, 11, 12, 18, and 19 bulk ER results.

Test	Confidence Interval (%)	Sample Mean (Ohm-cm)	Confidence Interval (Ohm-cm)	
			Lower Value	Upper Value
8	95	29,663	28,147	31,360
10	95	22,556	19,235	22,048
11	95	20,556	19,348	21,213
12	95	16,094	15,627	16,957
18	95	9,678	9,538	10,943
19	95	6,018	5,932	6,271

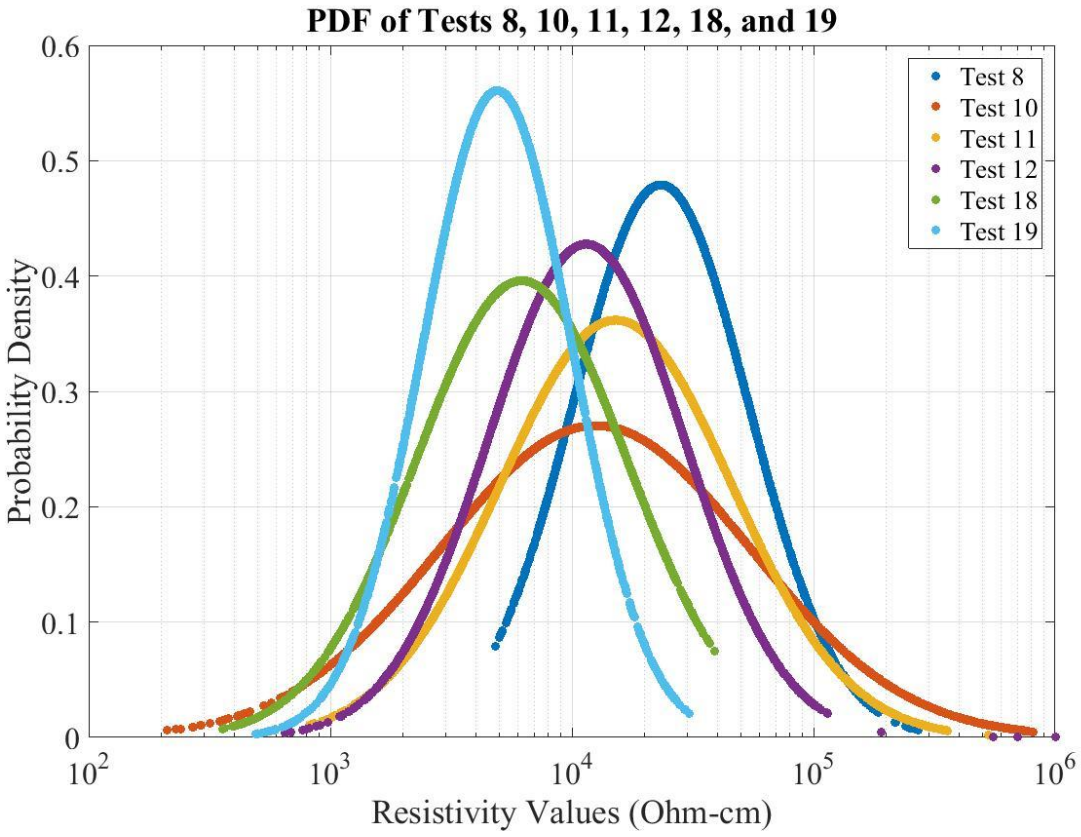

Fig. 4.14. PDF of Tests 8, 10, 11, 12, 18, and 19.

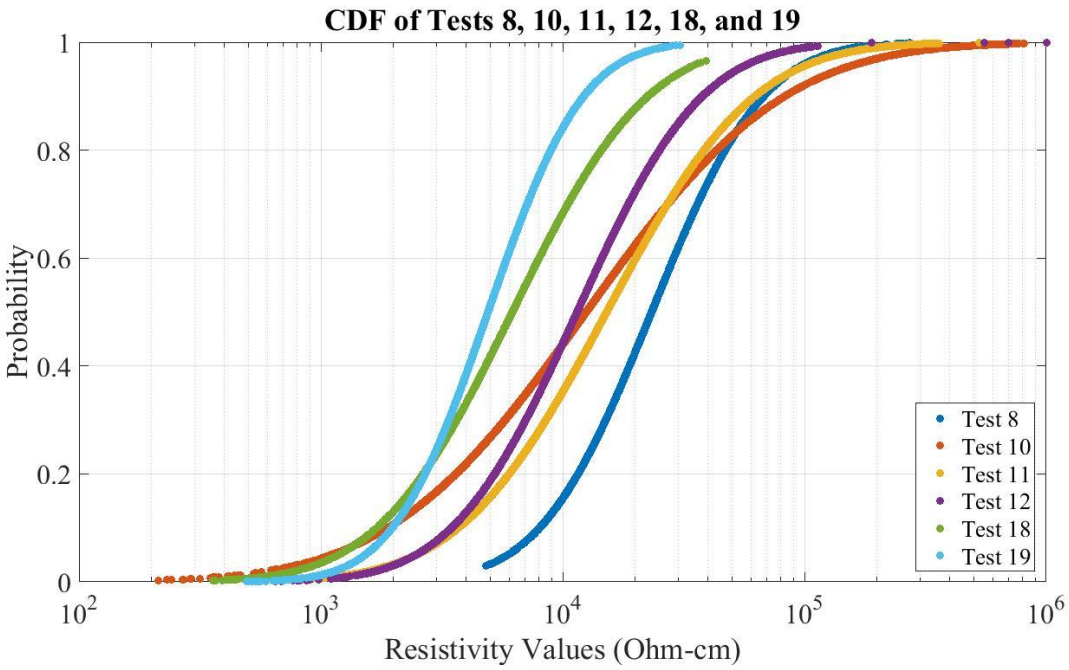

Fig. 4.15. CDF of Tests 4, 8, 10, 11, 12, 18, and 19.

Results of Tests 18 and 19 were extremely low due to low resistive material below the foundation that affected and skewed the ER results within the wall near the base. Based on results of Tests 8, 10, 11, and 12, the mean ranged from 16,000 to 30,000 Ohm-cm. Compared to the previous dry test cases, these four tests demonstrated water's effect of lowering the ER results. Variability of ER results of walls containing water was attributed to the degree of saturation; increased amounts of water provided decreased ER values.

4.3.6 Summary

Post-processing results removed the subjective nature of the EarthImager pseudosections. Results and showed that under similar testing conditions, ER imaging can provide valuable results used to determine the bulk ER of the wall. An ER greater than 20,000 Ohm-cm is representative of gravel material. ER imaging performed under similar testing conditions provided a smaller range between 36,400 to 59,300 Ohm-cm. However, compaction efforts, metallic reinforcement, and the presence of water all influence ER imaging. The effects of water may lower ER imaging values by 50%. Further testing in controlled environments is needed in order to define the effects of compaction, water, and metallic reinforcement.

Chapter 5 Conclusions, Recommendations, and Future Work

5.1 Conclusion

This thesis presents an experimental study that assesses the feasibility of utilizing ER imaging surveys to determine average bulk ER of backfills for earth retaining structures. The bulk ER of the aggregate backfill provides data on the uniformity of the ER during and after construction, corrosion potential, and potentially construction quality assurance information; though more research is needed regards to compaction. A quantitative post-processing algorithm was developed in this research to remove the qualitative uncertainty of ER imaging results and then to provide a bulk ER value. As expected, these results, shown in Table 5.1, are significantly higher than those gathered through laboratory experimentation because the materials and test conditions are different. AASHTO method T 288-12 laboratory test requires that the test sample pass a No. 10 sieve (2.0 mm) and water be added to obtain a minimum resistivity measurement. KDOT uses coarse aggregates as backfill material in many of their retaining walls. The coarse aggregates, do not pass through the No. 10 sieve and instead, AASHTO method T 288-12 is performed on the dust from the aggregates or crushed aggregate materials. These results are considered to be not indicative of the corrosion potential of the aggregates used for MSE walls. AASHTO method T 288-12 also requires a minimum measurement be recorded which is achieved when the material is in a slurry or water-dominated state. These results are also not indicative of the backfill conditions as the backfill should never be fully saturated when proper construction is achieved and water can drain through and away from the retaining walls. If the wall was to be fully saturated there would likely either be damage to the wall or the wall would have failed due to the hydrostatic back pressure. ER imaging also provides information of the entire wall rather than a point source that AASHTO method T 288-12 provides; providing more information on the bulk aggregates.

As seen in this study, ER imaging is a suitable in-situ test method that can produce ER values of aggregate backfill of MSE walls and retaining walls. As seen in Table 5.1, ER from dry and partially saturated conditions are significantly higher and results are not comparable to AASHTO method T 288-12 laboratory results. At this time more data are needed under dry and partially saturated conditions to determine the relationship between AASHTO test T 288-12 results and ER imaging so that the method can be successfully implemented to determine the bulk ER of

retaining walls and identify corrosion potential. With more data, it will be advantageous to use the proposed method because AASHTO test T 288-12 is thought to be overly conservative.

ER imaging was applied to not only MSE walls, but a gravity wall as well. Only one metallic reinforced MSE wall was available for testing. The metallic reinforcement lowered ER measurements due to the conductive nature of the reinforcement, although the effect of the metallic reinforcement dissipates with the depth of imaging. Additional testing is needed to understand the impact of metallic reinforcement on ER imaging. However, the results show that ER imaging is an applicable method. Geosynthetic reinforced MSE walls produced results similar to the gravity wall containing no reinforcement. This implies that the geosynthetic reinforcement has no effect on ER imaging. Additional testing of MSE walls and other retaining walls is required to evaluate the full potential of ER imaging for assessing aggregate corrosion potential.

One limitation of ER imaging is the contact between the electrode stakes and the coarse aggregates. As seen at one of the site, if the backfill aggregate is loosely compacted, the poor contact between the electrodes and the ground will result in a low injection of current and lead to noisy and erroneous ER measurements. Geosynthetic Wall 3 aggregate backfill was loosely compacted producing results significantly higher than the other tested walls (ER of approximately 1,000,000 Ohm-cm). ER imaging must be applied to areas that have recently been compacted. Further research is needed to define the correlation between the level of compaction and ER imaging.

Results of this study demonstrate ER imaging is a suitable in-situ testing method for measuring bulk ER of aggregate backfill of retaining walls. Additionally, ER imaging has the potential to be used as a monitoring technique for retaining walls due its ability to detect variation within the backfill. Further testing is necessary to understand the effects that reinforcement type, partial water saturation, and compaction have on bulk ER of aggregates in order to successfully implement the method for construction monitoring and for determining corrosion potential.

Table 5.1. Summary of bulk ER testing results.

Wall Type	No. of Test	Wet or Dry	Reinforcement	AASHTO T 288-12 (Ohm-cm)	Bulk ER (Ohm-cm)	Corrosion Potential	
						AASHTO T 288-12	Bulk ER
Geosynthetic Wall 1	4	Dry	Geosynthetic	3,808	48,696	Moderate	None
Geosynthetic Wall 2	7	Dry	Geosynthetic	3,808	49,702	Moderate	None
Geosynthetic Wall 2	8	Wet	Geosynthetic	3,808	29,663	Moderate	None
Geosynthetic Wall 3	9	Dry	Geosynthetic	Not provided	Not Applicable		
Metal Reinforced	12	Wet	Metal	6,036	16,094	Mild	None
Metal Reinforced	13	Dry	Metal	6,036	39,425	Mild	None
Gravity Wall	17	Dry	None	3,895	42,132	Moderate	None
Gravity Wall	18	Wet	None	3,895	9,678	Moderate	Mild

5.2 Recommendations

ER imaging can be successfully applied to earth retaining structures that are reinforced with metallic, geosynthetic, or unreinforced for determining bulk in-place ER of the aggregate. The inverted Schlumberger array is recommended due to its shorter duration of approximately 35 minutes. The method also provides good vertical resolution when compared to the Wenner and dipole-dipole processes. It is recommended to maximize electrode spacing to image deeper than the walls height into the native foundation material underneath the wall. However, imaging too much of the native material may alter the results for the aggregates near the base of the wall during the inversion process when native material is highly conductive. It can skew the bulk ER calculation as shown in the testing of the gravity wall. 3D testing is not recommended as the duration of the testing time dramatically increases with minimal extra data gain.

ER imaging should be done near or at the end of construction. Testing during earlier construction stages provides minimal data, especially for a small retaining wall. Depending on the size of the retaining wall, ER imaging may require construction to be halted during testing. The effects of continued construction activity, compaction of each layer, and the weight of each additional layer further the compaction and alter the ER imaging results. If possible, it is recommended that testing be performed when the backfill is known to be dry and also when known to be partially saturated to determine the corrosion potential under different conditions. Further testing is needed in varying conditions (varying partial saturations). It is anticipated that the dry and partial saturation conditions will be analyzed in a complimentary laboratory study to fully understand the influence water has on bulk ER of aggregates.

Surface compaction influences ER imaging with higher compaction allowing increased injection of current into the ground and diminished noisy data. Bulk ER values decrease with the increase of compaction and vice versa. It is recommended that survey be run at the end of construction when compaction should be more uniform so the ER of the aggregate itself can be determined. The contact resistance test performed prior to any ER imaging survey is important and should not be ignored. This study determined contact resistance values between 0 and 20,000 Ohm allow enough current into the ground to provide quality data typically with lower RMS and low noise. Current in between 20,000 to 40,000 Ohm typically ensures enough current for ER measurements, but decreases the accuracy of the results, leading to higher RMS, increase in data

noise, and higher ER results. Contact resistance results above 40,000 Ohm does not provide enough current to receive reliable data that becomes too noisy for interpretation in the event of poor compaction. It is advised that the test be moved to another section of the wall with recent compaction. The more contact between the electrode stake and the gravel, the greater the current supplied to the ground and the more accurate the measurement.

Performing ER after completion of the retaining wall is favored because the native material placed over the aggregates is typically finer-grained providing better contact, increased injected current, and less noisy and erroneous ER measurements. However, few tests were performed in this study after construction, and the testing followed recent rains. More post-construction tests are needed.

Based upon the limited data gathered during this study, it is recommended that the corrosion potential be reevaluated for coarse aggregates. AASHTO test T 288-12 results are not indicative of coarse aggregates KDOT uses as MSE wall backfill materials. The test requires the soil sample to pass through a No. 10 sieve and a minimum ER value be determined which is achieved at saturation. Table 5.2 outlines an update to the corrosion potential for coarse aggregates. Note that no testing was performed in a very corrosive or corrosive environment.

Table 5.2. Corrosion potential using ER imaging.

Test Method	**T 288-12**	**ER Imaging**
Aggressiveness	**Resistivity (Ohm-cm)**	
Very corrosive	<700	Unknown
Corrosive	700 to 2,000	Unknown
Moderately corrosive	2,000 to 5,000	10,000 to 20,000
Mildly corrosive	5,000 to 10,000	20,000 to 40,000
Noncorrosive	>10,000	>40,000

5.3 Future Work

Additional ER imaging testing of MSE walls with varying types of reinforcement is needed to further define the effects of reinforcement. Only one wall containing metallic reinforcement

was made available by KDOT for testing in this study. The other MSE walls were geosynthetically reinforced, which appeared to have no effect to the results as compared to an unreinforced structure, though more tests are needed. Similarly, Test of aggregates that is thought to be corrosive is needed to better define ER of AASHTO test 288-12.

The walls tested in this study had many different compaction methods which affected the ER results. More testing in a controlled environment with varying types of compaction equipment is required to further define the correlation that exists between compaction and ER. Further testing is needed with varying proximity to the face of the wall utilizing the same compaction method to ensure that compaction is the cause of varying ER results rather than the proximity to the face to the wall.

ER imaging was also performed after and during rain events with water known to be present within the backfill, lowering ER results. It is advised that further testing be completed to fully understand the correlation of water and water chemistry to ER and corrosion potential. Ideally, it is recommended that partial water saturation be tested to determine the effects water has on ER imaging.

Contractors and agencies unrelated to KDOT construct MSE and retaining walls utilizing material other than coarse aggregates for backfill. It is suggested that these walls with material other than coarse aggregate be tested as results will be significantly different from this study. The field method should be applied to retaining walls that have or are failing to determine possible irregularities between non-failure and failed walls and other buried structures. ER imaging has the potential to be used as a monitoring technique for not only retaining wall structures, but also for other buried infrastructure, such as pipes.

Results from this study need to be compared to a complementary study which expands AASHTO T 288-12 testing scope by increasing the size of the testing box and performing tests in a saturated state of the coarse aggregates rather than the finer materials and. Based upon the results from this particular study, compaction, varying types of reinforcement (metallic and geosynthetic), partial water saturation, and water chemistry should be analyzed to determine their effect in a controlled laboratory setting. Material other than coarse aggregates should also be tested as other agencies than KDOT may use non-aggregate materials for backfill which would produce different results than those seen in this study.

References

AGI. (2007). *EarthImager 2D Resistivity and IP Inversion Software Instruction Manual,* Advanced Geosciences, Inc., Austin, Texas.

Arjwech, R., Everett, M., Briaud, J., Hurlebaus, S., Cetina, Z., Tucker, S., Yousefpour, N. (2013). "Electrical Resistivity Imaging of Unknown Bridge Foundations." *Near Surface Geophysics,* 11(6), 591-598.

Armour, T., Bickford, J., Pfister, T. (2004). "Repair of failing MSE railroad bridge abutment." American Society of Civil Engineers, 380-394.

ASTM. (2012). *Standard Test Method for Measurement of Soil Resistivity using the Two-Electrode Soil Box Method (G187 12a),* American Society of Testing Materials.

ASTM. (2006). *Standard Test Method for Field Measurement of Soil Resistivity using the Wenner Four-Electrode Method,* American Society of Testing Materials, .

Baecher, G. B., and Christian, J. T. (2005). *Reliability and Statistics in Geotechnical Engineering,* John Wiley & Sons.

Bai, W., Kong, L., Guo, A. (2013). "Effects of Physical Properties on Electrical Conductivity of Compacted Lateritic Soil." *Journal of Rock Mechanics and Geotechnical Engineering,* 5(5), 406-411.

Bernstone, C., Dhalin, T., Ohlsson, T., Hogland, W. (2000). "DC-Resistivity Mapping of Internal Landfill Structures: Two Pre-Excavation Surveys." *Environmental Geology,* 39(3-4), 360-371.

Chambers, J. E., Wilkinson, P. B., Penn, S., Meldrum, P. I., Kuras, O., Loke, M. H., Gunn, D. A. (2013). "River Terrace Sand and Gravel Deposit Reserve Estimation using Three-Dimensional Electrical Resistivity Tomography for Bedrock Surface Detection." *Journal of Applied Geophysics,* 93(0), 25-32.

De Carlo, L., Perri, M. T., Caputo, M. C., Deiana, R., Vurro, M., Cassiani, G. (2013). "Characterization of a Dismissed Landfill via Electrical Resistivity Tomography and Mise-À-La-Masse Method." *Journal of Applied Geophysics,* 98(0), 1-10.

Devore, J. (2004). *Probability and Statistics for Engineering and Sciences,* 6th Ed., Thomson Learning, Inc., Canada.

Edwards, L. (1977). "A Modified Pseudosection for Resistivity and IP." *Geophysics,* 42(5), 1020-1036.

Elias, V., Fishman, K. L., Chrisopher, B. R., Berg, R. R. (2009). *Corrosion/Degradation of Soil Reinforcements for Mechanically Stabilized Earth Walls and Reinforced Soil Slopes*, US Department of Transportation Federal Highway Administration, Washington, DC.

FHWA. (2015). "Geotechnical engineering." <http://www.fhwa.dot.gov/engineering/geotech/> 2015).

Furman, A., Ferre, T., Warrick, A. (2003). "A Sensitivity Analysis of Electrical Resistivity Tomography Array Types using Analytical Element Modeling." *Vadose Zone Journal*, 2(3), 416-423.

Google Maps, 2013.

Hallof, P. (1957). *On the Interpretation of Resistivity and Induced Polarization Measurements*, Massachusetts Institute of Technology, Department of Geology and Geophysics.

KDOT. (2007). "KDOT geotechnical manual." <https://www.ksdot.org/descons.asp> 2014).

Knight, R. J., and Endres, A. L. (2005). "An Introduction to Rock Physics Principles for Near-Surface Geophysics." *Near Surface Geophysics*, Society of Exploration Geophysics, Tulsa, Ok, 31-70.

LaBrecque, D. J., Miletto, M., Daily, W., Ramirez, A., Owen, E. (1996). "The Effects of Noise on Occam's Inversion of Resistivity Tomography Data." *Geophysics*, 61(2), 538-548.

Loke, M. H. (1999). *Electrical Imaging Surveys for Environmental and Engineering Studies*.

Lowrie, W. (2007). "Earth's Age, Thermal and Electrical Properties." *Fundamentals of Geophysics*, Cambridge University Press, UK, 207-280.

Lucius, J. E., Abraham, J. D., Burton, B. L. (2008). *Resistivity Profiling for Mapping Gravel Layers that may Control Contaminant Migration at the Amargosa Desert Research Site, Nevada*, US Geological Survey, Reston, VA.

Lucius, J. E., Langer, W., Ellefsen, K. J. (2007). *An Introduction to using Surface Geophysics to Characterize Sand and Gravel Deposits*, US Geological Survey, Reston, VA.

McInnis, D., Silliman, S., Boukari, M., Yalo, N., Orou-Pete, S., Fertenbaugh, C., Sarre, K., Fayomi, H. (2013). "Combined Application of Electrical Resistivity and Shallow Groundwater Sampling to Assess Salinity in a Shallow Coastal Aquifer in Benin, West Africa." *Journal of Hydrology*, 505(1), 335-345.

Moylan, J. (2012). "Hydrostatic failure of an MSE wall; associated change in groundwater regime caused damage to a nearby residence." *Proc., 55th Annual Meeting of Association of Engineering Geologists,* Salt Lake City, Utah.

Nenna, V., Pidlisecky, A., Knight, R. (2011). "Informed Experimental Design for Electrical Resistivity Imaging." *Near Surface Geophysics,* 9(5), 469-482.

Reinforced Earth. "Determining the resistivity of MSE backfills through correct implementation of AASHTO T288-12." <http://www.reinforcedearth.com/sites/default/files/resistivity_flyer_reco_.pdf> 2015).

Stummer, P., Maurer, H., Green, A. G. (2004). "Experimental Design: Electrical Resistivity Data Sets that Provide Optimum Subsurface Information." *Geophysics,* 69(1), 130-139.

Thapalia, A., Borrok, D., Nazarian, S., Garibay, J. (2011). "Assessment of Corrosion Potential of Coarse Backfill Aggregates for Mechanically Stabilized Earth Walls." *Transportation Research Board,* 2253, 63-72.

Thornley, J. D., and Siddharthan, R. V. (2010). "Effects of corrosion aggressiveness on MSE wall stability in nevada." *Proc., 2010 Earth Retention Conference,* American Society of Civil Engineers, Bellevue, Washington, 539-547.

Vaudelet, P., Schmutz, M., Pessel, M., Franceschi, M., Guérin, R., Atteia, O., Blondel, A., Ngomseu, C., Galaup, S., Rejiba, F., Bégassat, P. (2011). "Mapping of Contaminant Plumes with Geoelectrical Methods. A Case Study in Urban Context." *Journal of Applied Geophysics,* 75(4), 738-751.

Zhou, Q. Y., Shimada, J., Sato, A. (2001). "Three Dimensional Spatial and Temporal Monitoring of Soil Water Content using Electrical Resistivity Tomography." *Water Resources Research,* 37(2), 273-285.

Zonge, K., Wynn, J., Urquhart, S. (2005). "Resistivity, Induced Polarization, and Complex Resistivity." *Near Surface Geophysics,* Society of Exploration Geophysics, Tulsa, OK, 265-300.

Appendix A Geosynthetic Wall 1

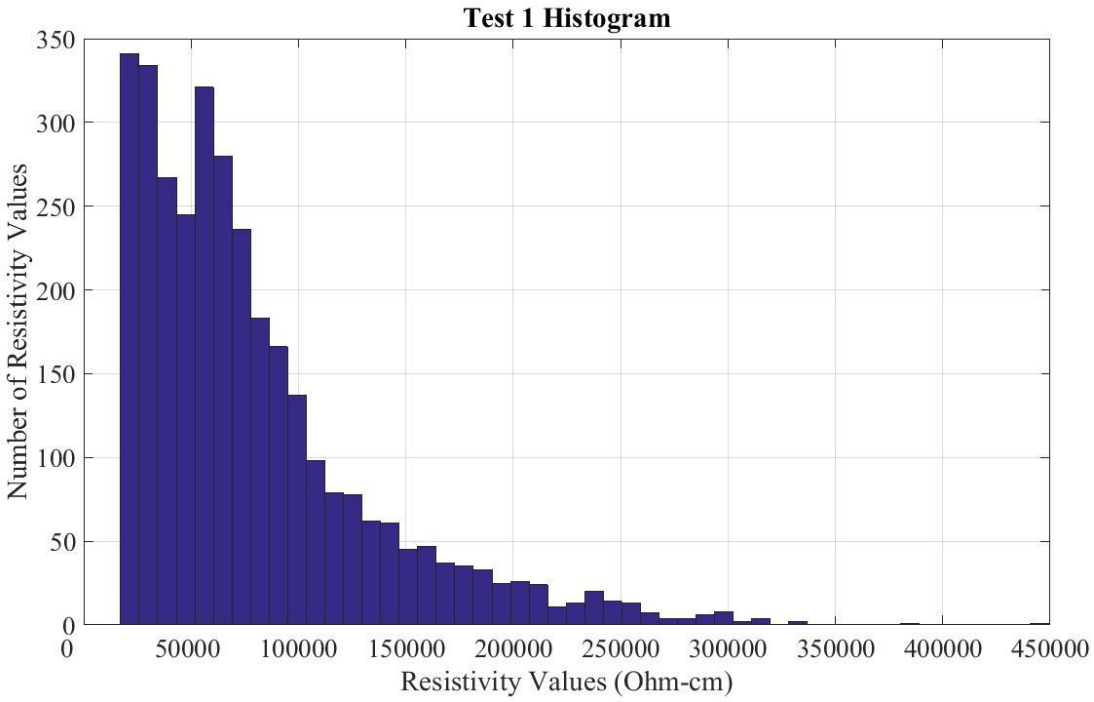

Fig. A.1. Test 1 histogram.

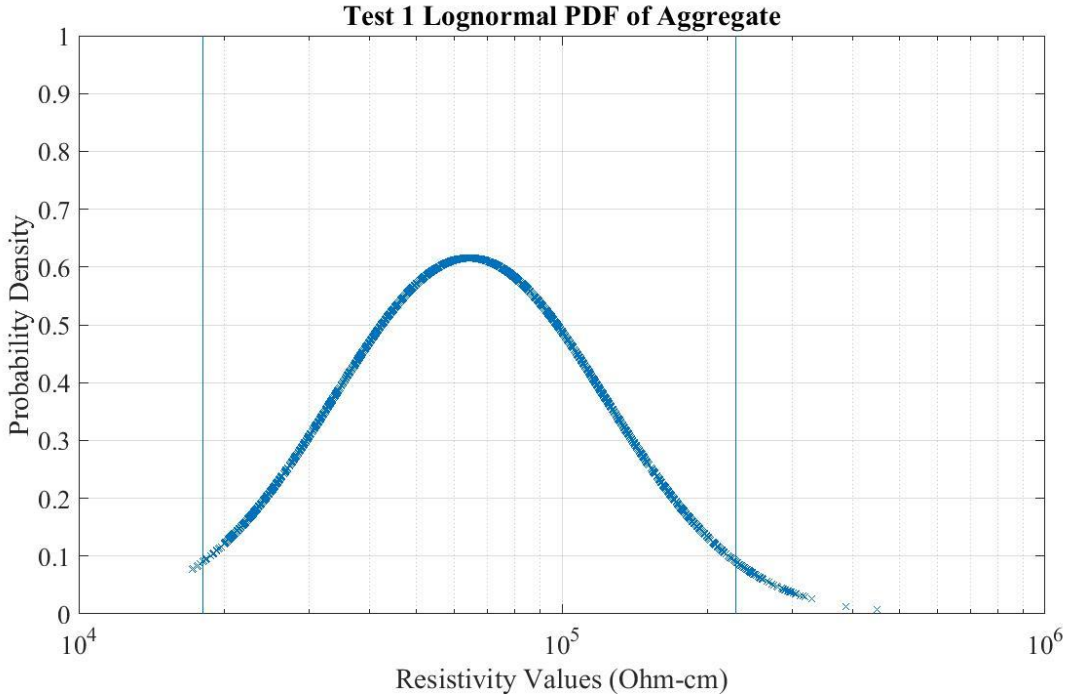

Fig. A.2. Test 1 PDF.

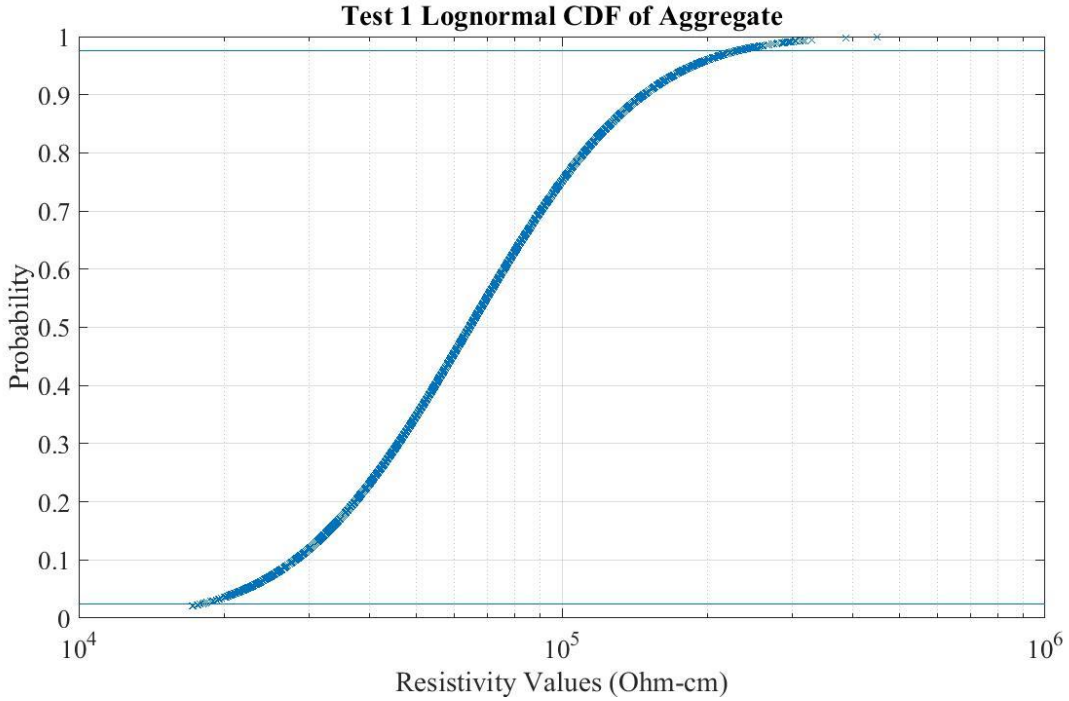

Fig.A.3. Test 1 CDF.

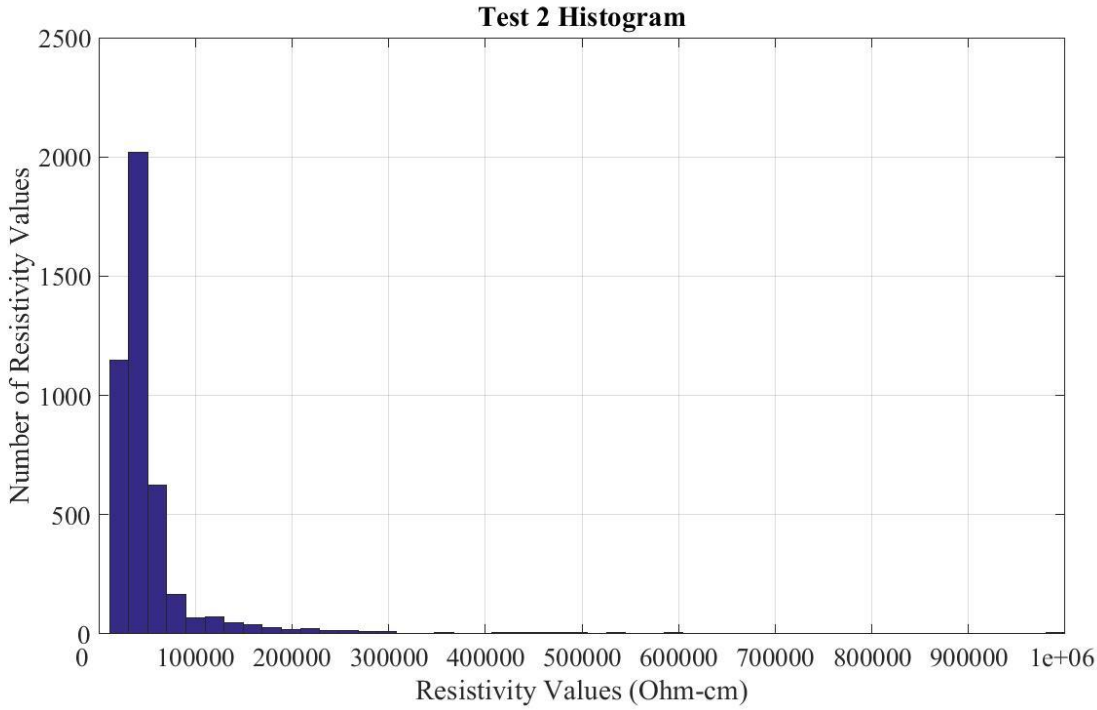

Fig.A.4. Test 2 Histogram.

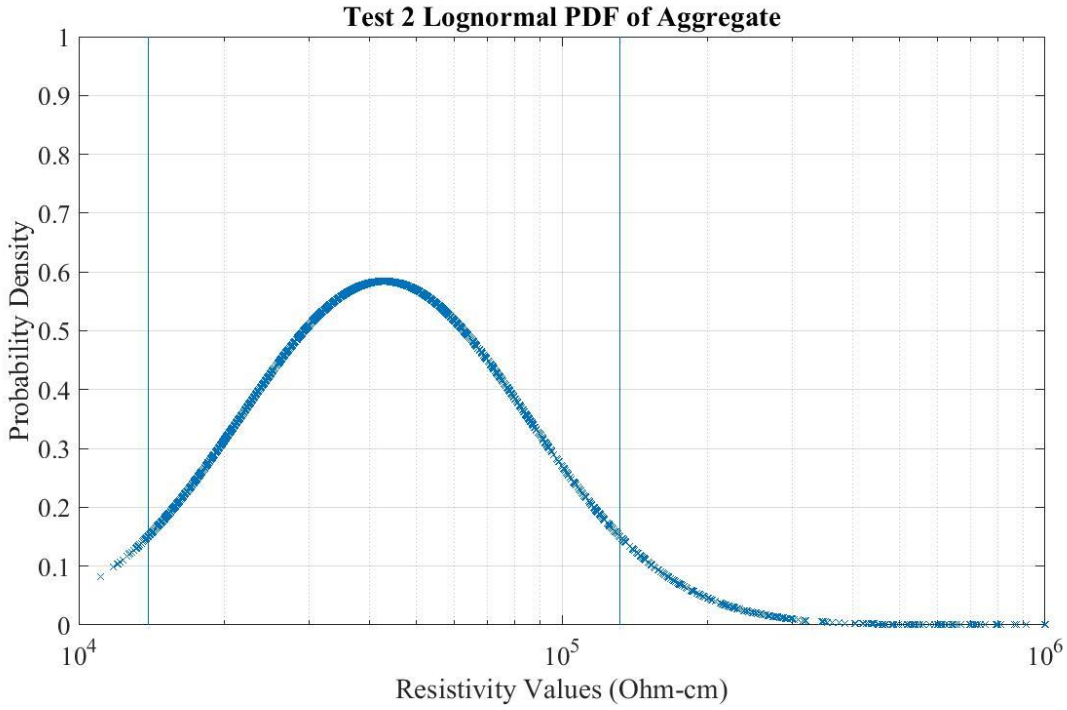

Fig.A.5. Test 2 PDF.

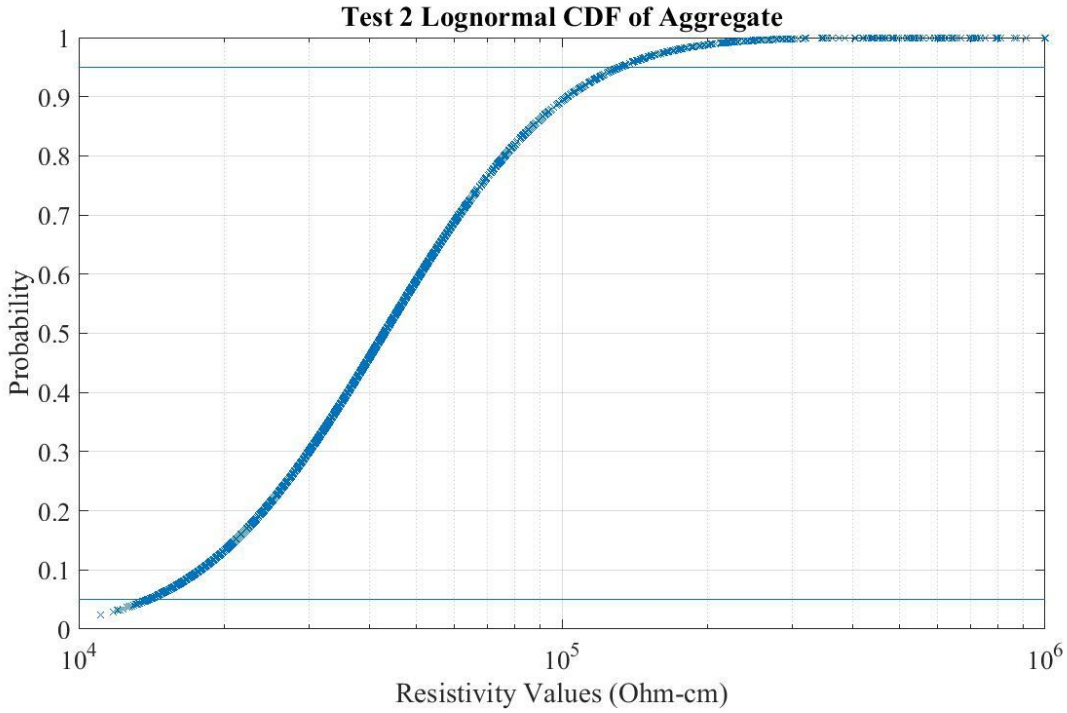

Fig. A.6. Test 2 CDF.

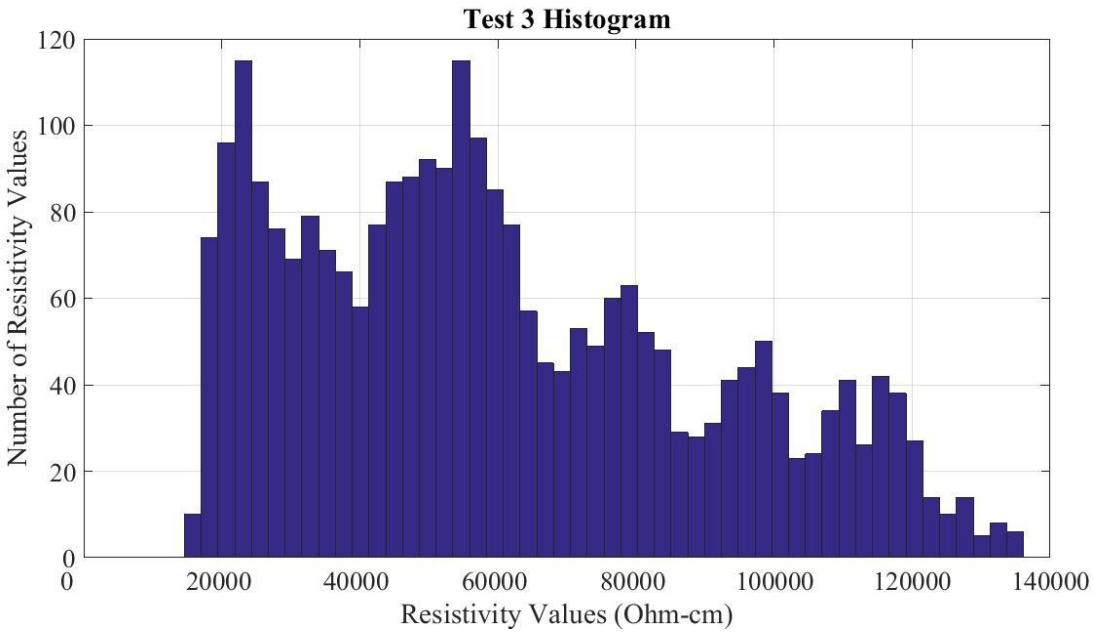

Fig. A.7. Test 3 Histogram.

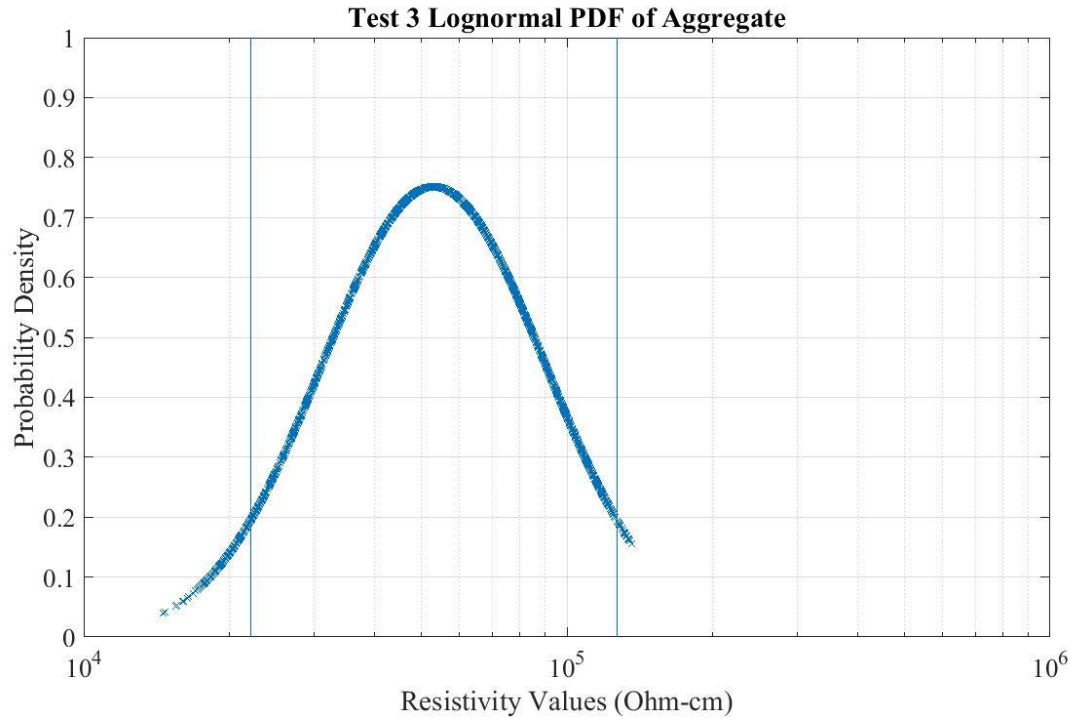

Fig. A.8. Test 3 PDF.

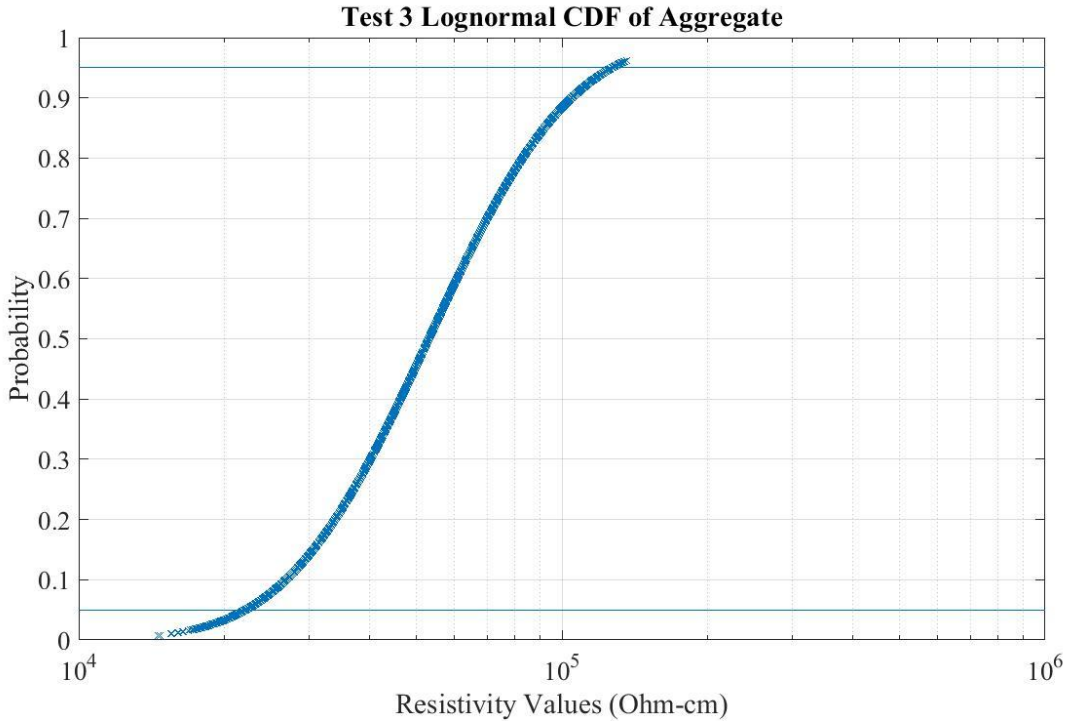

Fig. A.9. Test 3 CDF.

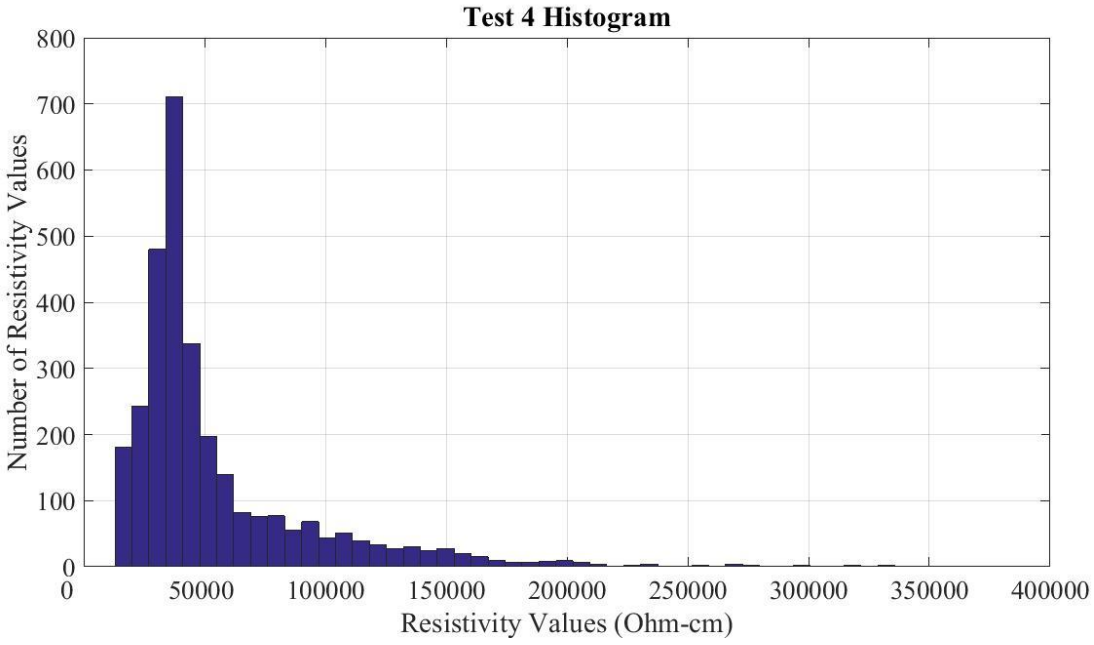

Fig. A.10. Test 4 Histogram.

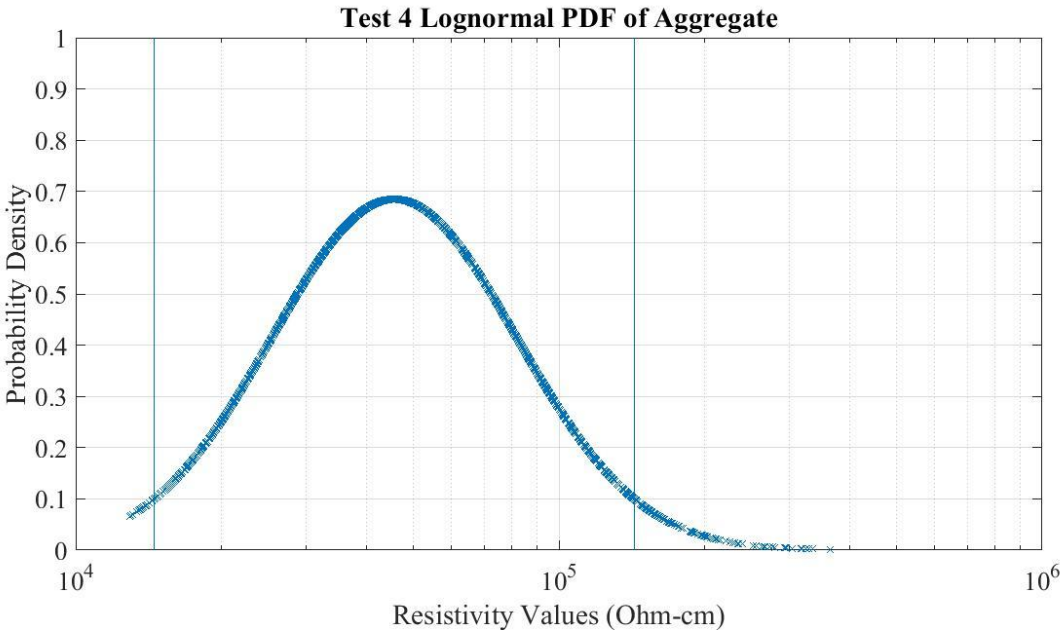

Fig. A.11. Test 4 PDF.

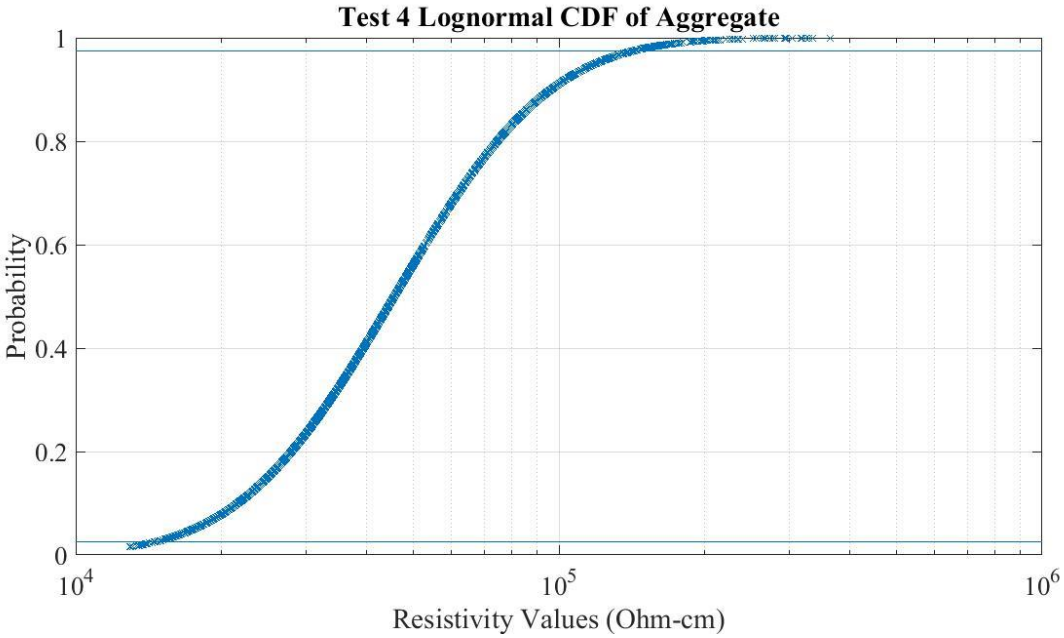

Fig. A.12. Test 4 CDF.

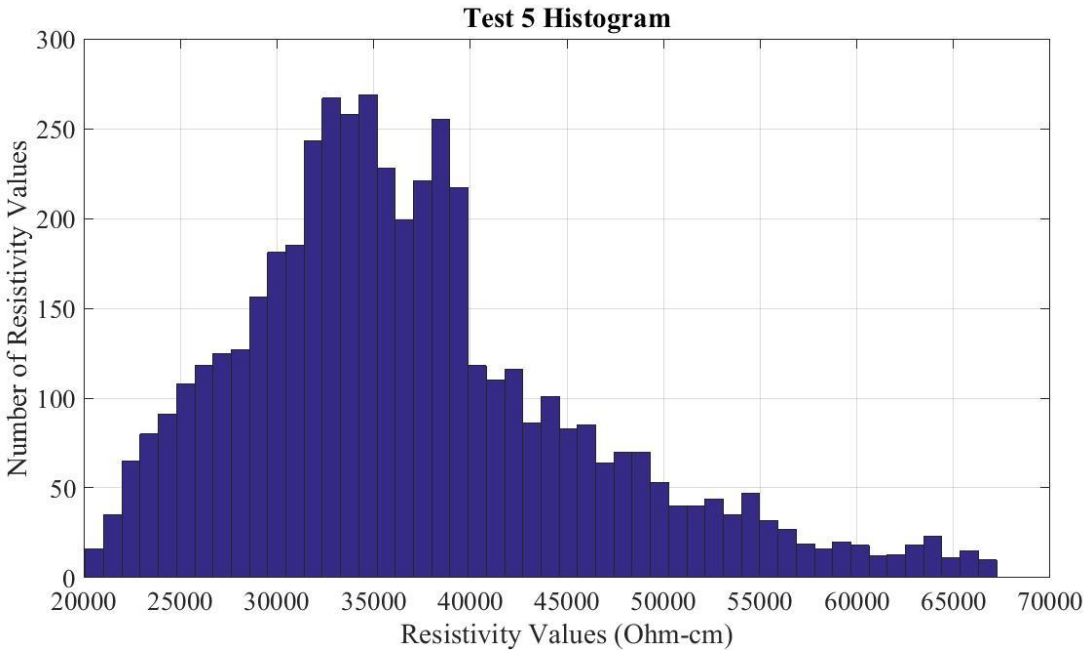

Fig. A.13. Test 5 Histogram.

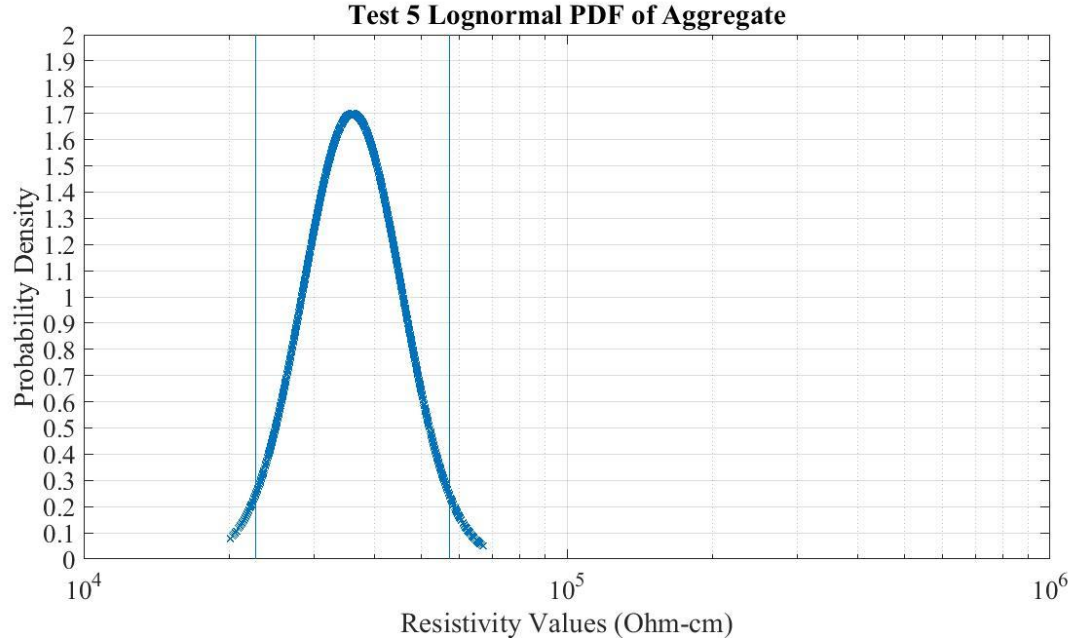

Fig. A.14. Test 5 PDF.

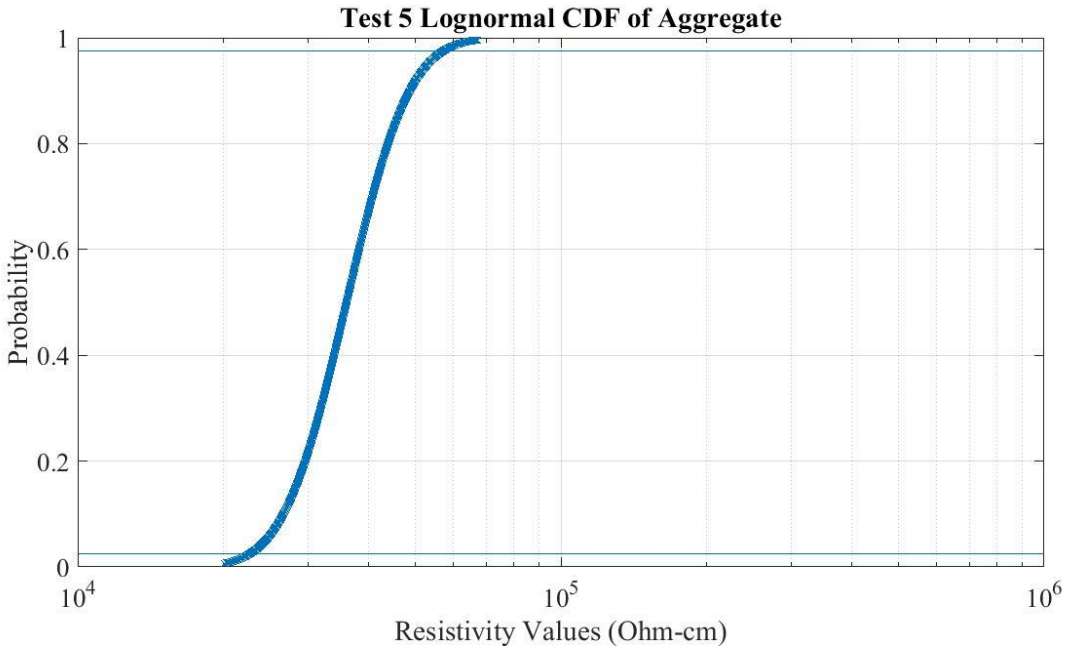

Fig. A.15. Test 5 CDF.

Appendix B Geosynthetic Wall 2

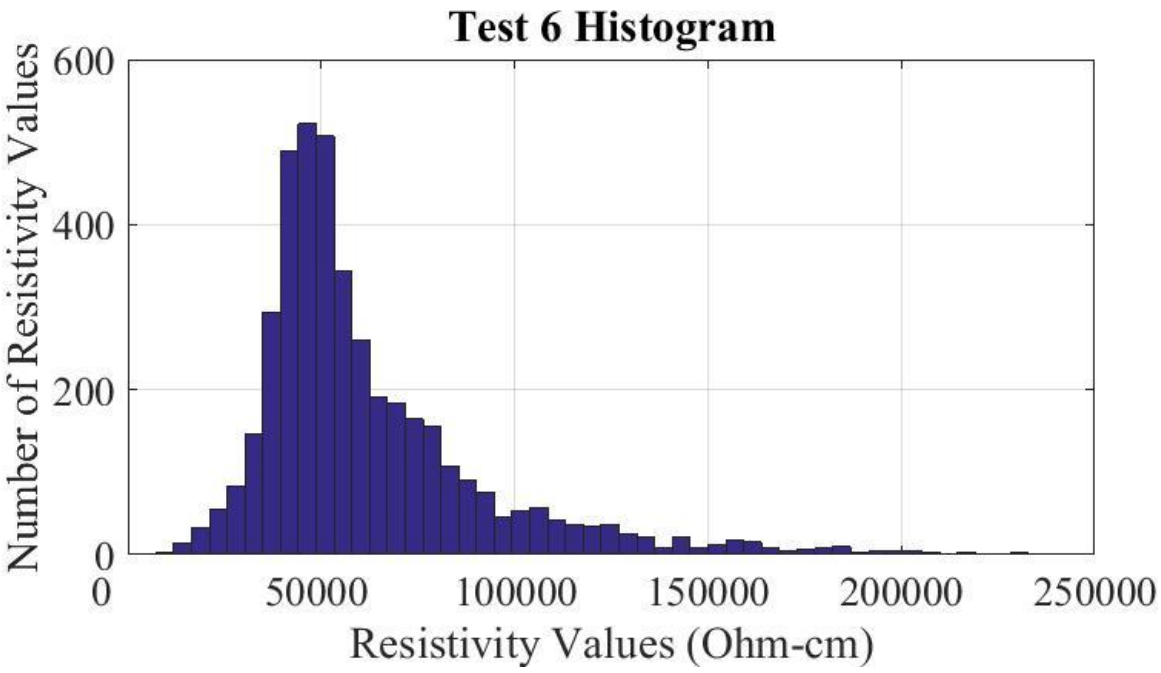

Fig. B.1. Test 6 Histogram.

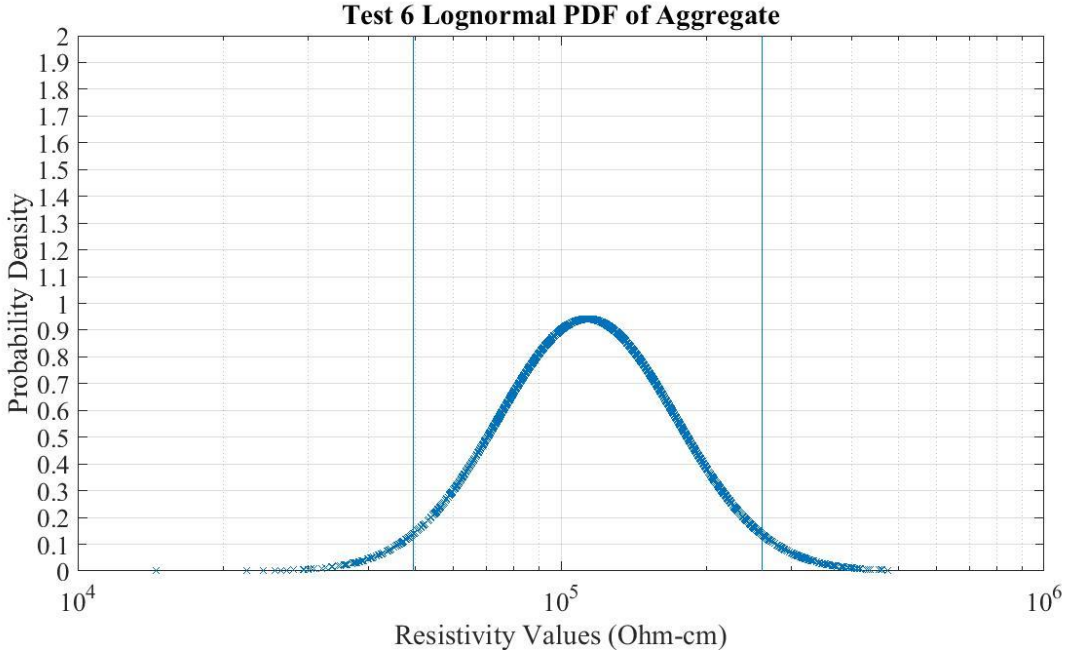

Fig. B.2. Test 6 PDF.

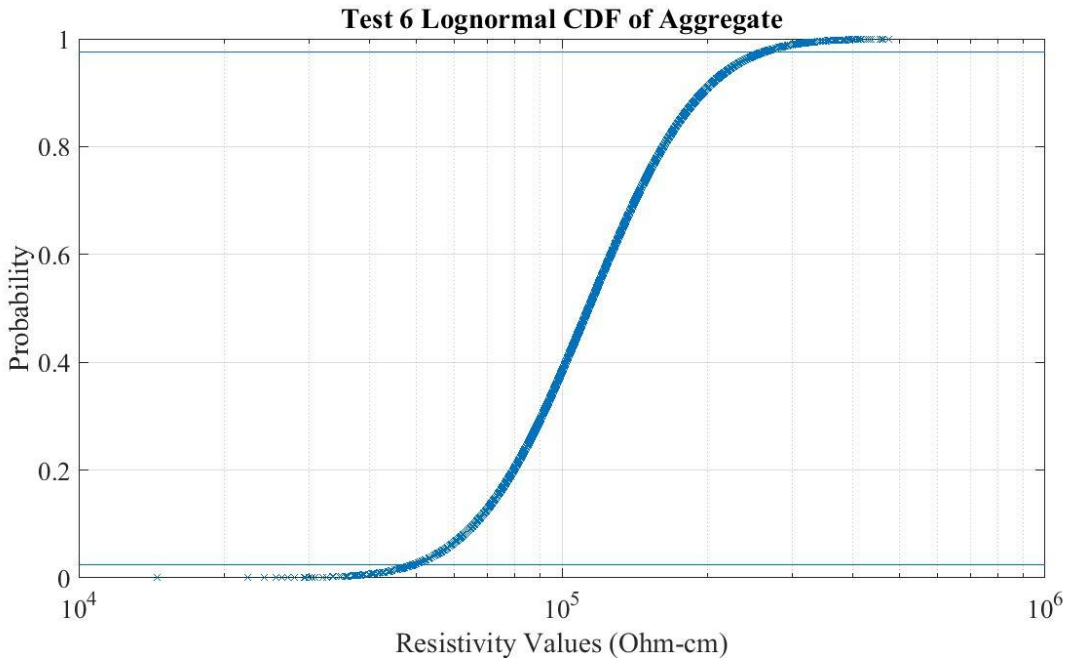

Fig. B.3. Test 6 CDF.

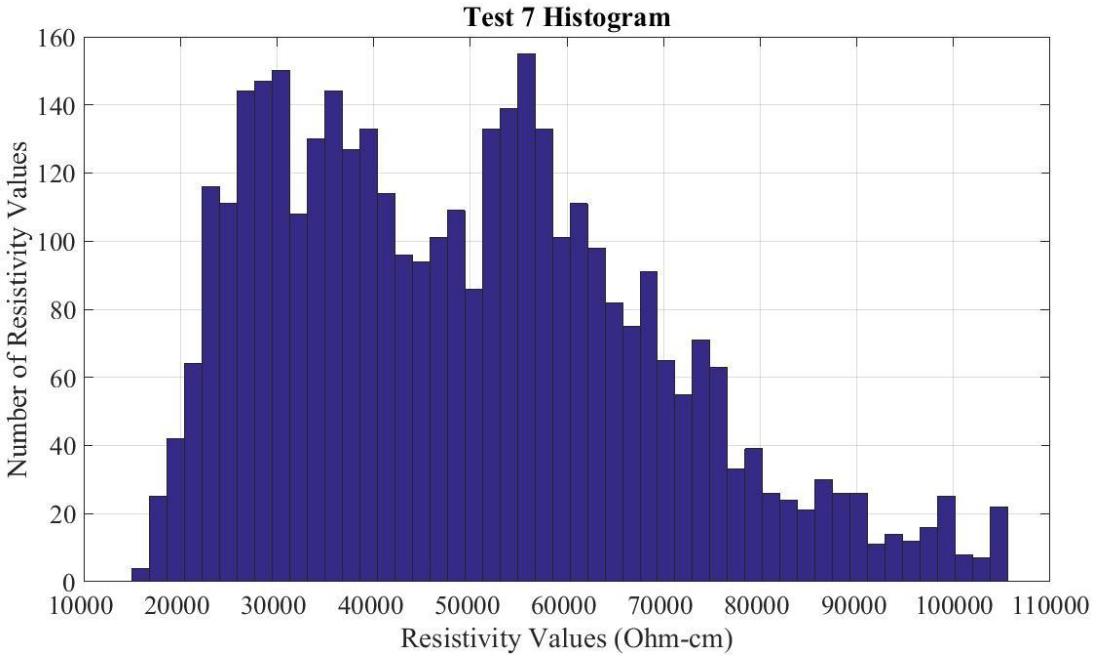

Fig. B.4. Test 7 Histogram.

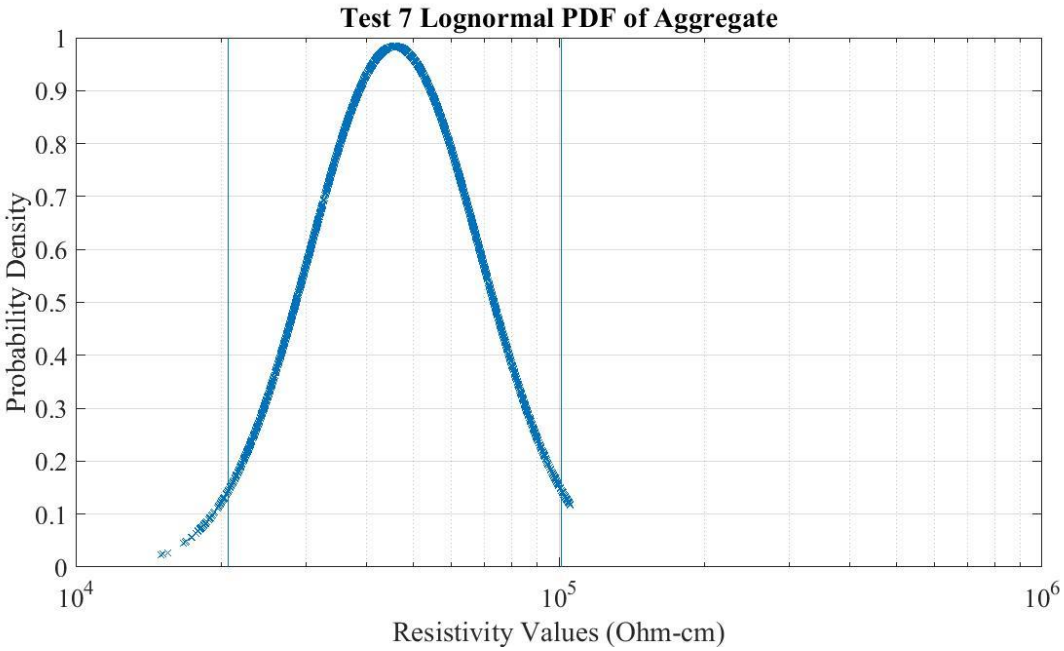

Fig. B.5. Test 7 PDF.

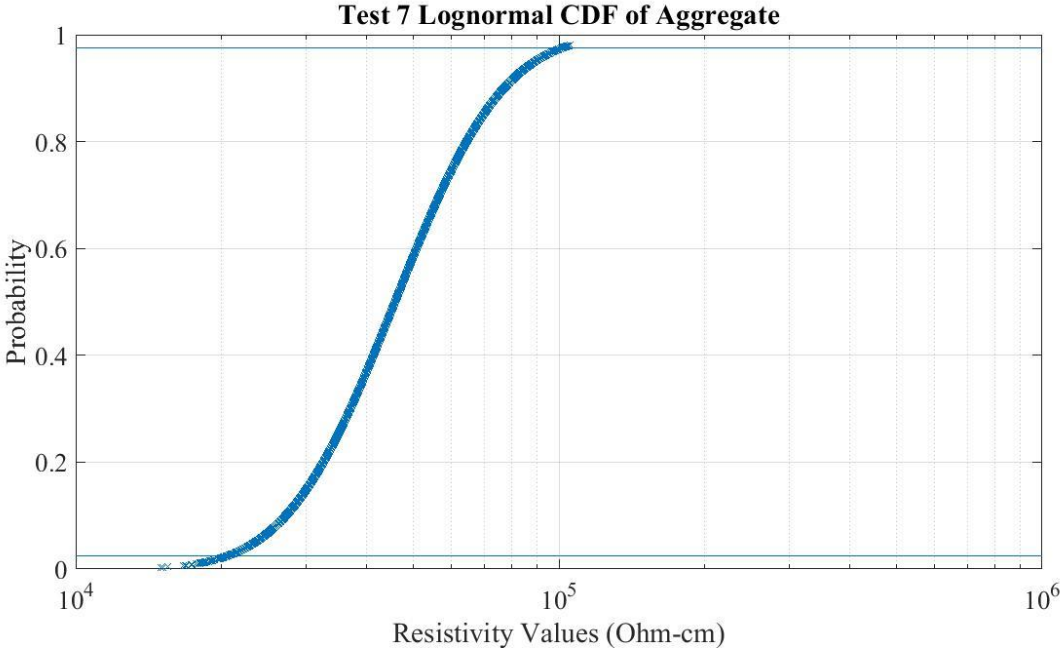

Fig. B.6. Test 7 CDF.

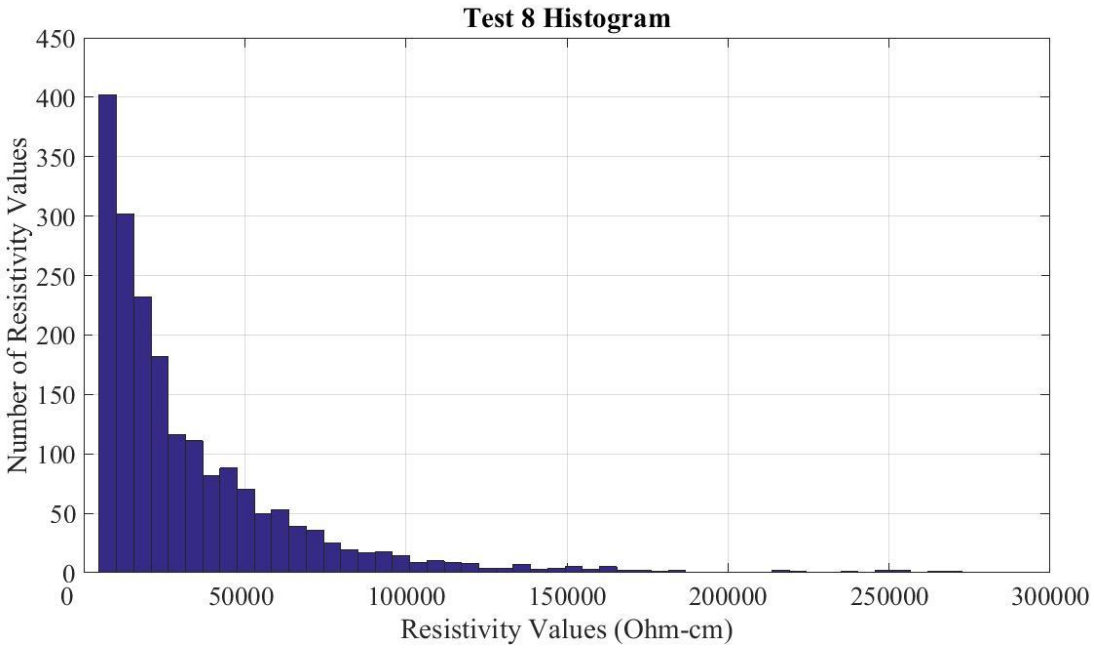

Fig. B.7. Test 8 Histogram.

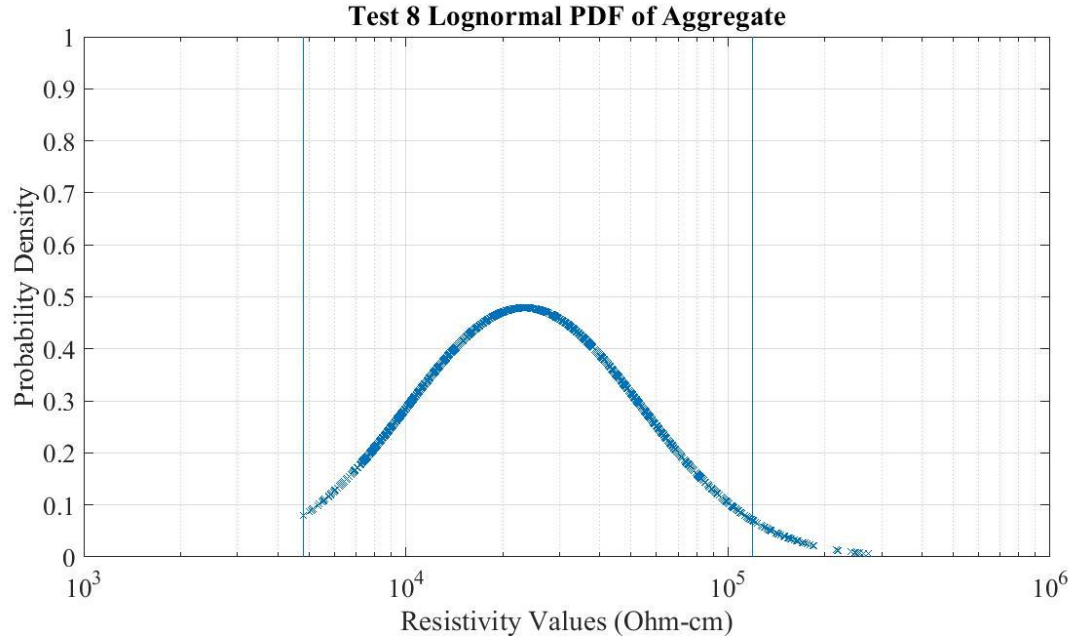

Fig. B.8. Test 8 PDF.

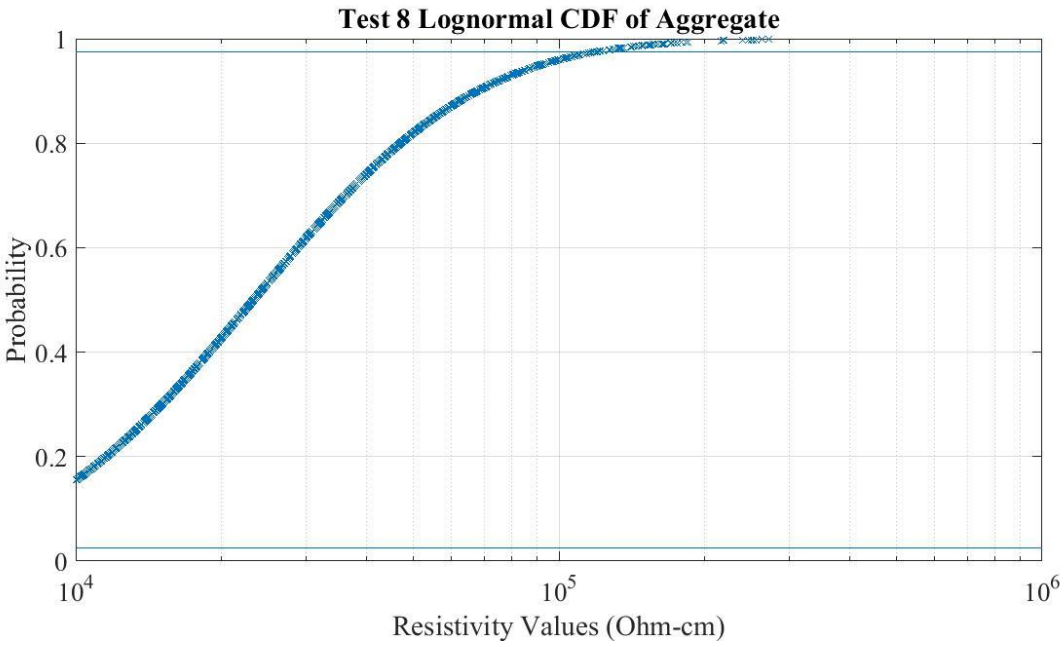

Fig. B.9. Test 8 CDF.

Appendix C Metal Wall

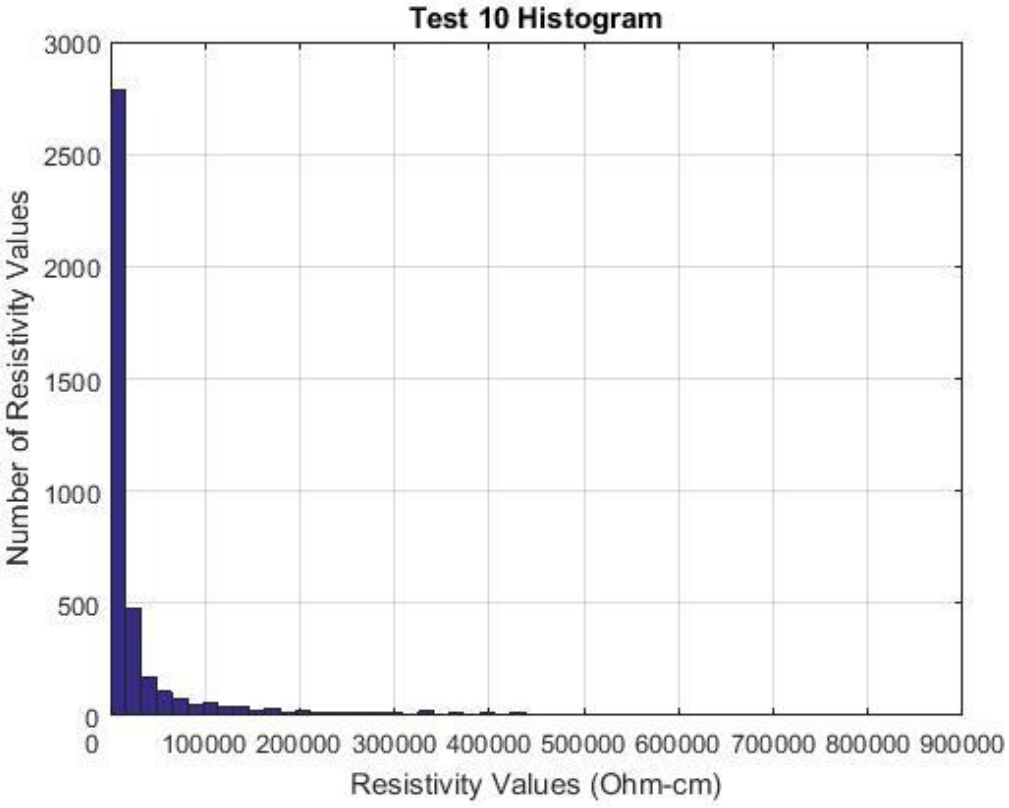

Fig. C.1. Test 10 Histogram.

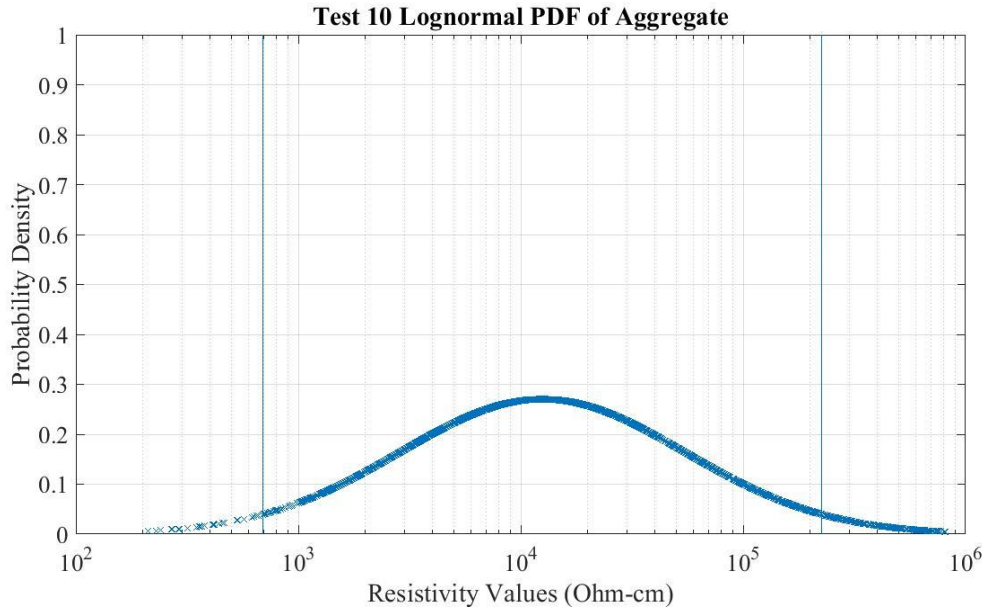

Fig. C.2. Test 10 PDF.

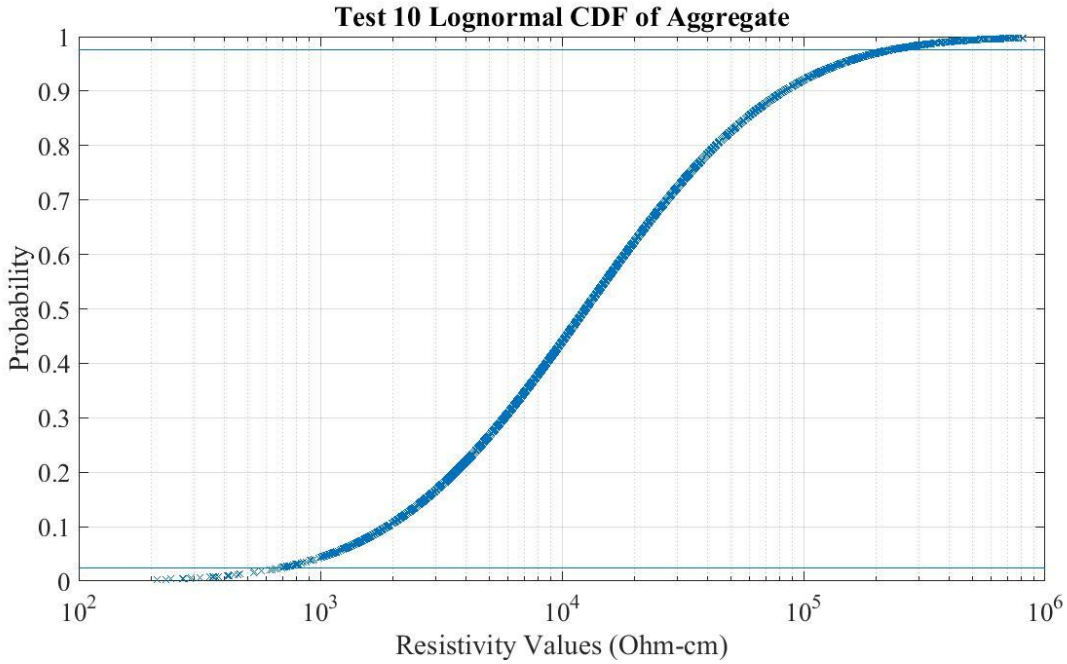

Fig. C.3. Test 10 CDF.

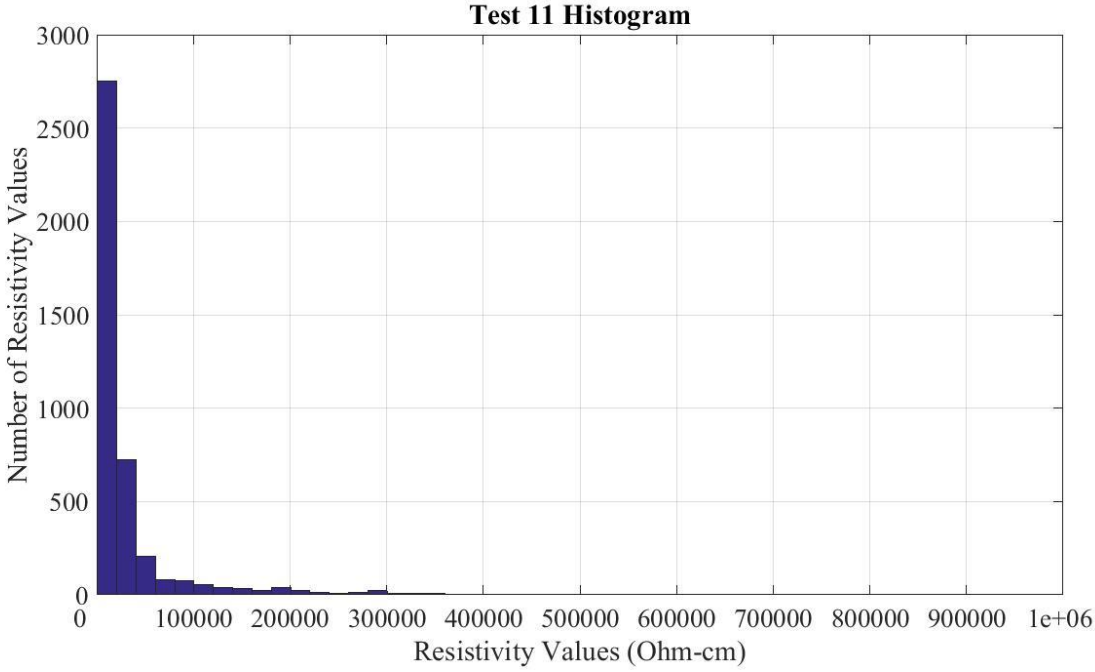

Fig. C.4. Test 11 histogram.

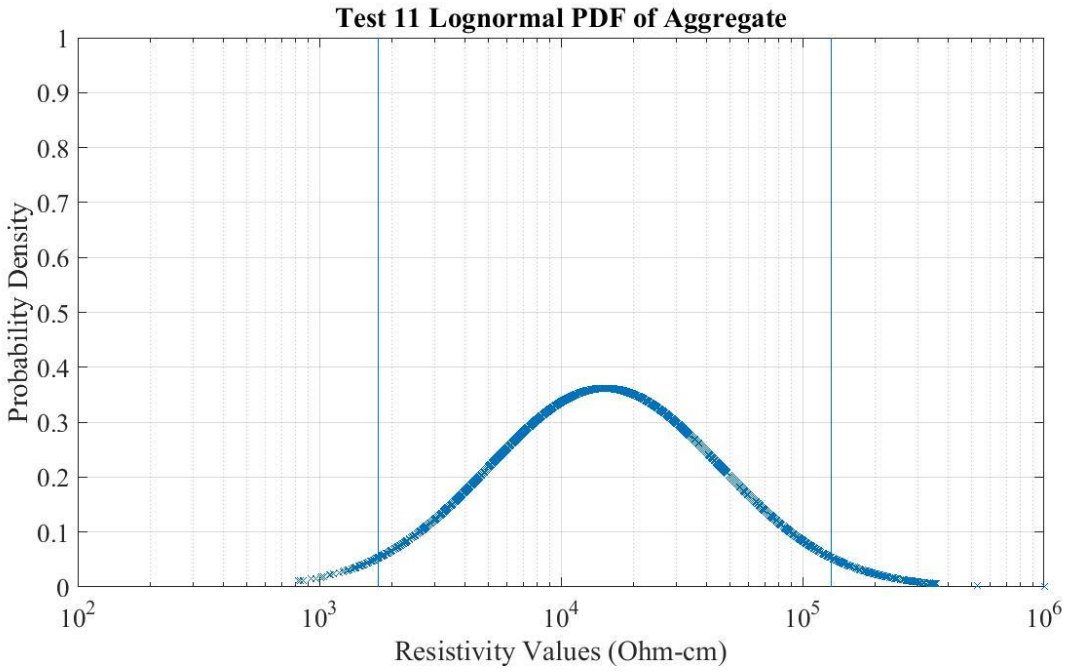

Fig. C.5. Test 11 PDF.

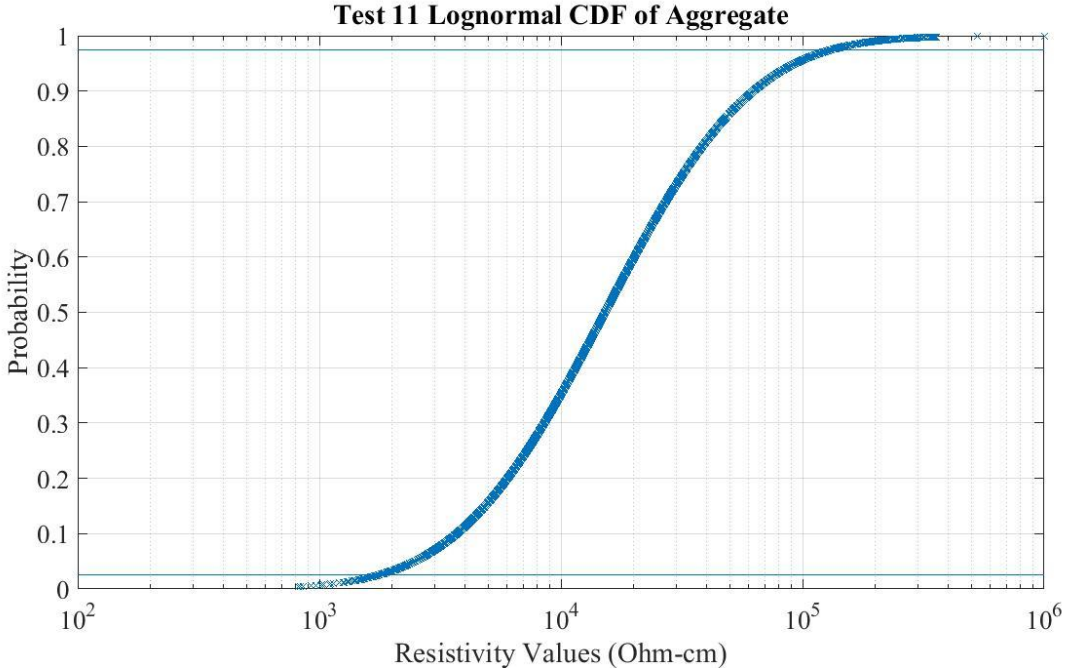

Fig. C.6. Test 11 CDF.

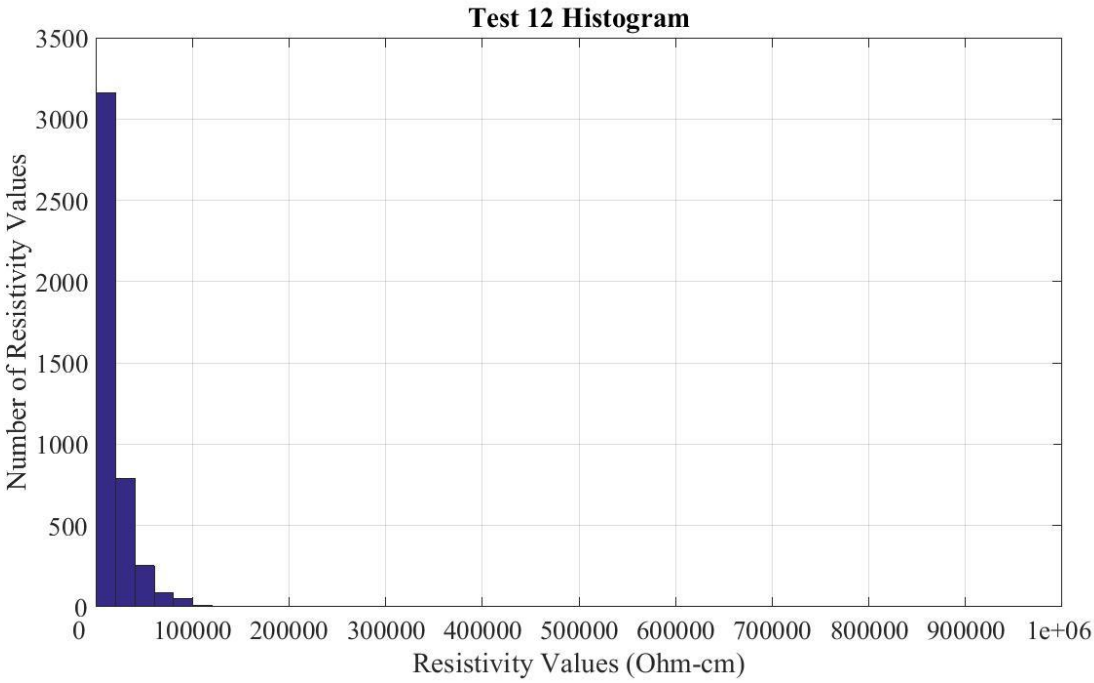

Fig. C.7. Test 12 histogram.

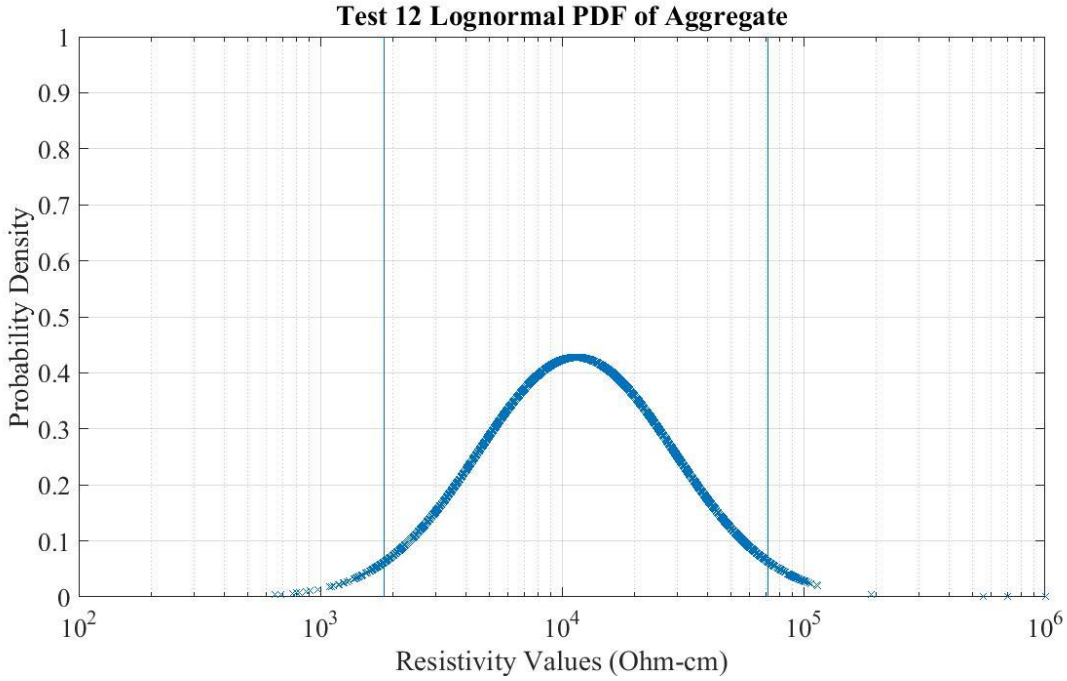

Fig. C.8. Test 12 PDF.

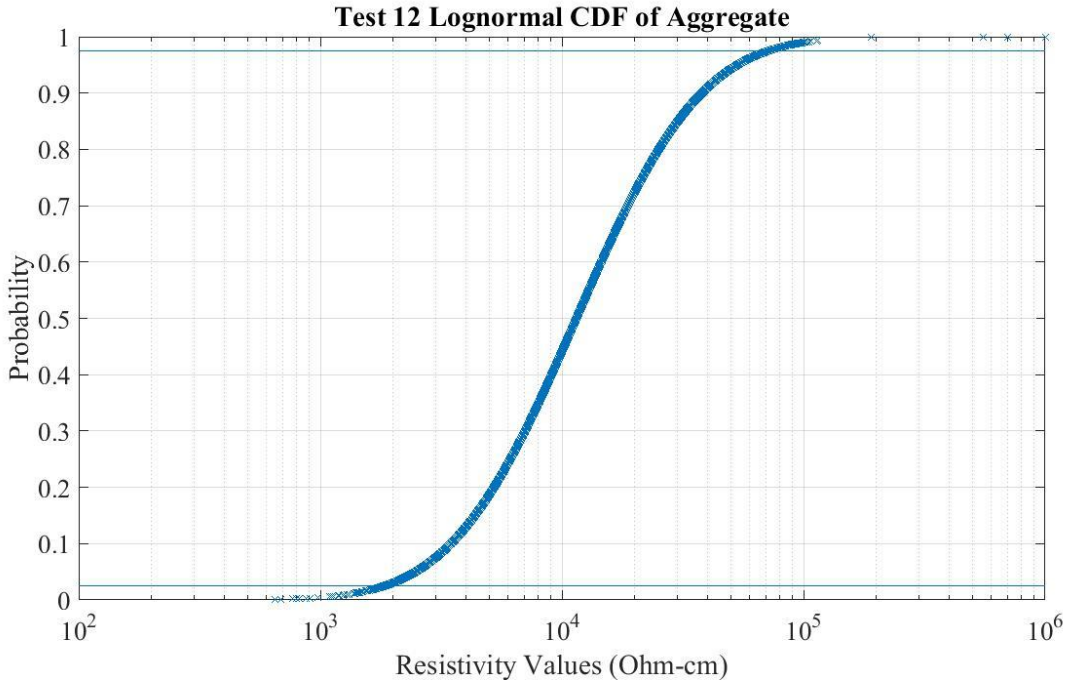

Fig. C.9. Test 12 CDF.

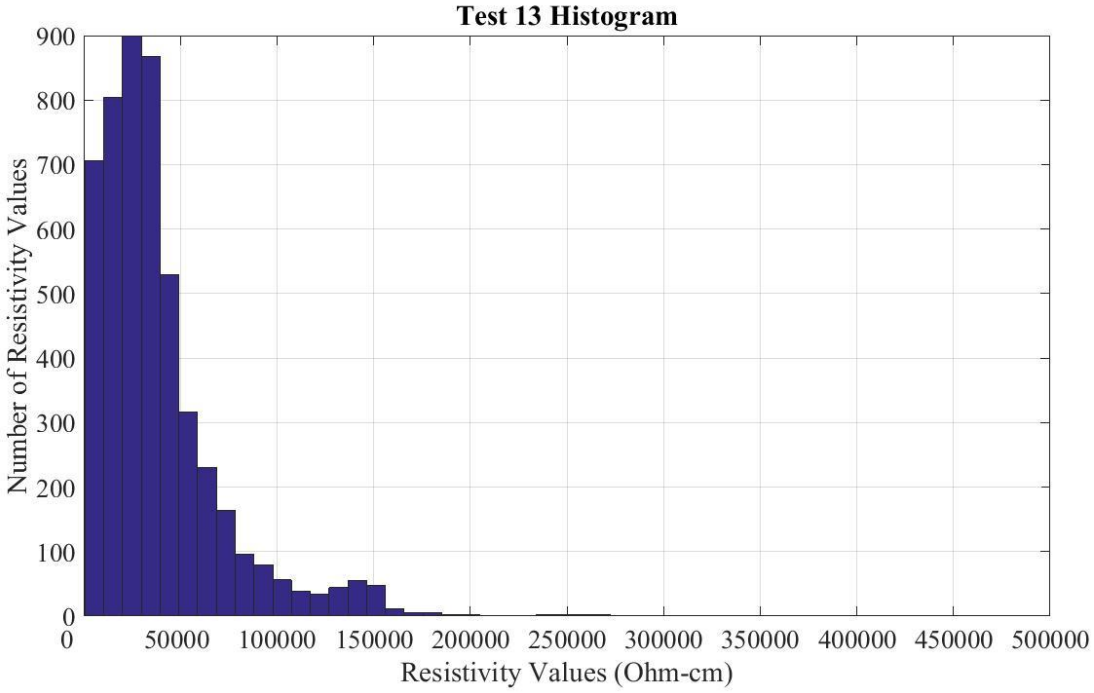

Fig. C.10. Test 13 histogram.

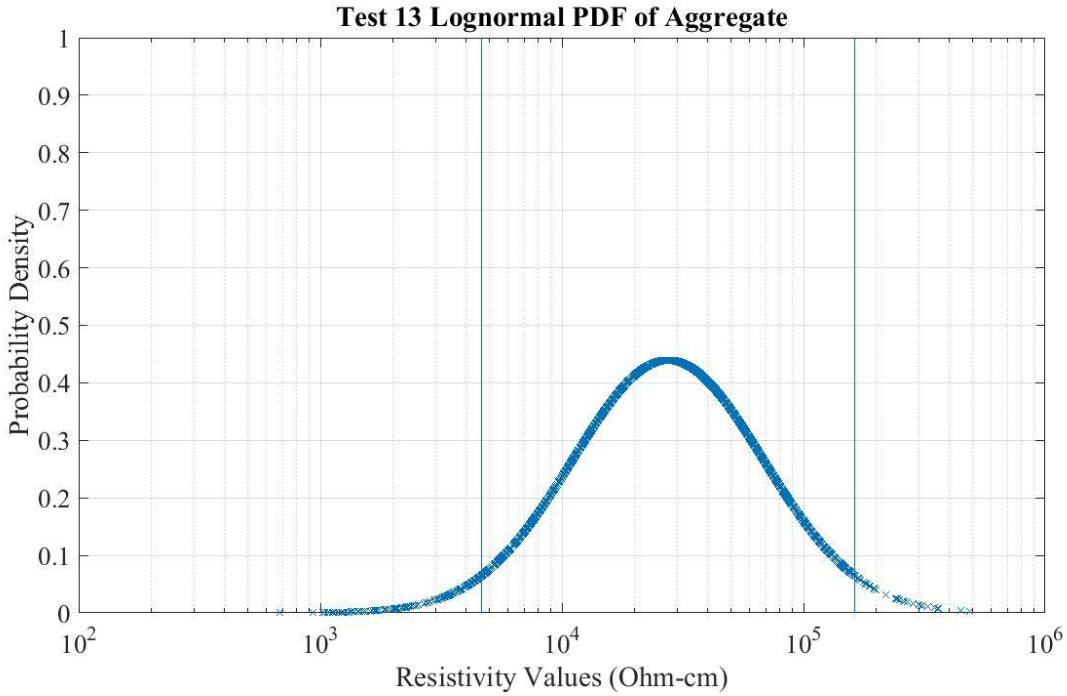

Fig. C.11. Test 13 PDF.

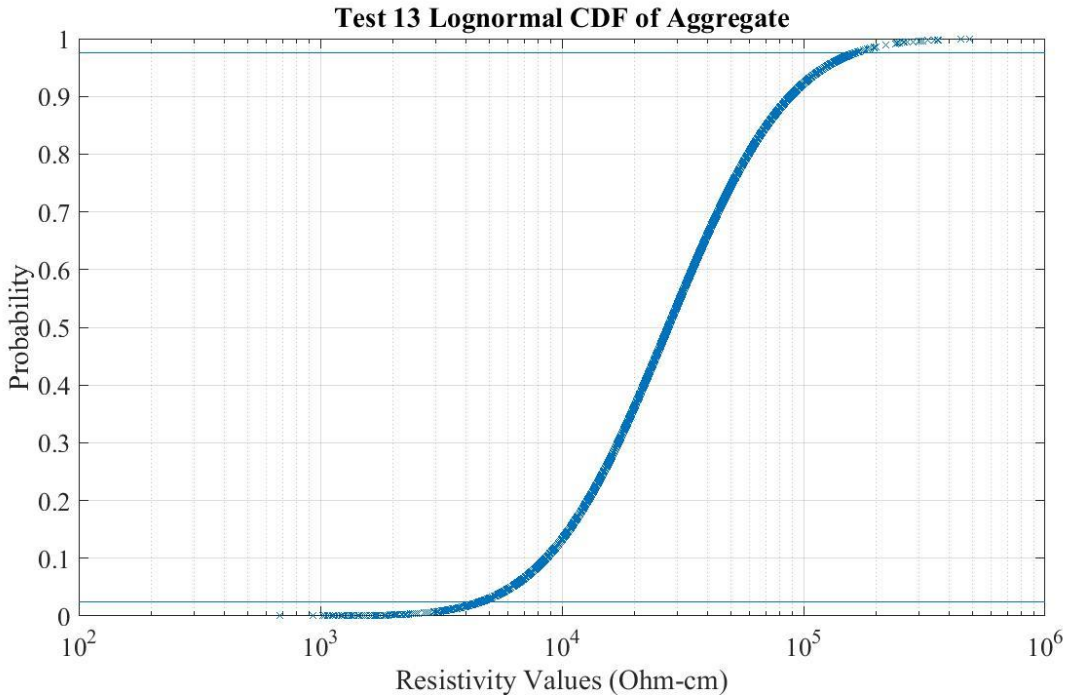

Fig. C.12. Test 13 CDF.

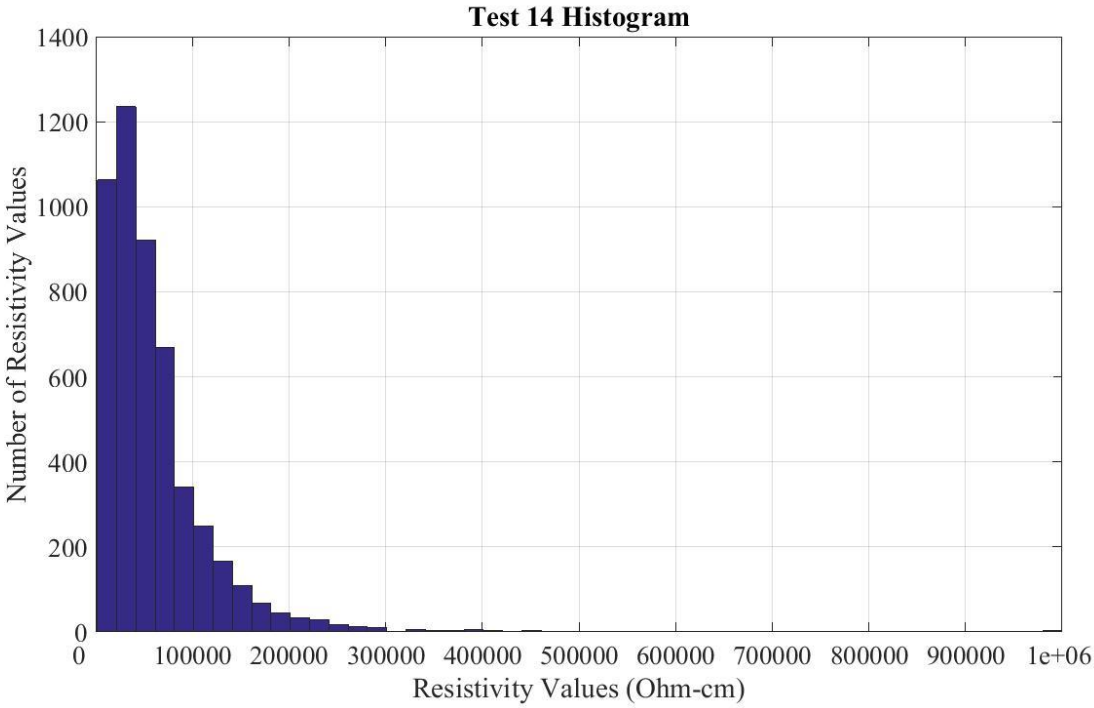

Fig. C.13. Test 14 histogram.

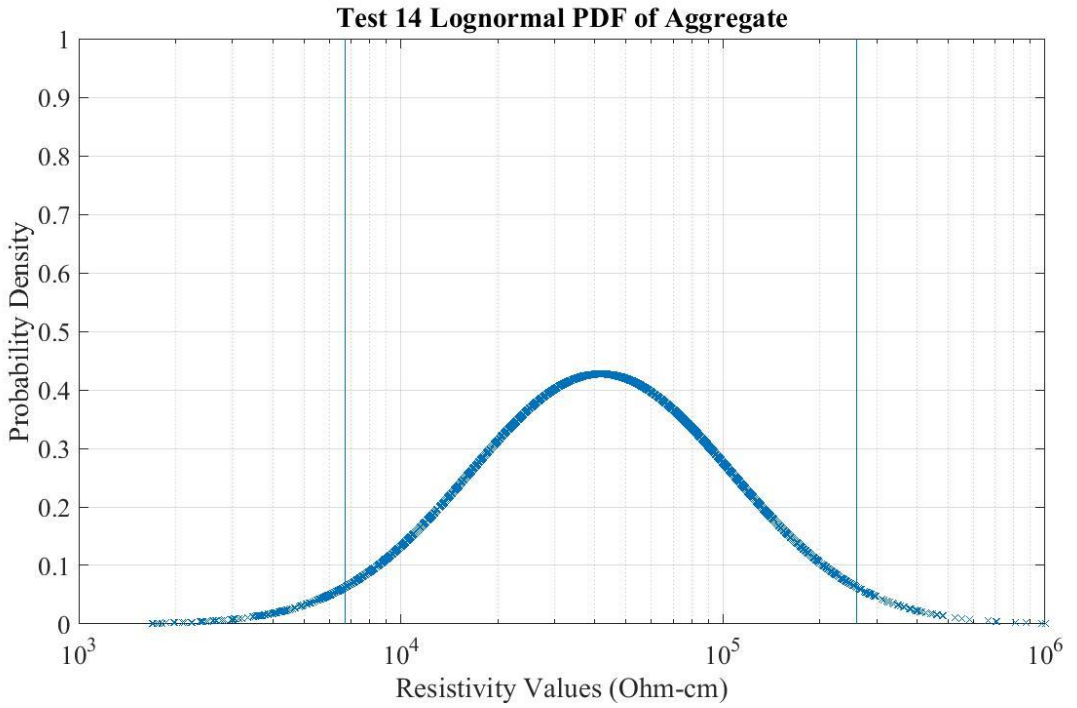

Fig. C.14. Test 14 PDF.

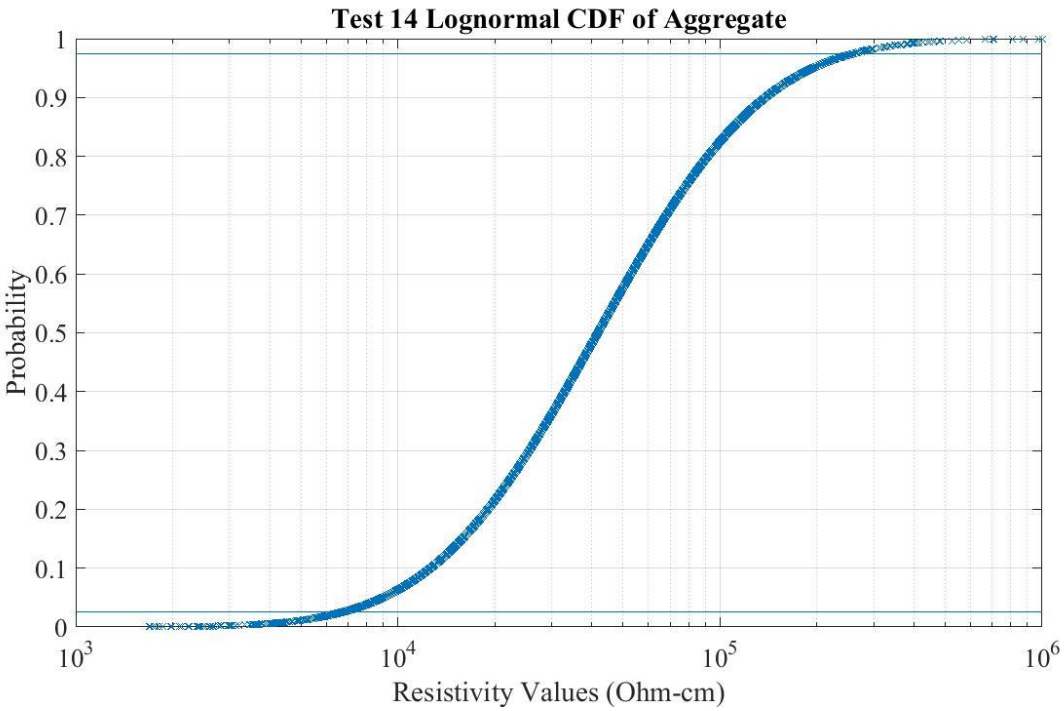

Fig. C.15. Test 14 CDF.

Appendix D Gravity Wall

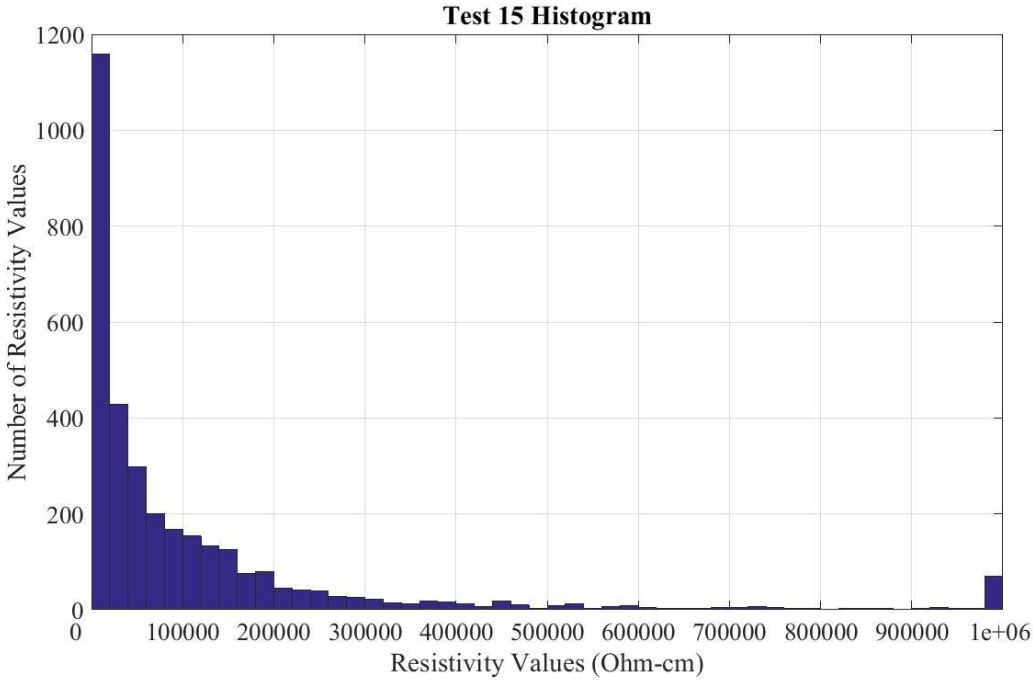

Fig. D.1. Test 15 histogram.

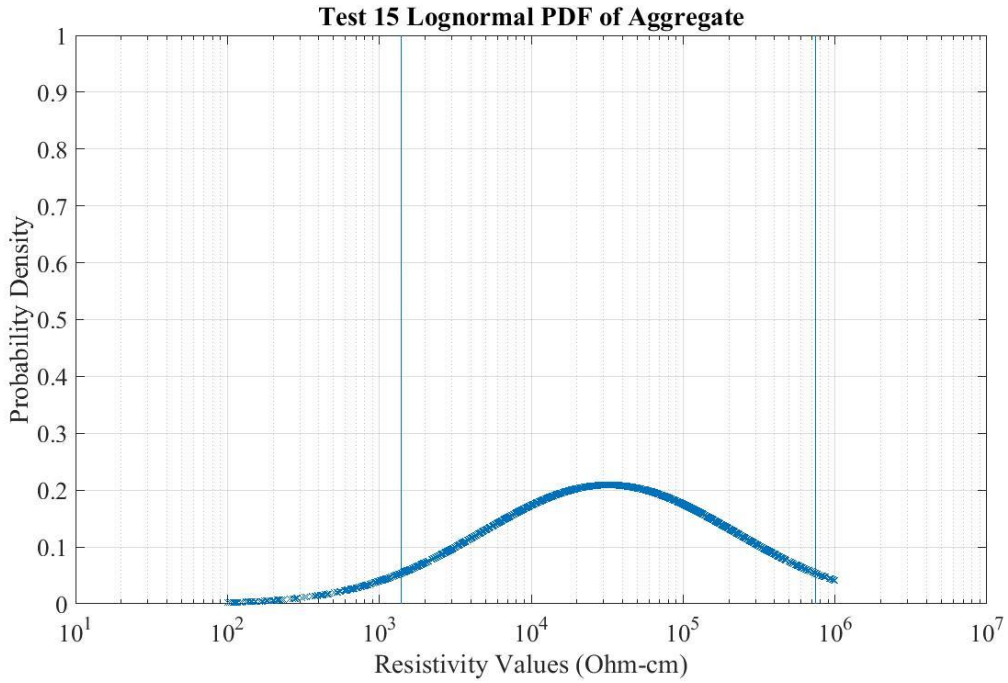

Fig. D.2. Test 15 PDF.

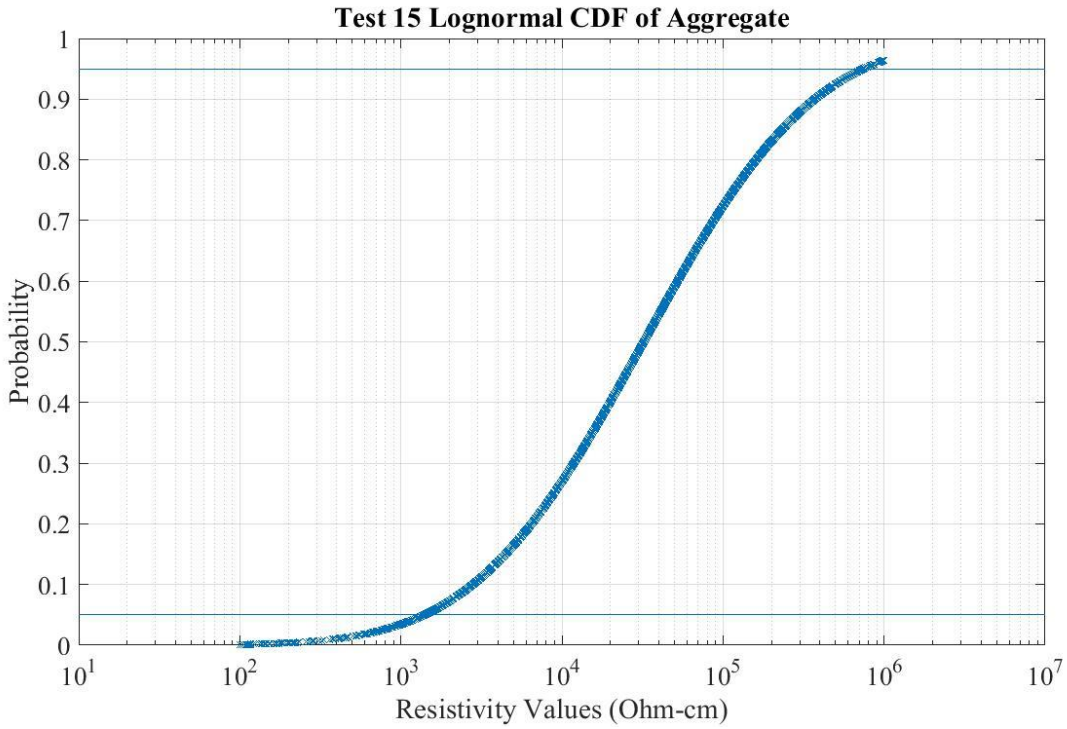

Fig. D.3. Test 15 CDF.

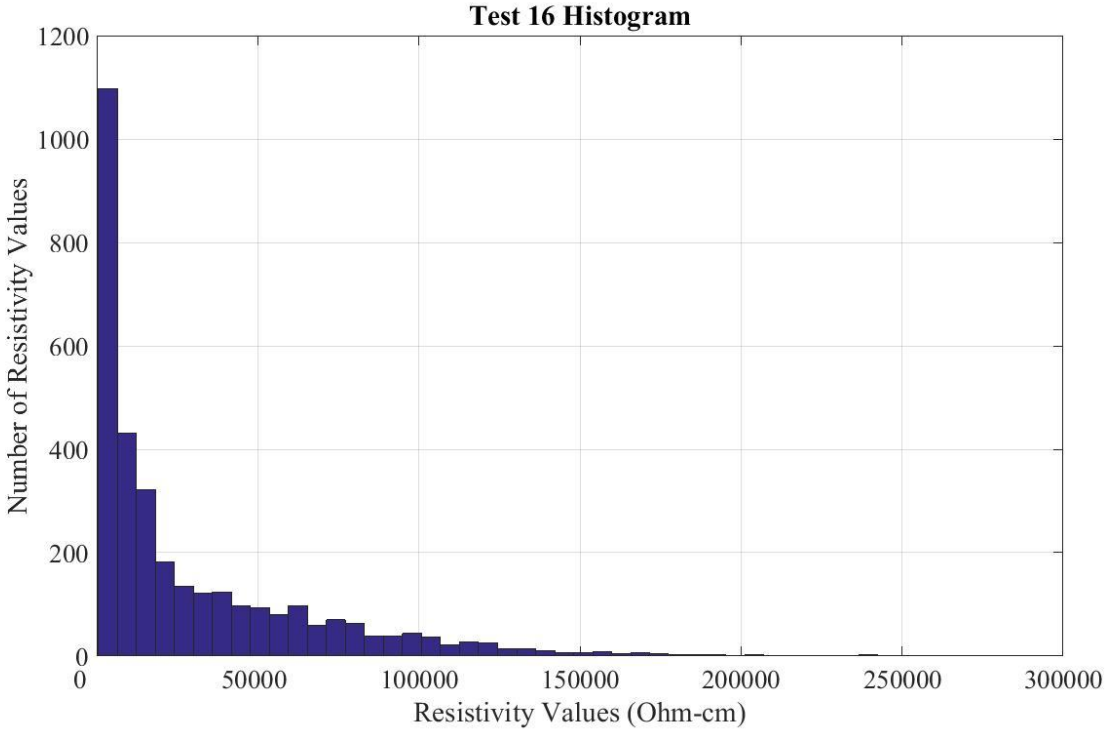

Fig. D.4. Test 16 histogram.

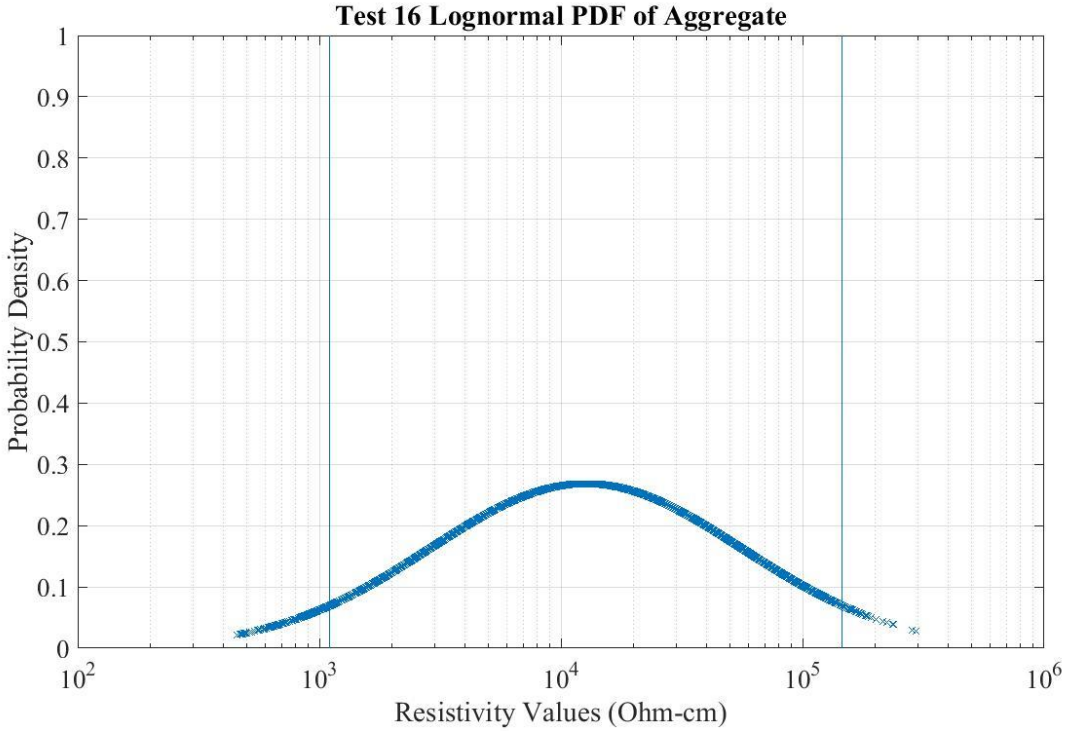

Fig. D.5. Test 16 PDF.

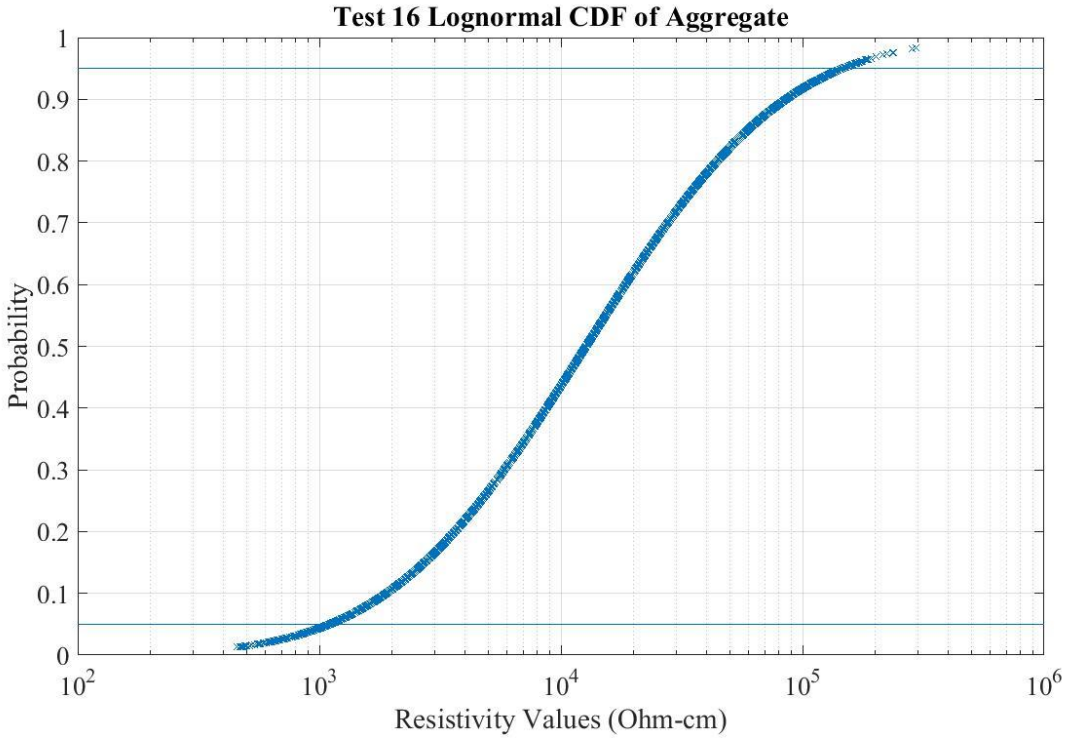

Fig. D.6. Test 16 CDF.

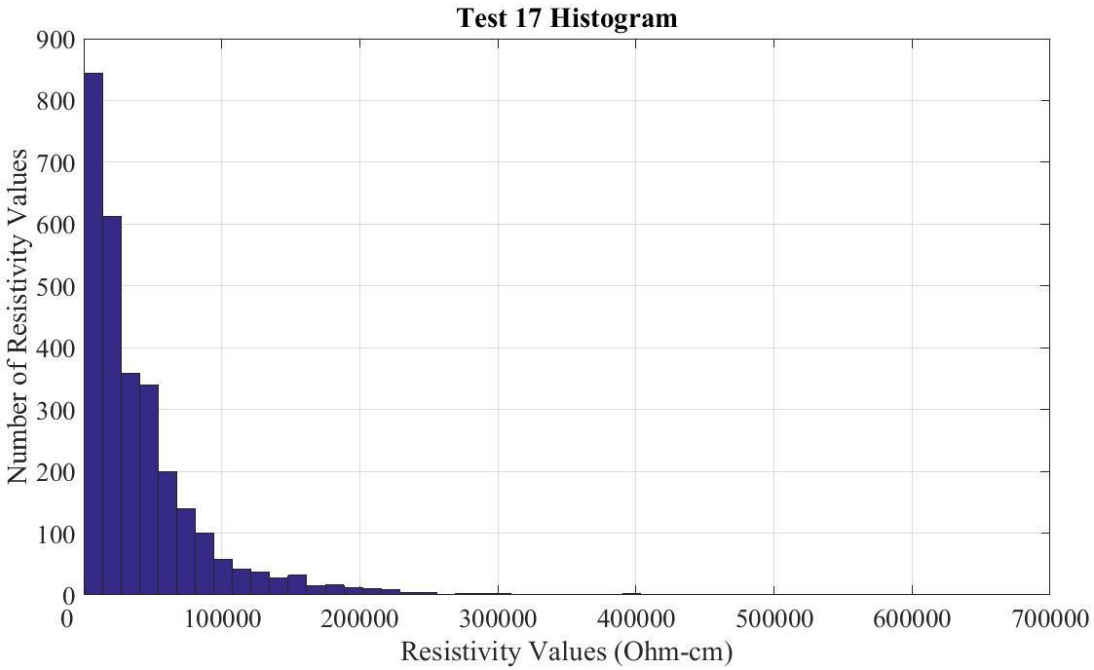

Fig. D.7. Test 17 histogram.

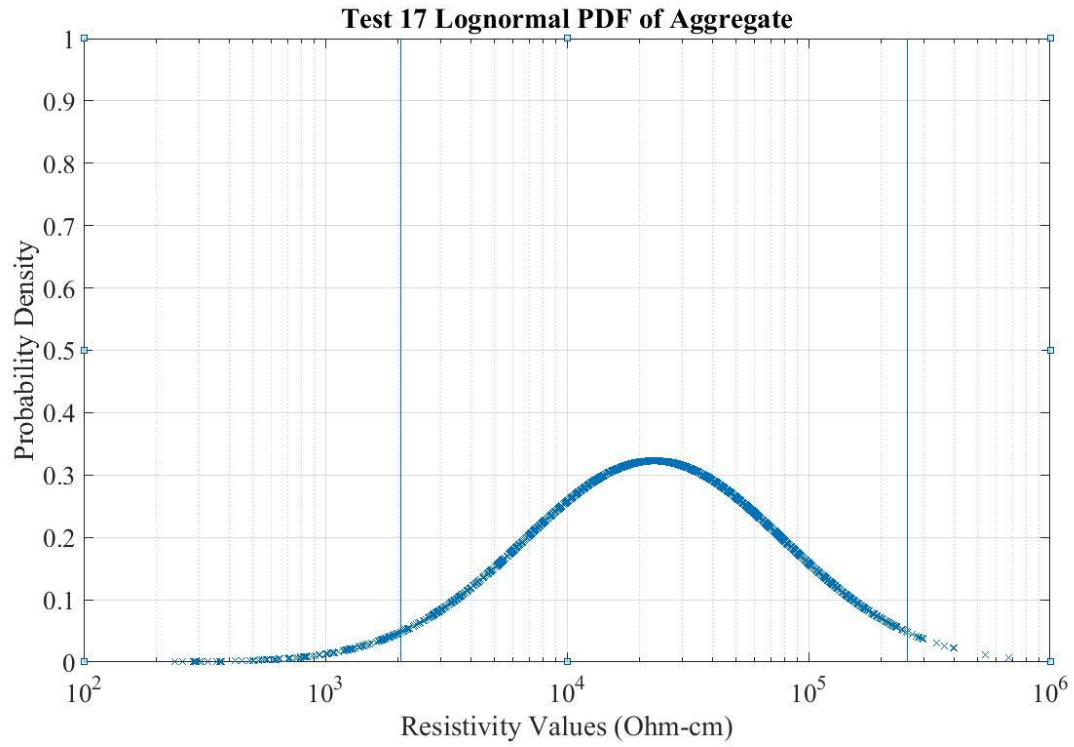

Fig. D.8. Test 17 PDF.

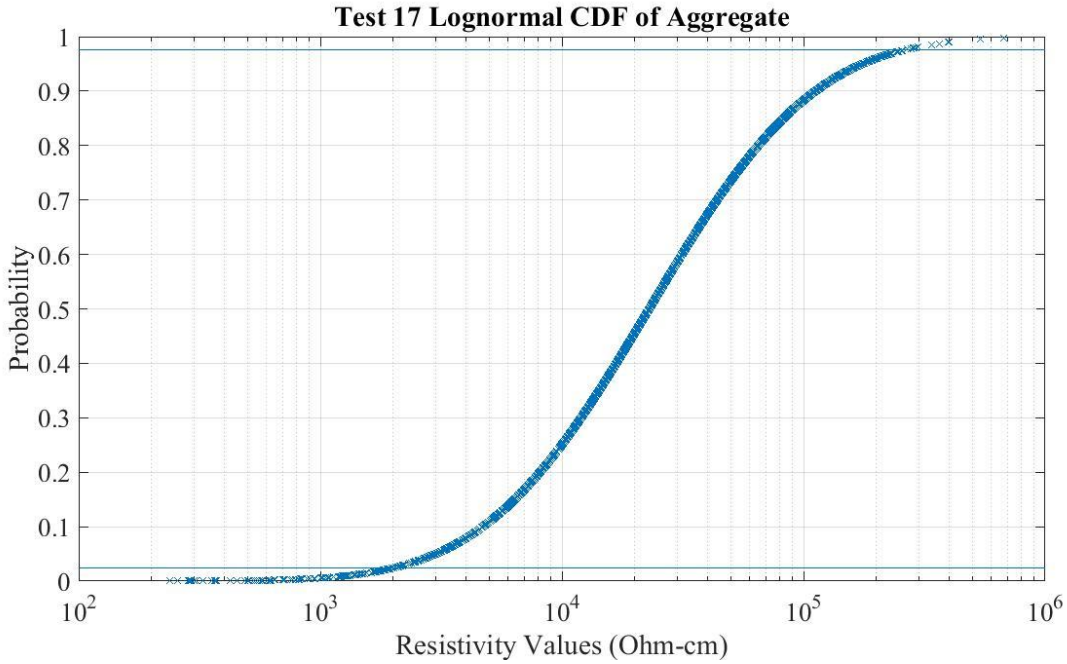

Fig. D.9. Test 17 CDF.

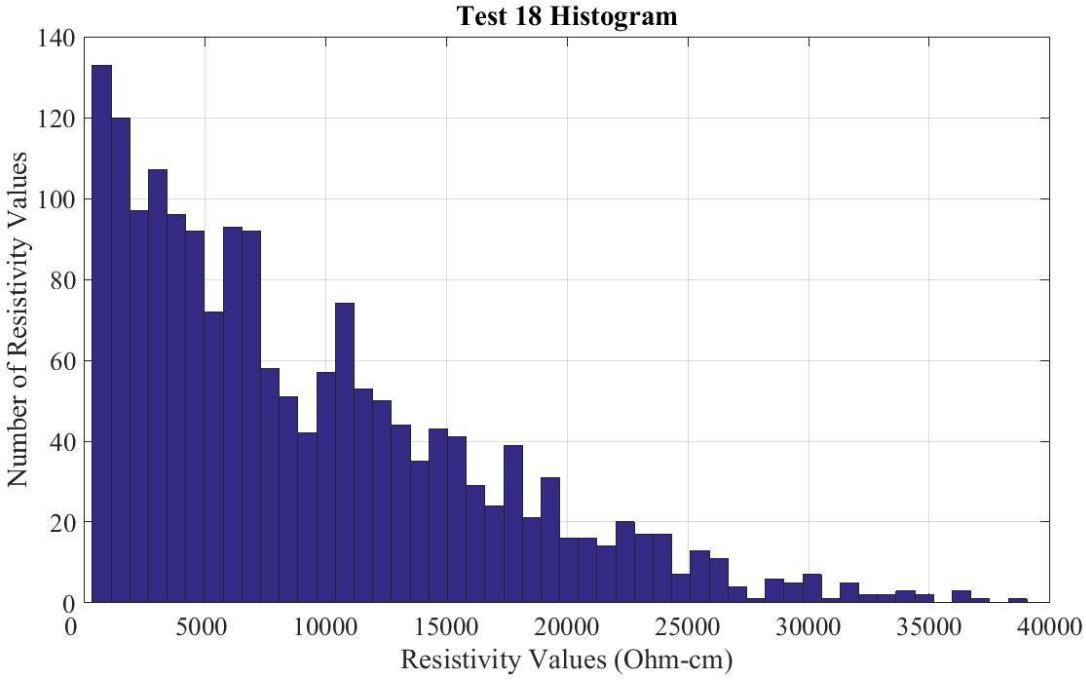

Fig. D.10. Test 18 histogram.

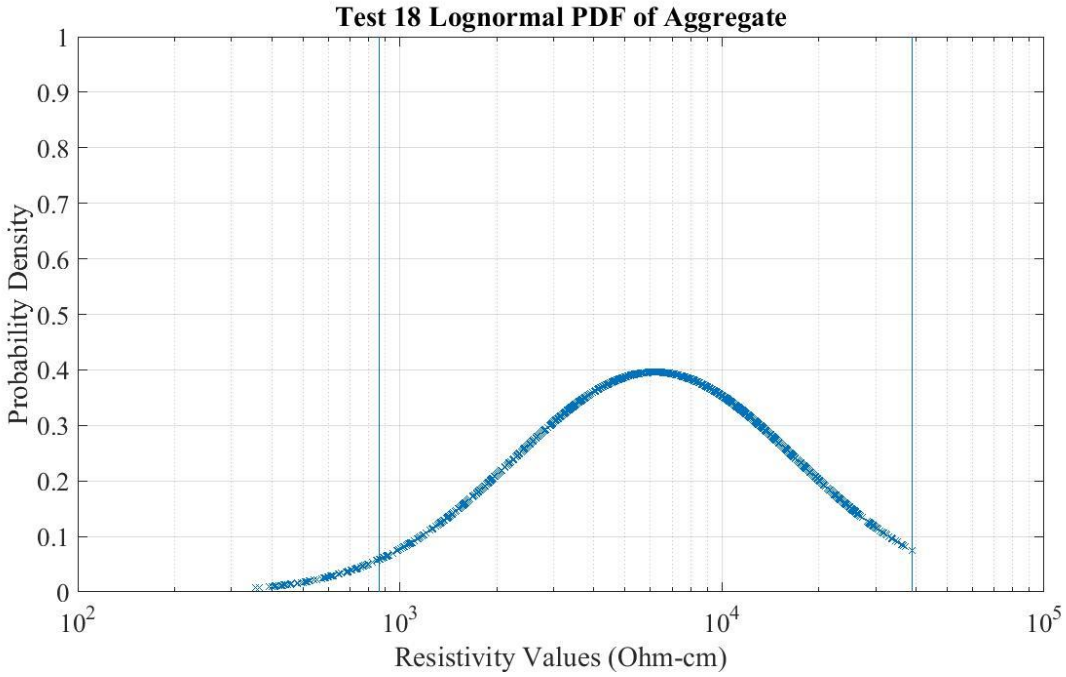

Fig. D.11. Test 18 PDF.

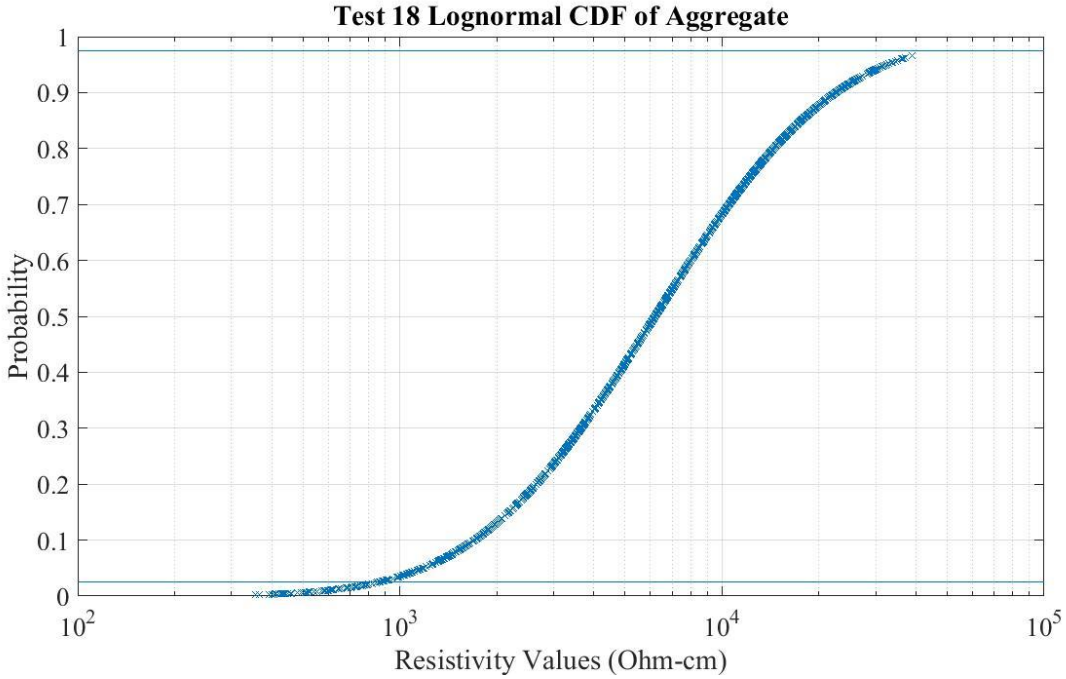

Fig. D.12. Test 18 CDF.

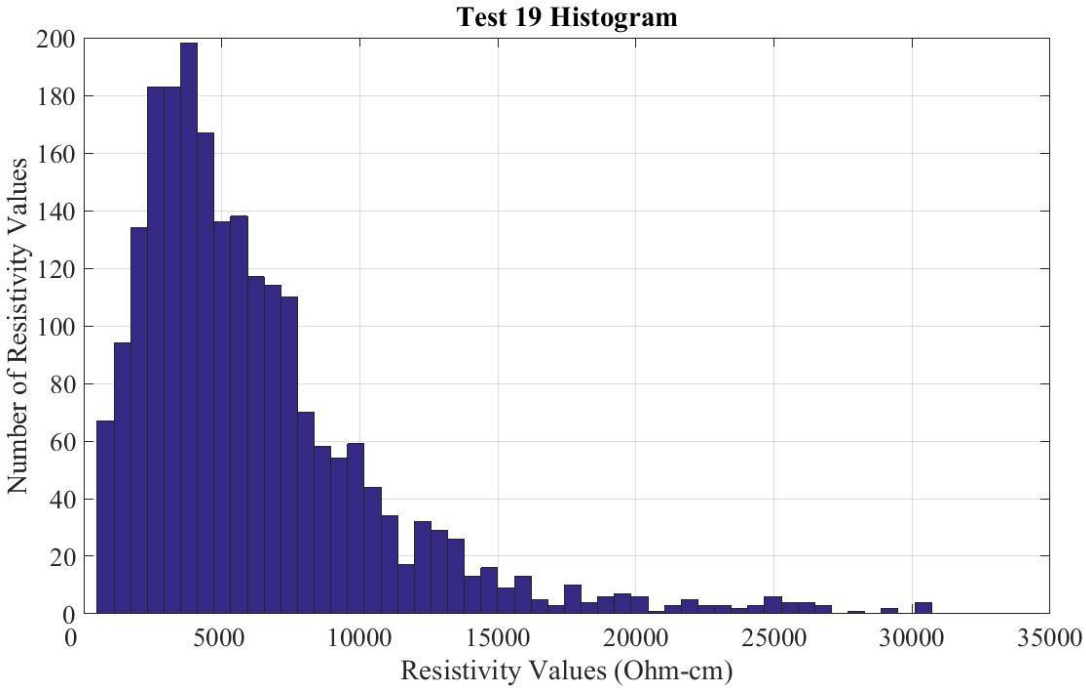

Fig. D.13. Test 19 histogram.

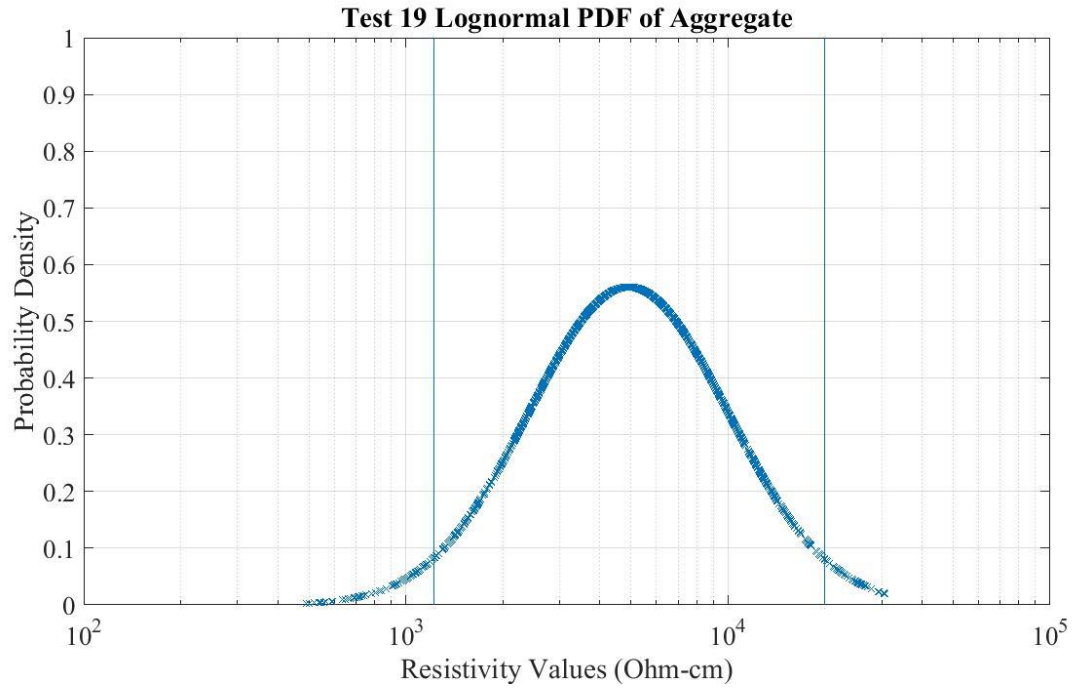

Fig. D.14. Test 19 PDF.

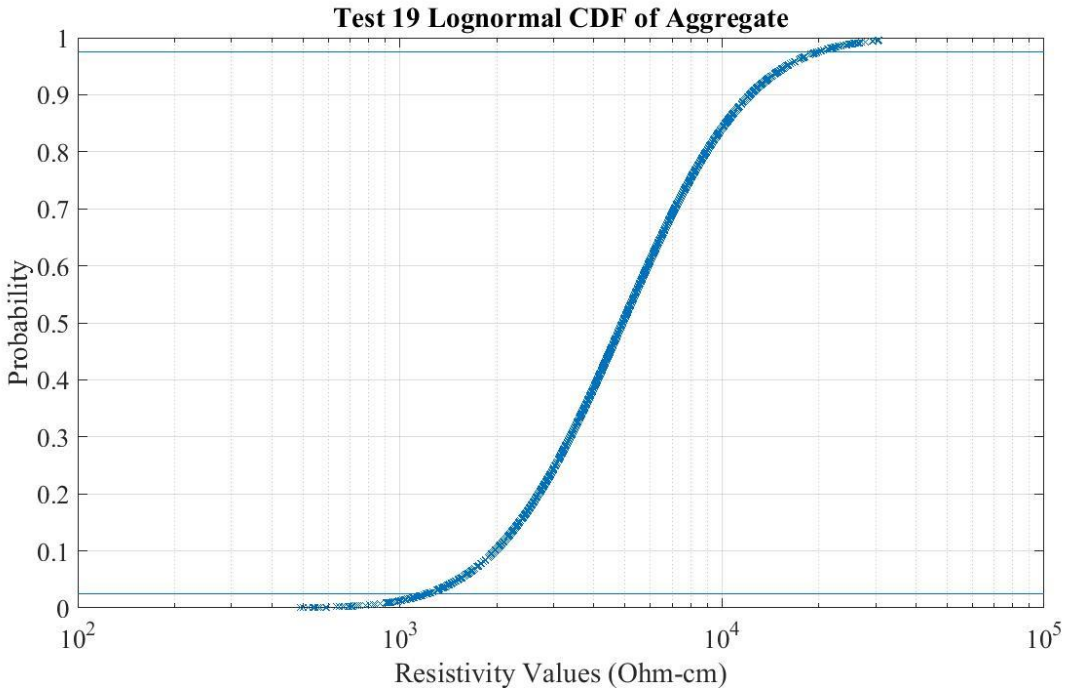

Fig. D.15. Test 19 CDF.